Uniform semiclassical methods and their applications

A thesis presented

by

Jiří Vaníček

to

The Department of Physics

in partial fulfillment of the requirements

for the degree of

Doctor of Philosophy

in the subject of

Physics

Harvard University

Cambridge, Massachusetts

May 2003

Dedicated to my parents, Jiří and Jana Vaníček, and my sister Marcela.

Thesis advisor:
Professor Eric J. Heller

Author:
Jiří Vaníček

Uniform semiclassical methods and their applications

Abstract

This thesis presents several uniform methods improving the accuracy of semiclassical approximations to quantum mechanics when the WKB approximation breaks down due to nonlinear underlying dynamics. In our alternative approach, the complicated Lagrangian manifold supporting a singular WKB wavefunction is replaced by a series of simpler Lagrangian manifolds, and the singular wavefunction is replaced by a convergent series of well-behaved semiclassical wavefunctions. This method is successfully applied to a model of homoclinic tangle, for which the WKB wavefunction has an infinite number of singularities, and to the problem of wave scattering from a corrugated wall.

A generalized replacement-manifold method is employed to find a uniform wavefunction describing coherent branched flow through a two-dimensional electron gas, a phenomenon recently discovered by direct imaging of the current using scanned probed microscopy. While the formation of branches has been explained by classical arguments, the semiclassical simulations necessary to account for the coherence are difficult due to the proliferation of catastrophes in phase space. The problem is solved here by using replacement manifolds with complex momenta. The method is first explained and tested on a single cusp catastrophe and then on a realistic model of the coherent branched flow.

Another uniform method is used to evaluate the quantum fidelity (Loschmidt echo). This method, based on the classical perturbation approximation and the Initial Value Representation, is numerically tractable and gives remarkably accurate results. Our method explicitly contains the Fermi-Golden-Rule and Lyapunov regimes of fidelity decay as well as the "building blocks" of analytical theories of recent literature, and thus permits a direct test of the approximations made by other authors. The thesis ends with a discussion of what remains from the theory of the decay of survival probability and the parametric dependence of the local density of states in one-dimensional Hamiltonian and disordered systems. We show that a remarkably accurate uniform approximation captures the physics of both perturbative and non-perturbative regimes, though it cannot take into account the strong localization effect.

Contents

List of Figures

List of Tables

Acknowledgments

First of all, I would like to thank my thesis advisor, Eric Heller, without whose support and encouragement completion of this dissertation would not have been possible. Most of the work in this thesis (especially Chapters 3-5) was done in collaboration with him. I am also indebted to Doron Cohen for many discussions and particularly because Chapter 6 is a result of our collaboration. I would like to express my thanks to Alex Barnett, Michael Haggerty, Bertrand Halperin, Lev Kaplan, Charles Marcus, Areez Mody, Steven Tomsovic, and Diego Vaz Bevilaqua, for many inspiring discussions and suggestions.

I am much obliged to other members of the Heller group, Bill Bies, Greg Fiete, Jesse Hersch, Alison Kalben, Sheng Lee, Natasha Lepore, Robert Parrott, Scot Shaw, Emmanuel Tannenbaum, Jay Vayshnav, and Troy Van Voorhis, for many discussions and their wonderful company both inside and outside of the office.

I would like to thank the faculty and the staff of the Department of Physics, Bonnie Currier, Carol Davis, Sheila Ferguson, Victoria Greene, Mary Lampros, Margaret Law, Ann Levy, Dayle Maynard, Stuart McNeal, Marilyn O'Connor, Kathy Ryan, Michal Spalinski, director David Norcross, and Judy Morrison from the Department of Chemistry.

I am very grateful to the National Science Foundation, to the Institute of Theoretical Atomic and Molecular Physics at the Harvard Smithsonian Center for Astrophysics, and to the Mathematical Sciences Research Institute at Berkeley for their financial support of my research. I am extremely indebted to Harvard University which has financially supported both my undergraduate and graduate studies. Studying at Harvard was a great experience: after spending seven and a half years there, I consider Cambridge and Harvard in particular to be my second home.

Last but not least, I would like to thank my parents, Jiří and Jana Vaníček, and my sister Marcela, for their lifelong encouragement and support of my studies and everything else they have done for me over the years. Without their help I would not have been able to not only finish but even start the research leading to this thesis.

Citations to Previously Published Work

Parts of this thesis have been previously published:

- "Replacement manifolds: A method to uniformize semiclassical wave functions," J. Vaníček and E. J. Heller, *Phys. Rev. E* **64**, 026215 (2001).
- "Uniform semiclassical wave function for coherent two-dimensional electron flow," J. Vaníček and E. J. Heller, *Phys. Rev. E* **67**, 016211 (2003).
- "Semiclassical evaluation of fidelity in the Fermi-golden-rule and Lyapunov regimes," J. Vaníček and E. J. Heller, submitted to *Phys. Rev. Lett.* Preprint: quant-ph/0302192 (2003).
- "Survival probability and the local density of states for one-dimensional Hamiltonian systems," J. Vaníček and D. Cohen, submitted to *J. Phys. A: Math. Gen.* Preprint: quant-ph/0303103 (2003).

Electronic preprints are available on the Internet at the following URL:

http://arXiv.org

Chapter 1

Introduction and summary

Semiclassical approximation to quantum mechanics remains an indispensable tool in many areas of physics and chemistry. Despite the extraordinary evolution of computer technology in the twentieth century, exact numerical solution of the Schrödinger equation is impossible for problems with more than a few degrees of freedom. Another great advantage of the semiclassical approximation lies in that it facilitates an intuitive understanding of the underlying physics, which is usually hidden in blind numerical solutions of the Schrödinger equation.

Quite generally, semiclassical wave functions (and other quantities) can be written as a sum of terms arising from classically allowed trajectories,

$$\psi^{sc} = \sum_j A_j e^{iS_j/\hbar}, \tag{1.1}$$

where amplitudes A_j are square roots of classical probabilities and phases in the exponent are determined by classical actions S_j. From expression (1.1) it is clear how semiclassical approximation accounts for interference. However, with small extension semiclassical approximation can account for many other quantum phenomena, such as potential or dynamical tunneling [35], which are forbidden in classical mechanics.

Although semiclassical mechanics is as old as the quantum theory itself, the field is continuously evolving: There still exist many open problems in the mathematical aspects of the approximation as well as in the quest for new effective ways to apply the approximation to various physical systems. Above all, implementation of semiclassical methods becomes difficult when complicated classical dynamics results in divergences of amplitudes A_j or in an exponential growth of terms in Eq. (1.1). These divergences can be corrected by

so-called *uniform* approximations, which are also the main focus of this thesis. Various uniform approximations, capable of correcting a *finite* number of singularities near classical catastrophes, have been known for many years. To name a few, these are the Airy [18, 9], Bessel [116], Pearcy [97, 29], and Laguerre [22] uniform methods. The replacement-manifold method developed in Chapters 3 and 4 of this thesis is a uniform approximation which can account for an *infinite* number of singularities at the same time.

As recently as in the 1980s, it was thought that the semiclassical approximation would break down in chaotic systems after the Ehrenfest time, i.e., the time when quantum wave packets become completely delocalized. However, Heller, O'Connor, Sepúlveda, and Tomsovic [58, 91, 92, 111, 119, 120] used more sophisticated versions of the WKB approximation (e.g., homoclinic orbit sum of Ref. [120]) to find that the approximation remains accurate long after the Ehrenfest time, as long as all of the terms[1] in Eq. (1.1) are properly taken into account. In Chapter 5 we present an alternative method based on the classical perturbation approximation and the initial value representation that not only corrects the singularities but also avoids the summation over an exponentially growing number of terms.

The thesis is organized as follows: Chapter 2 gives an overview of the evolution of semiclassical methods, uniform approximations, and their applications, in order to build a context for the uniform approximations introduced in the following chapters. For this purpose, Sections 2.3 and 2.4 are most important. Section 2.3 describes the simplest example of a uniform method, namely the Airy uniformization of a fold catastrophe. In Section 2.4 we explain the initial value representation [83, 84], a uniform method closely related to the methods developed in this thesis.

Chapter 3 introduces the replacement-manifold method and its first applications.[2] In general, semiclassical wave function can be associated with a Lagrangian manifold in phase space, which is evolved according to Hamilton's equations of motion. Singularities in Eq. (1.1) arise when the projection of this manifold on an appropriate coordinate plane is singular. The number of these singularities grows as the manifold becomes increasingly convoluted due to the nonlinear classical dynamics. The uniform method of Chapter 3 is based on the idea of replacing the original convoluted Lagrangian manifold by a series of simpler Lagrangian manifolds, and replacing the singular semiclassical wave function associated with the original manifold by a convergent series of well-behaved semiclassical

[1] $30,000$ semiclassical terms are used in Ref. [120].

[2] Most of Chapter 3 has been published in Ref. [125].

wave functions associated with these simpler manifolds. The replacement-manifold method is then successfully applied to a realistic model of a homoclinic tangle, a ubiquitous structure near unstable periodic orbits in chaotic systems. Replacement manifolds give very accurate results in spite of the fact that an infinite number of oscillations in the manifold are present in any neighborhood of the unstable point. The method is equally successfully applied to the problem of wave scattering from a corrugated wall, which physically corresponds, e. g., to a simple version of quantum-mechanical scattering of atoms from the surface of a solid.

In the original applications of the replacement-manifold method in Chapter 3, a special use was made of an infinite number of oscillations in the Lagrangian manifolds. In Chapter 4 that assumption is relaxed. The goal of Chapter 4 is to find a semiclassical description of the coherent branched electron flow from a quantum point contact, a phenomenon observed recently by the R. Westervelt group at Harvard University [121, 122].[3] In the experiments, the electron current was directly imaged using scanned probed microscopy. While the formation of branches can be explained by classical arguments [122], semiclassical simulation was needed to account for the coherence observed experimentally. However, due to the proliferation of catastrophes, such a simulation was deemed impossible because the standard WKB approximation is inapplicable and usual uniform semiclassical methods would be numerically intractable. The branched electron flow results from combination of focusing and/or defocusing properties of a weak random potential. In Chapter 4 we simulate impurities in the sample by Gaussian potential wells (or bumps) for which a generalized replacement-manifold expansion of the electron wave function can be found analytically. Propagation of the wave functions associated with these replacement manifolds again yields surprisingly accurate semiclassical wave functions. This is true even for times when proliferating caustic singularities result in the failure of the standard WKB approximation at *every* position with nonzero probability of finding an electron.

Chapter 5 describes a semiclassical method to calculate quantum fidelity.[4] Quantum fidelity stands for the overlap of two initially identically states, which have evolved in slightly different environments. It has attracted much attention recently because of its relevance to quantum computation and decoherence in complex environments. The same quantity is sometimes called "Loschmidt echo" because it can be regarded as the survival probability of a state evolved for time t in one environment, and then backward in time for

[3] Most of Chapter 4 has been published in Ref. [126].

[4] The main results of Chapter 5 have been published in Ref. [127].

time t in a slightly perturbed environment. In chaotic Hamiltonian systems, depending on the strength of perturbation, the decay of quantum fidelity can be either Gaussian or exponential in time. In the exponential regime, the decay rate first grows with the second power of the perturbation strength, but eventually saturates at the Lyapunov exponent λ of the unperturbed system. In fact, various other regimes have been observed in numerical simulations for either extremely short or very long times. Before this work, several authors used various qualitative semiclassical approaches to derive an approximate analytical behavior of the decay in various limits. In Chapter 5, we find a uniform semiclassical method which is numerically accurate over a wide range of perturbations strengths. It was thought that direct numerical evaluation would be impossible because of an exponentially growing number of semiclassical terms and singularities. As we show, however, this exponential "barrier" can be circumvented, using an approach based on the semiclassical perturbation approximation and the initial value representation.[5] Not only is this method numerically fast and accurate, it also provides a means to directly test all approximations used in deriving analytical results in recent literature [66, 19].

In Chapter 6 we explore properties of the survival probability and of the local density of states in the setting of non-adiabatic transitions, in which an eigenstate of an original Hamiltonian is propagated with a perturbed Hamiltonian.[6] For chaotic systems, there exists a theory for the decay of the survival probability, and for the parametric dependence of the local density of states. This theory leads to the distinction between "perturbative" and "non-perturbative" regimes, and the observation that standard semiclassical tools are useful in the latter case. Chapter 6 discusses what is left from this theory in the case of one-dimensional systems. In particular, we show that even in one dimension, we can find an intermediate regime in which the local density of states is Lorentzian and the survival probability decays exponentially. We demonstrate that a remarkably accurate uniform semiclassical approximation captures the physics of all different regimes, although it cannot take into account the effect of strong localization.

[5] This is because our approach facilitates the use of Monte Carlo integration which cannot be efficiently used in other representations.

[6] Most of Chapter 6 has been published in Ref. [124].

Chapter 2

Uniform semiclassical approximations and quantum chaos

2.1 Historical overview

Semiclassical approximation is as old as quantum theory itself: in fact, the old quantum theory of Bohr and Sommerfeld later turned out to be a semiclassical approximation to Schrödinger's wave mechanics. Before Schrödinger's equation was discovered, Bohr [14] had successfully described the hydrogen spectrum, using the quantization condition[1]

$$\oint p\, dq = 2\pi\hbar n. \tag{2.1}$$

This equation selects only those classical states of the system for which the action integral equals an integer multiple of Planck's constant $h = 2\pi\hbar$. This condition was soon generalized to systems with more degrees of freedom: first by Epstein to separable systems [40] and later by Einstein to integrable systems [38]. A system with f degrees of freedom is integrable (in the sense of Liouville and Arnold [74, 4]) if there are f independent integrals of motion in involution. The phase space of integrable systems foliates into invariant tori on which the quantization condition becomes

$$\oint_{C_j} \mathbf{p}\cdot d\mathbf{q} = 2\pi\hbar n, \tag{2.2}$$

where $\{C_1, ..., C_f\}$ is a basis of non-contractible loops on the torus.

[1] For more detailed history of the semiclassical quantization conditions, see Ref. [71], which is roughly followed here.

Wentzel [135], Kramers [72], Brillouin [17] and Jeffreys [67] showed that the old quantization conditions follow from the Schrödinger's equation in the short-wavelength limit, or now so-called WKB or JWKB approximation (that we discuss in Section 2.2). It was found that the integer n in Eq. (2.1) has to be corrected by a small number depending on the character of motion (e.g., one half for each oscillating degree of freedom). A full derivation of the semiclassical quantization conditions was completed by Keller [70] who incorporated both the shift of the quantum numbers and the integrability concept of Einstein, to find

$$\oint_{C_j} \mathbf{p}\cdot d\mathbf{q} = 2\pi\hbar\left(n + \mu_j/4\right). \tag{2.3}$$

This is now known as Einstein-Brillouin-Keller (EBK) or torus quantization.

Almost simultaneously with the derivation of the WKB approximation for the stationary solutions of the Schrödinger equation, Van Vleck [129] derived a semiclassical form of the quantum propagator, a quantity useful in quantum dynamics. Mathematically, the propagator is the kernel $K\left(\mathbf{q},\mathbf{q}';t\right)$ of the linear transformation that enables finding the wave function $\psi\left(\mathbf{q};t\right)$ at time t if we know the wave function $\psi\left(\mathbf{q}';0\right)$ at time 0:

$$\psi\left(\mathbf{q};t\right) = \int d\mathbf{q}\, K\left(\mathbf{q},\mathbf{q}';t\right)\, \psi\left(\mathbf{q}';0\right).$$

Van Vleck derived the short-wavelength approximation,

$$K_{sc}\left(\mathbf{q}'',\mathbf{q}';t\right) = (2\pi i\hbar)^{-f/2} \sum_j \left|\frac{\partial^2 S_j}{\partial\mathbf{q}''\partial\mathbf{q}'}\right|^{f/2} \exp\left[iS_j\left(\mathbf{q}'',\mathbf{q}';t\right)/\hbar - i\nu_j\pi/2\right], \tag{2.4}$$

in which $S_j\left(\mathbf{q}'',\mathbf{q}';t\right)$ denotes the action along the jth classical trajectory connecting $\mathbf{q}'$ with $\mathbf{q}''$ in time t,

$$S_j\left(\mathbf{q}'',\mathbf{q}';t\right) = \int dt\, L\left[\mathbf{q}_j\left(t\right), \dot{\mathbf{q}}_j\left(t\right); t\right]$$

and L is the Lagrangian. The phase $\nu_j\pi/2$ was not part of Van Vleck's original derivation: it was added later by Gutzwiller [47]. Without going into details, we note two properties of the Van Vleck-Gutzwiller propagator (2.4): first, it can be derived from the Feynman propagator [87, 94], if the integral over all trajectories (even those classically forbidden) is evaluated by the stationary-phase approximation: this process selects only the classically allowed trajectories. Second, the semiclassical propagator satisfies the "composition rule" satisfied by the exact quantum propagator,

$$K_{sc}\left(\mathbf{q}'',\mathbf{q}';t\right) = \int_{S.P.} d\mathbf{q}\, K_{sc}\left(\mathbf{q}'',\mathbf{q};t-t'\right)\, K_{sc}\left(\mathbf{q},\mathbf{q}';t'\right),$$

as long as the integral is evaluated by the method of stationary phase (S.P.). This method is an underlying feature of all of semiclassics: the final result is always the same, as long as all integrals used in its derivation are evaluated by the stationary phase approximation.

2.2 WKB approximation

Here we present a very quick review of the WKB approximation. For a more detailed physical presentation, see, e. g., Refs. [16, 2]. For a rigorous mathematical treatment, see, e.g., Refs. [36, 78]. The goal of the WKB approximation is to find the asymptotic solution to the time-independent Schrödinger equation,

$$\hat{H}\psi\left(\mathbf{q}\right) = E\psi\left(\mathbf{q}\right), \tag{2.5}$$

for $\hbar \to 0$. Here ψ is a square-integrable function and $\hat{H}$ is a Weyl operator with symbol

$$H\left(\mathbf{q},\mathbf{p}\right) = H_0\left(\mathbf{q},\mathbf{p}\right) + \hbar H_1\left(\mathbf{q},\mathbf{p}\right) + O\left(\hbar^2\right).$$

For simplicity we assume that $H_1\left(\mathbf{q},\mathbf{p}\right) = 0$ and that

$$H_0\left(\mathbf{q},\mathbf{p}\right) = \mathbf{p}^2/2m + V\left(\mathbf{q}\right).$$

We look for a solution of Eq. (2.5) in the form

$$\psi_{WKB}\left(\mathbf{q}\right) = \sum_{j=0}^{\infty} \hbar^j \, a_j\left(\mathbf{q}\right) \, \exp\left[\frac{i}{\hbar} S\left(\mathbf{q}\right)\right]. \tag{2.6}$$

Substituting the ansatz (2.6) into Eq. (2.5) and requiring that equality holds for each power of $\hbar$ in the resulting asymptotic expansion, we get the condition

$$H\left(\nabla S, \mathbf{q}\right) = E, \tag{2.7}$$

and a sequence of transport equations,

$$\begin{aligned} &\left(\nabla S \cdot \nabla + \frac{1}{2}\Delta S\right) a_0 = 0, \\ &\left(\nabla S \cdot \nabla + \frac{1}{2}\Delta S\right) a_j = \frac{i}{2}\Delta a_{j-1}, \;\; for \;\; j \geq 1. \end{aligned} \tag{2.8}$$

Eq. (2.7) can be immediately recognized as the Hamilton-Jacobi equation of classical mechanics. Most of the time, we are only interested in the leading order term a_0, which requires the solution of only the first of the transport equations (2.8).

2.3 Standard uniformization: The Airy function

The paradigm example of a uniform method is the *Airy uniformization*, most often used to correct the WKB wave function near a potential turning point. We discuss the simplest example, for which the uniform wave function turns out to be exact: we look for the stationary wave function for a linear ramp potential in one dimension,

$$V(q) = -\beta q \tag{2.9}$$

For this potential, the Schrödinger equation (2.5) becomes

$$-\frac{\hbar^2}{2m}\psi_E''(q) - (\beta q + E)\psi_E(q) = 0 \tag{2.10}$$

After the shift $\psi_E(q) = \psi_0(q + E/\beta)$ and change of variables

$$u = \frac{m^{1/3}\beta^{1/3}}{\hbar^{2/3}} q \equiv \gamma q,$$
$$\Psi(u) = \psi_0(q),$$

the Schrödinger equation reads

$$\frac{1}{2}\Psi''(u) + u\Psi(u) = 0. \tag{2.11}$$

Eq. (2.11) can be exactly solved in the momentum representation where it becomes

$$\left(\frac{1}{2}p^2 - i\frac{\partial}{\partial p}\right)\Phi(p) = 0. \tag{2.12}$$

Up to normalization, this equation is satisfied by the momentum wave function

$$\Phi(p) = e^{-ip^3/6} \tag{2.13}$$

It turns out that for the linear potential, applying the WKB method in the momentum representation gives the same result (2.13), $\Phi_{\rm WKB}(p) = \Phi_{\rm exact}(p)$. The Airy uniformization procedure works more generally, as long as there are no caustics in the momentum representation and we have at least an approximate equality $\Phi_{\rm WKB}(p) \approx \Phi_{\rm exact}(p)$. The position wave function is obtained via the Fourier transform,

$$\Psi(u) = \frac{1}{\sqrt{2\pi}}\int_{-\infty}^{\infty} e^{ipu}\Phi(p)\ dp \approx \frac{1}{\sqrt{2\pi}}\int_{-\infty}^{\infty} e^{ipu}\Phi_{\rm WKB}(p)\ dp$$
$$= \frac{2}{\sqrt{2\pi}}\int_{0}^{\infty} \cos(p^3/6 - pu)\ dp \tag{2.14}$$

If the Fourier transform (2.14) is evaluated by the stationary-phase approximation, we obtain the standard WKB wave function

$$\begin{aligned}\Psi_{\rm WKB}(u) &\sim \left(i\sqrt{2u}\right)^{-1/2} \exp\left[-i(\sqrt{2u})^3/6 + i\sqrt{2u}\ u\right] + \text{c.c.} \\ &\sim \frac{2^{3/4}}{u^{1/4}} \cos\left(\frac{2^{3/2}}{3}u^{3/2} - \frac{\pi}{4}\right)\end{aligned} \tag{2.15}$$

Noting that $\int^u p(u')\ du' = (2u)^{3/2}/3$ we get the more familiar WKB form

$$\Psi_{\rm WKB}(u) \sim \frac{2}{\sqrt{p(u)}} \cos\left(\int^u p(u')\ du' - \frac{\pi}{4}\right). \tag{2.16}$$

Figure 2.1 displays the semiclassical position wave function $\psi_{E,\ \rm WKB}(q) = \langle q|E\rangle_{\rm WKB}$, which

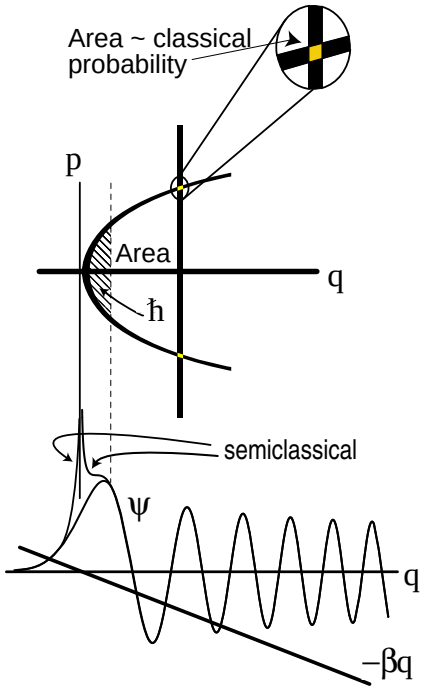

Figure 2.1: Diagram showing the areas in phase space important to the semiclassical approximation to the Airy function.

becomes inaccurate when the area enclosed by the vertical line ($q = const.$) and the energy contour corresponding to the state $|E\rangle$ falls below Planck's constant. Upon entering the highlighted "problematic" region, the original momentum integral (2.14) may be substituted

for the position WKB result (2.16), giving a uniformization,

$$\Psi_{\rm unif}(u) = \frac{1}{\sqrt{2\pi}} \int\limits_{-\infty}^{\infty} e^{ip\ u} \Phi_{\rm WKB}(p)\ dp = 2^{5/6}\pi^{1/2} {\rm Ai}\left(-2^{1/3}u\right),$$

$$\psi_{\rm unif}(q) \propto {\rm Ai}(-2^{1/3}\gamma q) = {\rm Ai}\left[-\left(\frac{2m\beta}{\hbar^2}\right)^{1/3} q\right]. \tag{2.17}$$

Of course in this case we know that the result of the integral is an Airy function, but in general there may be integrals which are not known analytically or even close to those that are known. Moreover, for the linear potential we have an exact equality $\psi_{\rm unif}(q) = \psi_{\rm exact}(q)$ since the momentum WKB wave function is exact, $\Phi_{\rm WKB}(p) = \Phi_{\rm exact}(p)$.

To summarize, Airy uniformization is based on two steps, which characterize almost every other uniform method: first we find a representation in which the WKB wave function is accurate, then we transform into the required representation exactly instead of using the stationary-phase approximation.

In this thesis we encounter more complex situations for which Airy uniformization is not a sufficient tool. Examples include singularities induced by nonlinear interactions, including chaos (Section 3.4, Chapter 4, Chapter 5), reflection from corrugated surfaces (Section 3.6), disordered one-dimensional systems (Chapter 6), etc.

2.4 Initial value representation

Another successful uniform method is the *initial value representation* introduced by Miller in Ref. [83]. In this section we describe at least its basic version since various uniform approximations developed in this thesis are closely related to this method. The initial value representation has greatly evolved since its original form and this evolution has recently been summarized in a review article [84].

Here we follow the presentation of this article and show how to apply the method to a generic matrix element of the semiclassical evolution operator. This matrix element is the probability amplitude for a transition from state $\mathbf{n}_1$ at time zero to state $\mathbf{n}_2$ in time t,

$$K_{\mathbf{n}_2,\mathbf{n}_1}(t) = \left\langle \psi_{\mathbf{n}_2} \left| e^{-iHt/\hbar} \right| \psi_{\mathbf{n}_1} \right\rangle = \int d\mathbf{q}'' \int d\mathbf{q}' \psi^*_{\mathbf{n}_2}(\mathbf{q}'') \left\langle \mathbf{q}'' \left| e^{-iHt/\hbar} \right| \mathbf{q}' \right\rangle \psi_{\mathbf{n}_1}(\mathbf{q}'), \tag{2.18}$$

where the exact propagator in the coordinate representation is replaced by the semiclassical

Van Vleck propagator (2.4),

$$K_{sc}\left(\mathbf{q}'',\mathbf{q}';t\right)=\left\langle \mathbf{q}''\left|e^{-iHt/\hbar}\right|\mathbf{q}'\right\rangle_{sc}$$
$$=(2\pi i\hbar)^{-f/2}\sum_{j}\left|\det\frac{\partial^{2}S_{j}}{\partial\mathbf{q}''\partial\mathbf{q}'}\right|^{f/2}\exp\left[iS_{j}\left(\mathbf{q}'',\mathbf{q}';t\right)/\hbar-i\nu_{j}\pi/2\right].$$

As written above, the matrix element is difficult to implement numerically: one needs to solve a nonlinear boundary value problem in order to find all classical trajectories that connect the initial point $\mathbf{q}'$ with the final point $\mathbf{q}''$ in time t. Moreover, there are caustic singularities in the Van Vleck propagator whenever the Van Vleck determinant $\det\frac{\partial^{2}S_{j}}{\partial\mathbf{q}''\partial\mathbf{q}'}$ becomes singular.

The initial-value-representation "trick" is based on realization that the Van Vleck determinant is nothing else but the Jacobian of the transformation from the final position to the initial momentum,

$$\det\frac{\partial^{2}S_{j}}{\partial\mathbf{q}''\partial\mathbf{q}'}=\det\left(-\frac{\partial\mathbf{p}'_{j}}{\partial\mathbf{q}''}\right). \tag{2.19}$$

If we change the integration variable in (2.18) from the final position $\mathbf{q}''$ to the initial momentum $\mathbf{p}'$, we obtain a simpler expression

$$K^{IVR}_{\mathbf{n}_2,\mathbf{n}_1}(t)=(2\pi i\hbar)^{-f/2}\int d\mathbf{p}'\int d\mathbf{q}'\left|\det\left(\frac{\partial\mathbf{q}_t\left(\mathbf{q}',\mathbf{p}'\right)}{\partial\mathbf{p}'}\right)\right| \tag{2.20}$$
$$\times\exp\left[iS\left(\mathbf{q}',\mathbf{p}';t\right)/\hbar-i\nu\pi/2\right]\psi^{*}_{\mathbf{n}_2}\left(\mathbf{q}_t\right)\psi_{\mathbf{n}_1}\left(\mathbf{q}'\right).$$

This is the initial value representation of the matrix element (2.18). The nonlinear boundary-value problem has been replaced by an initial value problem, which is much simpler since for each initial position and momentum, there is only one classical trajectory. Moreover the singularities of the Van Vleck determinant (2.19) have been replaced by zeroes of its inverse.

The initial value representation (2.20) can describe classically forbidden processes such as barrier or dynamical tunneling [35], using real-valued trajectories. It also makes it possible to treat systems with many degrees of freedom since the integrals in the initial value representation are much easier to treat by various Monte Carlo methods.

2.5 Other semiclassical propagation and uniform methods

Without going into much detail, let us at least mention several other semiclassical propagation and uniform methods.

As far as semiclassical dynamics is concerned, there exist many techniques besides the Van Vleck propagator (2.4) and the initial value representation of Section 2.4. In particular, there are many *Gaussian wavepacket propagation* methods. Depending on whether the Gaussians are fixed or not, we can distinguish between so-called *frozen* [54] and *thawed* [52, 53] *Gaussian methods*. Herman and Kluk combined the initial value representation with the frozen Gaussian approximation to obtain a coherent-state version of the semiclassical propagator [59]. Another method, so-called *Gaussian spawning* was developed by Martinez *et al.* [79, 80]. Although they are very efficient, most Gaussian wavepacket methods have one common undesirable feature: they all rely on an *ad hoc* choice of the Gaussians. An exception is the replacement-manifold method which (when applied to the coherent branched flow in Chapter 4) turns out to "spawn" uniquely defined Gaussian wavepackets.

Besides the *Airy uniform method* of Section 2.3 which is useful for a fold singularity, there are similar methods for all classes of singularities from the *catastrophe theory* [118, 4]. The second simplest class is the cusp singularity, for which there is a uniform method based on *Pearcy's integral* [97, 29]. We shall find an alternative cusp uniformization based on replacement manifolds in Chapter 4. From various other uniform methods useful in molecular dynamics calculations let us mention the *Bessel* [116] and *Laguerre* [22] *uniform approximations*. Bessel uniformization appears whenever the quantity of interest can be expressed as an overlap of semiclassical eigenstates associated with an integrable Hamiltonian H and a slightly perturbed Hamiltonian H^V. If the perturbation is classically small, perturbed torus action can be written in terms of the unperturbed *action-angle variables*[2] as

$$\mathbf{I}^V(\theta,\,\mathbf{I}) \approx \mathbf{I} + \sum_{\mathbf{n}\in\mathbb{Z}^f} \left(a_{\mathbf{n}} \cos \mathbf{n}\cdot\theta + b_{\mathbf{n}} \sin \mathbf{n}\cdot\theta\right). \tag{2.21}$$

Quantum overlap amplitude of the two states is approximately given by

$$O \approx (2\pi)^{-f} \int d\theta \, \exp\left[\frac{i}{h}(\mathbf{I}_V - \mathbf{I})\right]. \tag{2.22}$$

If the perturbation is large quantum mechanically, i.e., the change of action is large compared to Planck's cell, overlap integral (2.22) can be evaluated semiclassically, by the stationary phase approximation. In the opposite case, integral (2.22) must be evaluated exactly. In case that there is only one non-zero harmonic term (say $a_{\mathbf{n}_0}$) in the series in Eq. (2.21),

[2] See, e.g. Ref. [4].

integral (2.22) can be found analytically, giving the Bessel uniform result

$$O \approx J_0(a_{\mathbf{n}_0}/h).$$

2.6 Periodic orbit theory and quantum chaos

Phase space of classically chaotic systems does not foliate into tori as it does for integrable systems. As a result, quantization of chaotic systems is much more difficult. While semiclassical quantization of the hydrogen atom was done before the discovery of the Schrödinger equation, helium, the second simplest atom of the periodic table, resisted semiclassical quantization until 1990s [137]. Although Schrödinger's equation is linear and therefore does not allow chaos as Newton's equations do, it appears reasonable that classically chaotic dynamics should reflect itself in the quantum spectrum and wave functions. In particular, this should be the case in the semiclassical limit when Planck's constant is small compared to the characteristic phase space structures. The study of imprints of classical chaos in quantum mechanics has given rise to a whole new field of physics and mathematics: *quantum chaos*.

In chaotic systems, the EBK quantization of Section 2.1 is replaced by the *periodic orbit theory*, developed by Gutzwiller [48].[3] The so-called *Gutzwiller trace formula* expresses the oscillatory part of the level density in terms of a sum over periodic orbits of the classical system. While the original formulation was only valid for isolated orbits, it was extended in the work of Strutinsky [117], Berry and Tabor [12] to degenerate orbits. If there are no real degenerate orbits, but the system is near a bifurcation, the accuracy of the trace formula can be improved by including so-called *ghost orbits* (complex orbits that become real only after the bifurcation) [73, 75].

Completely different approach to the study of quantum properties of classically chaotic systems comes from the point of view of *Bohigas-Giannoni-Schmit conjecture* [13] which states that statistical properties of quantum spectra of classically chaotic systems are governed by the *random matrix theory* [81]. The most direct consequence is on the distribution of spacings between adjacent energy levels: while for integrable system this distribution is *Poisson*,

$$P(s) \approx \exp(-s), \tag{2.23}$$

[3] For more detailed derivation and discussion, see, e.g., Refs. [49, 16].

for chaotic systems it closely follows *Wigner's surmise*,

$$P(s) \approx \frac{\pi}{2} s \exp(-\pi s^2/4), \tag{2.24}$$

(s is the adjacent energy spacing in units of the mean level spacing Δ). In practice, there are deviations from the random matrix theory, the most important being due to *scars* in the eigenstates near the least unstable periodic orbits [55, 69]. In this thesis, random matrix theory is used only in Chapter 5 and there only for the purpose of comparison with our uniform result.

2.7 Applications of semiclassical theory and experimental manifestations of quantum chaos

While semiclassical theory is a beautiful theory that poses many interesting mathematical questions, its utility lies especially in applications to experiment. Besides successfully explaining the hydrogen spectrum (using the torus quantization), and at least some features of the helium spectrum (using the periodic orbit theory), it is particularly useful in describing molecular dynamics.

Various semiclassical methods can successfully describe Raman scattering, photodissociation, molecular collisions, rotation-vibration spectra, etc. For review of applications in molecular dynamics, see, e.g., monographs [21, 109] and references therein. The main reason for the success of semiclassical approximation in molecular processes is the applicability of the *Born-Oppenheimer approximation* in which the dynamics of nuclei is separated from the dynamics of electrons.

A paradigm system for the exploration of quantum chaos is the *Rydberg atom*[4] in a uniform magnetic field [43, 51].[5] Classical chaotic dynamic reflects itself in *quasi-Landau resonances* in atomic photoabsorption [46]. Experimental realization of the *standard map* (also known as the *kicked rotor*) of Section 5.6.1 has been accomplished by Raizen *et al.* [104, 86] using ultracold sodium atoms in a near-resonant periodic standing wave of light. Until these experiments, which even demonstrated the *dynamical localization effect*, the standard map had been used as a theoretical tool only. Validity of the semiclassical

[4] I.e., a highly excited hydrogen atom.

[5] Due to a scaling property, the same chaotic dynamics can be achieved for an atom in a low-lying excited state but in a strong magnetic field.

approximation of the atomic interaction with a laser standing wave has been analyzed by Vaníček *et al.* in the setting of atomic lithography [128]. While the approximation is fairly accurate, it obviously cannot account for such quantum effects as spontaneous decay and Landau-Zener transitions which can be important [93].

Semiclassical methods have also been quite successful in explaining transport properties of electrons in mesoscopic systems. Examples include experiments measuring electron transport through a tunneling diode in crossed electric and magnetic fields [136, 89, 88], magnetoresistance in a two-dimensional antidot array of scatterers [134, 133, 132], or conductance fluctuations in quantum dots [77, 76]. By using quantum dots in the shape of a stadium billiard and a circle, Marcus *et al.* [77, 76] were able to compare transport properties of classically chaotic and integrable systems. Again, some effects, such as the spin-orbit coupling, must be treated quantum-mechanically [50].

Chapter 3

Replacement manifolds: A method to uniformize semiclassical wave functions

In this chapter, we present a new semiclassical technique which relies on replacing complicated classical manifold structure with a series of simpler manifolds, which are then evaluated by the usual semiclassical rules. Under circumstances where the original manifolds give poor or useless results semiclassically, the replacement manifolds can yield remarkably accurate wave functions. We give several working examples to illustrate the theory presented here.

3.1 Introduction

Semiclassical methods are based on classical mechanics; the relevant classical manifolds form the "skeleton" to which the wave function is attached. However, associating a semiclassical wave function with a Lagrangian manifold is problematic when the manifold has structure within a phase space volume $\hbar^f$ (f is the number of degrees of freedom). In one dimension, where the Lagrangian manifold is just a curve in the two-dimensional phase space, these problems occur when the Lagrangian curve forms loops with areas smaller than $\hbar$. If that happens, typically two or more stationary phase points corresponding to distinct contributions to the semiclassical wave function are not well separated in phase.

Consequently, the stationary phase method, on which the standard semiclassical (WKB) approximation of Section 2.2 is based, breaks down. Worse, in some important situations, such as in the case of the universal homoclinic oscillations associated with chaotic regions of phase space, the problematic loops may be repeated infinitely many times in a small region.[1]

While the semiclassical wave function diverges in caustic regions lurking near the small area loops, the exact quantum wave function is of course well-behaved. This is one manifestation of how quantum mechanics smoothes over classical detail. In the following sections, we shall quantify how this smoothing occurs. We suggest and test a new way of looking at the smoothing process in terms of "replacement manifolds", in which new, well behaved classical manifolds are substituted for the original badly behaved ones. One application of this approach is uniformizing a semiclassical wave function in the vicinity of the ubiquitous homoclinic oscillations of a chaotic system.

It is widely understood that very small changes in potentials or walls of billiards can have little effect on quantum eigenstates, but can drastically affect the classical manifold structure. This immediately implies a many-to-one relationship between the classical manifolds and quantum wave functions. That is, many different underlying classical manifold patterns correspond to the same wave function. Now, whatever the choice of manifold (amongst these equivalent forms) we can suppose an appropriate uniformization exists which gives the correct wave function. However, the non-uniform, simple semiclassical limit for the various choices of manifolds can differ drastically in accuracy. It is this fact which we exploit in this chapter.

3.2 Replacement manifolds

Let us consider Lagrangian manifold defined by a position-momentum relation

$$P(Q) = p - \frac{3}{2}\,\hbar\epsilon\alpha Q^2 \sin \alpha Q^3 \tag{3.1}$$

(use of capital letters will become clear in the next section). This model was first introduced in Ref. [57] but was not fully explored there. The function (3.1) has oscillations of

[1] Somewhat surprisingly, softly chaotic systems resist semiclassical treatment often more than those with strongly chaotic behavior. It is because loop areas in phase space increase as chaos grows stronger. For semiclassical analysis of a strongly chaotic system see, e.g., Refs. [120, 91]. For semiclassical analysis of a mixed system (with weak chaos) see, e.g., Ref. [110].

increasing amplitude and frequency, which however have the same area $\int P(Q)dQ = \epsilon\hbar$ between successive zeros (see Fig. 3.1, small value of ϵ corresponds to small area of loops). This is also a characteristic property of homoclinic oscillations near a periodic orbit. The momentum $P(Q)$ spans an ever larger range as Q increases, but we now show that for $\epsilon < 1$ the manifold's semiclassical behavior can be understood by replacing it by three smooth manifolds. The rules for replacement are simple to derive.

The action function $S(Q)$ is the integral of $P(Q)$:

$$S(Q) = \int_0^Q P(Q')\, dQ' = pQ + \frac{1}{2}\,\hbar\epsilon\left(\cos\alpha Q^3 - 1\right). \tag{3.2}$$

The "wave function"

$$\psi(Q) = A(Q)\, e^{iS(Q)/\hbar} \tag{3.3}$$

can be approximated by

$$\psi(Q) \approx A(Q)\, e^{-i\epsilon/2} e^{ipQ/\hbar}\left(1 + i\frac{\epsilon}{2}\cos(\alpha Q^3)\right) \tag{3.4}$$

$$\psi(Q) \approx A(Q)\, e^{-i\epsilon/2} e^{ipQ/\hbar}\left(1 + i\frac{\epsilon}{4}e^{i\alpha Q^3} + i\frac{\epsilon}{4}e^{-i\alpha Q^3}\right) \tag{3.5}$$

if $\epsilon < 1$. For small ϵ this expression is nearly identical with (3.3) with the original action (3.2), because $\cos(\alpha Q^3)$ is bounded by ± 1. However semiclassically it has the interpretation of the sum of three smooth classical manifolds, i.e., $P = p$, $P = p + 3\,\hbar\alpha Q^2$ and $P = p - 3\,\hbar\alpha Q^2$. They have the weights $e^{-i\epsilon/2}A(Q)$, $i\frac{\epsilon}{4}e^{-i\epsilon/2}A(Q)$, $i\frac{\epsilon}{4}e^{-i\epsilon/2}A(Q)$, respectively. The situation is depicted in Fig. 3.2.

Almost every discussion of the relation of classical and quantum mechanics for chaotic systems alludes to quantum smoothing, but here we can see explicitly how this smoothing comes about. For all reasonable purposes the three smooth classical manifolds accurately replace the rapid oscillations of the original manifold. Note too that depending on the parameters the outlying manifolds $P = p + 3\,\hbar\alpha Q^2$, and $P = p - 3\,\hbar\alpha Q^2$ lie far from the original Lagrangian manifold (3.1). We shall discuss interesting consequences of this in the next section. Here let us just note that in this case the outlying manifolds give an exponentially suppressed contributions (as if due to tunneling).

So far, we have considered the wave function only in position representation where caustics are absent and the semiclassical form (3.3) was accurate. The situation is very different in momentum space. In order to find the wave function in momentum representation, we have to sum over all contributions from intersections of a horizontal line (corresponding

to a momentum eigenstate) with the oscillating manifold (3.1). When $\epsilon < 1$, the adjacent intersections will be separated by a phase $\Delta S \,/\, \hbar$ that is smaller than 1 for any classically allowed momentum, and therefore the standard semiclassical approximation will break down for *all classical momenta*! Usual Airy-type uniformization methods of Section 2.3 (also see Refs. [18, 9]) do not serve under these circumstances, because the manifold is completely covered with caustics (see the filled-in areas ΔS_1 and ΔS_2 in Fig. 3.1). Apparently, we have no other choice but to part with semiclassical method and use a numerical Fourier transform over the position wave function to obtain $\phi(P)$. However, using replacement manifolds is a much simpler and more intuitive approach which can rescue the situation. To find the

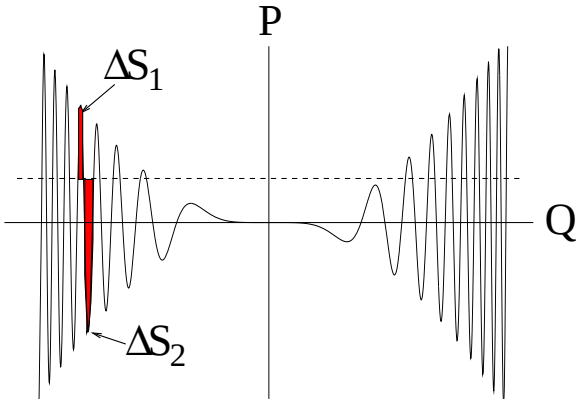

Figure 3.1: Areas in phase space important to momentum wave function associated with the manifold $P(Q) = p - \frac{3}{2}\hbar\alpha\epsilon Q^2 \sin(\alpha Q^3)$, $\epsilon = 0.5$. Primitive semiclassical approximation fails since both areas ΔS_1 and ΔS_2 can be smaller than $\hbar$.

momentum wave function $\phi(P)$ associated with the original manifold, we add (with appropriate weights) wave functions $\phi_n(P)$ corresponding to the three replacement manifolds. Each of these partial wave functions is equal to a Fourier transform of a corresponding position wave function $\psi_n(Q)$,

$$\phi_n(P) = \frac{1}{\sqrt{2\pi\hbar}} \int dQ\, \psi_n(Q)\, e^{-iPQ/\hbar}. \tag{3.6}$$

Except for a small region close to $P = p$ (highlighted in Fig. 3.2), this integral can be evaluated by the stationary phase method! In other words, although the semiclassical approximation completely fails for the original manifold, it works almost everywhere for the replacement manifolds. Moreover, the standard Airy uniformization procedure of Section 2.3 can be exploited to correct the only remaining inaccuracy in a narrow region near $P = p$. In the next section we will see that the momentum wave function found by applying

the stationary phase approximation to replacement manifolds is in excellent agreement with numerical solution.

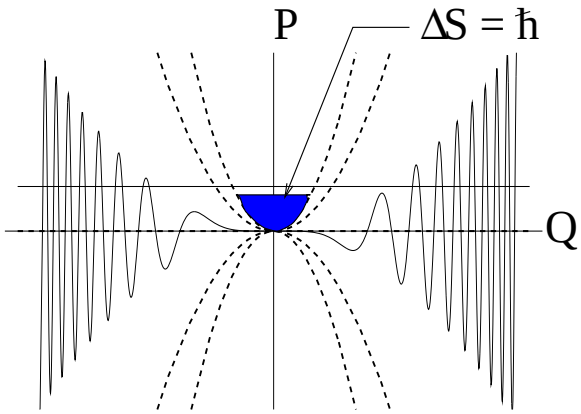

Figure 3.2: Original (solid line) and replacement manifolds (dashed lines) for $P(Q) = p - \frac{3}{2}\hbar\alpha\epsilon Q^2 \sin(\alpha Q^3)$, $\epsilon = 0.5$.

3.3 Uniformization with replacement manifolds in a generalized model

In order to capture other properties of homoclinic oscillations in our model, we consider a generalized manifold

$$P(Q) = p - \frac{1}{2}\hbar\epsilon \frac{d\xi(Q)}{dQ} \sin \xi(Q), \tag{3.7}$$

in which αQ^3 from (3.1) is replaced by a generic smooth function $\xi(Q)$. The presence of the derivative $\frac{d\xi(Q)}{dQ}$ ensures equal loop areas between successive zeros of $\xi(Q)$. Example of a manifold with $\xi(Q) = \alpha \log \frac{Q}{a}$ is displayed in Fig. 3.4. Manifold (3.7) can be obtained from a horizontal manifold representing a momentum state $|p\rangle$ by a canonical transformation of coordinates[2]

$$Q = q,\ P = p - \frac{1}{2}\hbar\epsilon \frac{d\xi}{dq} \sin \xi(q), \tag{3.8}$$

generated by the function

$$F_3(p, Q) = -pQ - \frac{1}{2}\hbar\epsilon \cos \xi(Q), \tag{3.9}$$

[2]We keep the discussion in terms of general canonical transformations although we often have in mind the semiclassical Van Vleck propagator when speaking of transformation elements.

Instead of looking for $\psi(Q)$ with a general prefactor $A(Q)$, we find the uniform semiclassical transformation element $\langle P|p\rangle$, and thereby fix the amplitude prefactor to be $A(Q) = (2\pi\hbar)^{-1/2}$; this retains all the problematic features of the manifold. We solve the problem to all orders in ϵ by replacing the original manifold with an infinite series of replacement manifolds. First we note that the semiclassical transformation element

$$\langle Q|p\rangle_{sc} = \frac{1}{\sqrt{2\pi\hbar}}\, e^{-iF_3(p,Q)/\hbar} \tag{3.10}$$

is fairly accurate since there are no caustics in this representation (to each final Q corresponds a single initial q). The momentum-representation element is obtained by a Fourier transform,

$$\begin{aligned}\langle P|p\rangle &\simeq \frac{1}{\sqrt{2\pi\hbar}} \int dQ\, e^{-iPQ/\hbar}\, \langle Q|p\rangle_{sc} \\ &= \frac{1}{2\pi\hbar} \int dQ\, \exp\left\{\frac{i}{\hbar}\left[-PQ - F_3(p,Q)\right]\right\}.\end{aligned} \tag{3.11}$$

If evaluated by the stationary phase method, the integral yields a very poor semiclassical result since there exist many coalescing stationary phase points. An accurate uniform answer is obtained by evaluating integral (3.11) exactly. The accuracy is usually further improved by changing the integration variable from Q to q (in our case both forms are equivalent since $Q = q$). This uniform version of $\langle P|p\rangle$ can be further simplified by writing $\langle Q|p\rangle$ as a sum over replacement manifolds. Recognizing that the factor $e^{i\frac{\epsilon}{2}\cos\xi(Q)}$ in $\langle Q|p\rangle_{sc} = (2\pi\hbar)^{-1/2} \exp\left[ipQ/\hbar + i\frac{\epsilon}{2}\cos\xi(Q)\right]$ is a generating function for Bessel functions, we can extend the sum from previous section beyond the first order in ϵ. In fact we obtain an infinite sum convergent for any ϵ,

$$\begin{aligned}\langle Q|p\rangle &= \frac{1}{\sqrt{2\pi\hbar}} e^{ipQ/\hbar} \sum_{n=-\infty}^{\infty} J_n\left(\frac{\epsilon}{2}\right) i^n e^{in\xi(Q)} \\ &= \sum_{n=-\infty}^{\infty} J_n\left(\frac{\epsilon}{2}\right) i^n \langle Q|p\rangle_n\end{aligned} \tag{3.12}$$

where $\langle Q|p\rangle_n = (2\pi\hbar)^{-1/2} \exp\left\{i\left[pQ + n\hbar\xi(Q)\right]/\hbar\right\}$. We can rewrite (3.11) as

$$\begin{aligned}\langle P|p\rangle &= \sum_{n=-\infty}^{\infty} J_n\left(\frac{\epsilon}{2}\right) \frac{i^n}{\sqrt{2\pi\hbar}} \int dQ\, e^{-iPQ/\hbar}\, \langle Q|p\rangle_n \\ &= \sum_{n=-\infty}^{\infty} J_n\left(\frac{\epsilon}{2}\right) i^n \langle P|p\rangle_n\end{aligned} \tag{3.13}$$

where

$$\langle P|p\rangle_n = \frac{1}{2\pi\hbar}\int dQ\, \exp\left\{\frac{i}{\hbar}\left[(p-P)Q + n\hbar\xi(Q)\right]\right\} \tag{3.14}$$

may be identified semiclassically as a transformation element corresponding to the n-th replacement manifold

$$P_n(Q) = p + n\hbar\frac{d\xi(Q)}{dQ}, \tag{3.15}$$

Unlike the original manifold (3.7), the n-th replacement manifold (3.15) does not have caustics as long as the function $\xi(Q)$ is simple enough. Consequently, $\langle P|p\rangle_n$ can be evaluated by the stationary phase method. As promised, we have expressed the uniform version of $\langle P|p\rangle$ as a weighted sum over semiclassical replacement manifolds,

$$\langle P|p\rangle_{\rm unif} = \sum_{n=-\infty}^{\infty} J_n\left(\frac{\epsilon}{2}\right) i^n \langle P|p\rangle_{n,sc}.$$

If this transformation element is applied to a well-behaved (i.e., decaying fast enough at $\pm\infty$) function of p, the resulting sum converges for any ϵ. The replacement-manifold method is therefore not restricted to the regime where loop areas are smaller than $\hbar$. It also works in the strongly chaotic regime where $\epsilon > 1$ (and where the standard semiclassical approximation holds) if all manifolds up to $|n| \simeq \epsilon$ are included in the sum. This follows since $J_n(\epsilon/2)$ considered as a function of n decays exponentially fast for $|n| > \epsilon/2$. In other words, we only need to include several replacement manifolds beyond those intersecting the original manifold. Physically, the manifolds outside of the range of the original one lie in a classically forbidden region in which the wave function is exponentially suppressed.

In the opposite case ($\epsilon < 1$) which interests us the most, considering replacement manifolds up to $|n| = 1$ will suffice while the "primitive" semiclassical approximation fails completely even for $P = p$. In this regime ϵ can be thought of as a parameter defining the strength of the perturbation which causes the manifold to oscillate around a simple manifold that describes the system if perturbation is absent.

To complete our solution for a specific function $\xi(Q)$, we must evaluate $\langle P|p\rangle_n$. For $n = 0$, we cannot use the stationary phase approximation (because the action is linear), but integral (3.14) is trivial and we obtain in general

$$\langle P|p\rangle_0 = \delta(P-p). \tag{3.16}$$

For $n \neq 0$, the stationary phase method applied to (3.14) yields a result in the form of a

sum over stationary phase points Q_{sp},

$$\langle P|p\rangle_{n,sc} = \frac{1}{\sqrt{2\pi\hbar}} \sum_{Q=Q_{sp}} \left|\frac{\partial^2 f_n}{\partial Q^2}\right|^{-1/2} \exp\left[i\left(\frac{f_n}{\hbar} + \frac{\pi}{4}\,\mathrm{sgn}\,\frac{\partial^2 f_n}{\partial Q^2}\right)\right] \tag{3.17}$$

where $f_n(Q,P,p) = (p-P)\,Q + n\hbar\xi(Q)$ and $\frac{\partial f_n}{\partial Q} = 0$ for $Q = Q_{sp}$. For manifold (3.1), each replacement manifold $P_n(Q) = p + 3n\hbar\alpha Q^2$ has two stationary phase points

$$Q_{sp} = \pm\left(\frac{P-p}{3n\hbar\alpha}\right)^{1/2} \tag{3.18}$$

whose contributions add to give

$$\langle P|p\rangle_{n,sc} = \pi^{-1/2}[3\,n\hbar^3\alpha(P-p)]^{-1/4}\cos\left[\frac{2}{(n\alpha)^{1/2}}\left(\frac{P-p}{3\hbar}\right)^{3/2} - \frac{\pi}{4}\right]. \tag{3.19}$$

Replacement manifolds still contain one caustic at $P = p$, which can be easily uniformized by evaluating integral (3.14) exactly, as in Section 2.3,[3]

$$\langle P|p\rangle_{n,\mathrm{unif}} = \frac{1}{(3\,|n|\alpha)^{1/3}\hbar} Ai\left(-\frac{(\mathrm{sgn}\ n)(P-p)}{(3|n|\alpha)^{1/3}\hbar}\right).$$

Having found $\langle P|p\rangle_n$, we can calculate $\langle P|p\rangle$ from (3.13) to all orders in ϵ. $\langle P|p\rangle_{1,sc}$ and $\langle P|p\rangle_{1,\mathrm{unif}}$ agree very well except for a small region near p (similarly as in Fig. 2.1). Fig. 3.3 demonstrates the excellent agreement of the replacement manifold method with the direct numerical computation of $\langle P|p\rangle$ using the fast Fourier transform.

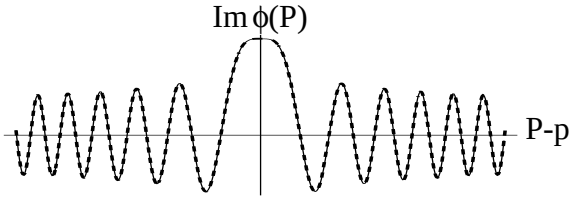

Figure 3.3: Momentum wave function: comparison of numerical initial value representation (solid line) with the replacement-manifold sum up to $|n| = 1$ (O(ϵ), dashed line) for original manifold with $\xi(Q) = \alpha Q^3$, $\epsilon = 0.5$ and $\alpha = 1$.

Here the replacement-manifold approach should be compared to the semiclassical perturbation approximation of Miller and Smith [85, 61] who used a perturbative approach to classical dynamics to calculate the semiclassical S matrix. They first applied this method

[3]Even if the integral is not analytic, an Airy-function uniformization procedure can be used. See, e.g., Refs. [18, 9].

to the collinear collision of an atom with a diatomic molecule [85]. The starting point is the initial value representation of the classical scattering matrix,

$$S_{n_f,n_i} = \frac{1}{2\pi}\int_0^{2\pi} dq_i \left[\frac{\partial q_f(q_i,n_i)}{\partial q_i}\right]^{1/2} \times \exp\left(i\left\{\Phi(q_i,n_i) + q_f(q_i,n_i)\left[n_f(q_i,n_i) - n_f\right]\right\}\right) \tag{3.20}$$

where $\hbar = 1$, n_i, n_f, q_i, q_f denote, respectively, the initial and final values of the action and angle variables describing the internal degree of freedom, and Φ is the action integral. For details, see Refs. [83] and [85]. If the classical quantities listed above are calculated using the first-order perturbation dynamics, the S matrix takes the form

$$S_{n_f,n_i} = \frac{e^{i\Phi_0}}{2\pi}\int_0^{2\pi} dq_i \exp\left\{-i\left[(n_f - n_i)\,q_i + A(q_i,n_i)\right]\right\}$$

where Φ_0 is twice the phase-shift for the unperturbed potential and $A(q_i,n_i)$ is the time integral of the perturbation potential along the unperturbed trajectory [85]. For various physical systems (such as ion-dipole collisions [85] or atom-surface scattering [61]), $A(q_i,n_i)$ has a sinusoidal dependence on q_i as long as perturbation remains small. In this regime we expect the semiclassical perturbation approximation and the replacement-manifold approximation to give the same answer. We shall verify that for the scattering by a corrugated wall in Section 3.6. The semiclassical perturbation approximation of Miller and Smith presently appears to be more widely applicable since it does not require any special property of the manifold. On the other hand, advantage of the replacement-manifold method lies in the fact that it is not subjected to the smallness of perturbation. Provided that the *full* action falls into one of the classes discussed above, we can apply the replacement-manifold method without approximating classical dynamics.

3.4 Model of homoclinic oscillations

Homoclinic oscillations in chaotic systems have another characteristic property besides having a constant area of loops that we required from the generalized model (3.7) in the previous section: the amplitude of homoclinic oscillations (i.e., "height" of loops) increases exponentially as we approach an unstable periodic orbit (see Fig. 3.4). To keep area of loops constant, the width of loops has to decrease accordingly. For bounded systems, the exponentially growing loops must eventually twist in a complicated manner in order to

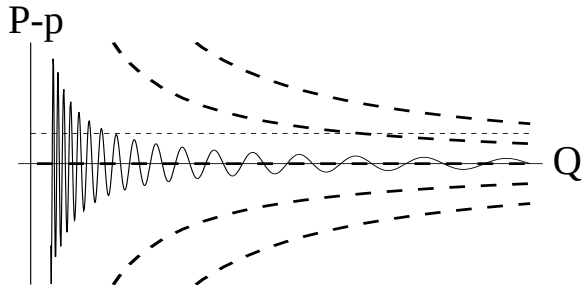

Figure 3.4: Original (solid line) and replacement manifolds (dashed lines) for $\xi(Q) = \alpha \log \frac{Q}{a}$, $\epsilon = 0.5$.

fit into available phase space. For sake of simplicity, we consider a model that satisfies the requirement of exponential growth, but is unbounded. Such a model can be found among generalized manifolds of previous section. Specifically, we want to find a manifold whose homoclinic points (i.e., intersections with line $P = p$ in our case) form a geometric series,

$$Q_n = a\, e^{n\lambda} \tag{3.21}$$

where λ is the Lyapunov exponent. In other words, we are looking for a function $\xi(Q)$ such that $\xi(Q_n) = 2\pi n$. The logarithmic function comes to mind first since $\log \frac{Q_n}{a} = n\lambda$. With the correct prefactor $\alpha = \frac{2\pi}{\lambda}$, we find the desired function

$$\xi(Q) = \alpha \log \frac{Q}{a} \tag{3.22}$$

because $\xi(Q_n) = \alpha \log \frac{Q_n}{a} = \frac{2\pi}{\lambda} n\lambda = 2\pi n$. Substituting $\xi(Q)$ from (3.22) into the general form (3.7), we obtain a manifold described by the relation

$$P(Q) = p - \frac{1}{2} \frac{\hbar \epsilon \alpha}{Q} \cos(\alpha \log \frac{Q}{a}) \tag{3.23}$$

and displayed in Fig. 3.4. Replacement manifolds (3.15) become

$$P_n(Q) = p + \frac{n\hbar\alpha}{Q}. \tag{3.24}$$

In the present case, function f_n from (3.17) becomes

$$f_n(Q, P, p) = (p - P)Q + n\hbar\alpha \log \frac{Q}{a},$$

and its single stationary phase point,

$$Q_{sp} = \frac{n\hbar\alpha}{P - p}. \tag{3.25}$$

For $P > p$, only manifolds with $n > 0$ contribute, and for $P < p$ only $n < 0$ is allowed. Defining $j = |n|$, for $P \neq p$ we replace the sum over n by sum over all positive j. In both cases, the j-th manifold gives a semiclassical contribution

$$\langle P|p\rangle_{j,sc} = \left(\frac{j\alpha}{2\pi}\right)^{1/2} \frac{1}{|P-p|} \exp\left\{ i \ \mathrm{sgn}(P-p) \left[j\alpha \log \frac{j\hbar\alpha}{ae|P-p|} - \frac{\pi}{4} \right] \right\} \tag{3.26}$$

with $j = |n| > 0$. In this case caustics are missing because there is a single stationary phase point Q_{sp}. We have a finite integration limit at zero, but it is separated from Q_{sp} by an infinite action (equal to the area delimited by lines $Q = 0$, $P = p$, and the n-th replacement manifold, see Fig. 3.4). In fact, it can be shown that further terms in the asymptotic expansion of $\langle P|p\rangle_{j,sc}$ have the same dependence on $\hbar$ and $P-p$ as (3.26), and only differ in their dependence on $j\alpha$. Luckily, these claims can be easily verified by analytical evaluation of integral (3.14) for $\xi(Q)$ given by Eq. (3.22), which is done in Appendix A.

In Fig. 3.5, the replacement-manifold expansion of $\langle P|p\rangle$ is applied to an initial Gaussian wave packet centered around q_0, p_0, namely

$$\phi^i(p) = \left(\frac{\sigma^2}{\pi\hbar^2}\right)^{1/4} \exp\left[\frac{i}{\hbar}(p_0 - p)q_0 - \frac{\sigma^2(p-p_0)^2}{2\hbar^2} \right].$$

The final position wave function is

$$\psi^f_{sc}(Q) = (\pi\sigma^2)^{-1/4} \exp\left[-\frac{i}{\hbar} F_3(p_0, Q) - \frac{(Q-q_0)^2}{2\sigma^2} \right]$$

and the uniform momentum wave function,

$$\begin{aligned} \phi^f_{\mathrm{unif}}(P) &= J_0\left(\frac{\epsilon}{2}\right) \phi^i(P) \\ &\quad + \frac{(2\pi\hbar)^{1/2}}{(\pi\sigma^2)^{1/4}} \sum_{j=1}^{\infty} J_j\left(\frac{\epsilon}{2}\right) i^j \langle P|p_0\rangle_{j,sc} \exp\left[-\frac{(Q_{sp,j} - q_0)^2}{2\sigma^2} \right] \end{aligned} \tag{3.27}$$

with $Q_{sp,j} = j\hbar\alpha/|P - p_0|$ and $\langle P|p_0\rangle_{j,sc}$ given by (3.26).

The large oscillation near $P = p_0$ in Fig. 3.5 corresponds to the zeroth replacement manifold contribution $\phi^i(P)$, the smaller wavelet to the right corresponds to the remaining replacement manifolds. The figure confirms the excellent accord between the replacement-manifold method and the numerical initial-value-representation evaluation by the fast Fourier transform.[4] We have thus succeeded in uniformizing something with many of the properties of homoclinic oscillations near an unstable periodic orbit using replacement-manifold "technology."

[4]The small difference is the result of our neglecting the shift of the stationary phase points due to the finite extent of $\phi^i(p)$.

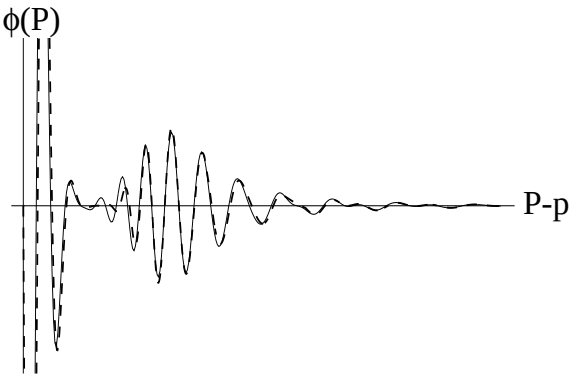

Figure 3.5: Momentum wave function: comparison of numerical initial value representation (solid line) with the replacement-manifold sum up to $j = 1$ ($O(\epsilon)$, dashed line) for original manifold with $\xi(Q) = \alpha \log\left(\frac{Q}{a}\right)$, $\epsilon = 0.5$ and $\alpha \approx 33$.

3.5 Comparison with the stationary phase method

It is instructive to check explicitly if the expansion in terms of replacement manifolds agrees with the stationary-phase method applied to the original manifold when areas of loops are larger than $\hbar$ ($\epsilon > 1$). Let us choose an analytically solvable example with $\xi(Q) = \alpha Q$. Corresponding manifold

$$P(Q) = p - \frac{1}{2}\,\hbar\epsilon\alpha \sin \alpha Q \tag{3.28}$$

has another advantage compared to manifolds in Figures 3.2 and 3.4. Unlike those, for $\epsilon \gg 1$ and small enough $P - p$, manifold (3.28) has all caustics in a safe distance. The replacement manifolds are horizontal lines $P_n = p + n\hbar\alpha$, independent of Q and corresponding transformation elements can be evaluated exactly as $\langle P|p\rangle_n = \delta(P - p - n\hbar\alpha)$. Using (3.13), the uniform expression for $\langle P|p\rangle$ is

$$\langle P|p\rangle_{\text{unif}} = \sum_{n=-\infty}^{\infty} J_n\left(\frac{\epsilon}{2}\right)\, i^n\, \delta(P - p - n\hbar\alpha), \tag{3.29}$$

so the wave function is determined by its Fourier coefficients $a_n(\epsilon) = J_n(\epsilon/2)\, i^n$, which is natural since manifold (3.28) is exactly periodic. Moreover, each replacement manifold contributes only to a single momentum (P_n). Put differently, we have calculated the wave function for any specific momentum to all orders in ϵ. Now let us find the semiclassical form of $\langle P|p\rangle$. For a given momentum P there is an infinite number of stationary phase points

Q_{sp} which occur in pairs (X_n, Y_n),

$$X_n = X_0 + \frac{2\pi}{\alpha}n, \quad Y_n = \frac{\pi}{\alpha} - X_0 + \frac{2\pi}{\alpha}n, \tag{3.30}$$

where $X_0 = -\frac{1}{\alpha}\arcsin\frac{2(P-p)}{\epsilon\hbar\alpha}$. In analogy with Eq. (3.17), the semiclassical transformation element for manifold (3.28) is

$$\langle P|p\rangle_{sc} = \frac{1}{\sqrt{2\pi\hbar}} \tag{3.31}$$
$$\times \sum_{n=-\infty}^{\infty} \left|\frac{\partial^2 S}{\partial Q^2}\right|_{Q=X_n}^{-1/2} \left\{\exp\left[\frac{i}{\hbar}\, S|_{Q=X_n} - i\frac{\pi}{4}\right] + \exp\left[\frac{i}{\hbar}\, S|_{Q=Y_n} + i\frac{\pi}{4}\right]\right\}$$

with

$$S \equiv S(Q,P,p) = -PQ - F_3(p,Q) = (p-P)\,Q + \frac{1}{2}\hbar\epsilon\cos\alpha Q.$$

Using (3.30), (3.31) and defining $r = \frac{P-p}{\hbar\alpha}$, we get

$$\langle P|p\rangle_{sc} = \frac{1}{\hbar\alpha}F(\epsilon,r)\sum_{n=-\infty}^{\infty} e^{2\pi i n r} \tag{3.32}$$

where

$$F(\epsilon,r) = \sqrt{\frac{2}{\pi}}e^{-ir\pi/2}\frac{\cos\left\{r\left(\frac{\pi}{2} + \arcsin\frac{2r}{\epsilon}\right) + \left[\left(\frac{\epsilon}{2}\right)^2 - r^2\right]^{1/2} - \frac{\pi}{4}\right\}}{\left[(\frac{\epsilon}{2})^2 - r^2\right]^{1/4}}. \tag{3.33}$$

Employing the Poisson summation formula

$$\sum_{n=-\infty}^{\infty} e^{2\pi i n r} = \sum_{m=-\infty}^{\infty}\delta(m-r)$$

and reverting to $P = p + r\hbar\alpha$, we obtain

$$\langle P|p\rangle_{sc} = \frac{1}{\hbar\alpha}F(\epsilon,r)\sum_{n=-\infty}^{\infty}\delta(n-r) = \frac{1}{\hbar\alpha}\sum_{n=-\infty}^{\infty}F(\epsilon,n)\,\delta(n-r)$$
$$= \sum_{n=-\infty}^{\infty}F(\epsilon,n)\,\delta(P-p-n\hbar\alpha). \tag{3.34}$$

Comparing (3.34) with (3.29), we see that the semiclassical and uniform versions of $\langle P|p\rangle$ will be asymptotically equal if $F(\epsilon,n) \sim J_n(\epsilon/2)\,i^n$ for large ϵ. That is indeed true since for $\epsilon \gg n^2$,

$$F(\epsilon,n) \sim \left(\frac{2}{\pi\frac{\epsilon}{2}}\right)^{1/2} e^{in\pi/2}\cos\left(\frac{\epsilon}{2} - \frac{n\pi}{2} - \frac{\pi}{4}\right) \sim J_n\left(\frac{\epsilon}{2}\right)i^n \tag{3.35}$$

Table 3.1 shows that for $\epsilon = 10$, stationary-phase and replacement-manifold values of a_n differ by less than 0.02 up to $n = 3$. In the opposite limit, for $\epsilon < 1$, the stationary phase method give a completely wrong value even for the first coefficient a_0 (not shown).

Table 3.1: Comparison of numerical, replacement-manifold (RM), and stationary-phase (SP) evaluation of $|\phi(P)|^2$ for $\xi(Q) = \alpha Q$, $\epsilon = 10$.

n	0	1	2	3	4	5
$\lvert a_n\rvert$ (num.)	0.1776	0.3276	0.0466	0.3648	0.3912	0.2611
$\lvert a_n\rvert$ (RM)	0.1776	0.3276	0.0466	0.3648	0.3912	0.2611
$\lvert a_n\rvert$ (SP)	0.1704	0.3324	0.0343	0.3622	0.4312	∞

3.6 Scattering from a corrugated wall

In this section, we apply the replacement-manifold method to a system that naturally generates the loop structure discussed in previous sections. Namely, we discuss scattering of a plane wave by a corrugated wall. This system has also been used as a simple model of elastic scattering of atoms by solid surfaces (for review see Ref. [60]).

Let us consider a plane divided into two parts by a periodically curved boundary consisting of the set of points with coordinates $(x, \tilde{y})$ related by the equation

$$\tilde{y}(x) = \frac{\varepsilon}{\beta} \sin \beta x \tag{3.36}$$

where β gives the spatial frequency of corrugation and ε the maximum slope $\frac{d\tilde{y}}{dx}$ of the wall. A plane wave with momentum $\hbar\mathbf{k}_1$ is incident from the upper half-plane at an angle α_1 from the y axis, so the incident wave vector is $\mathbf{k}_1 = k\,(\sin\alpha_1, -\cos\alpha_1)$. Classically, the wave reflects specularly from the curved boundary. The reflected rays are shown in Fig. 3.6. Notice the clearly visible caustics, emanating in pairs from cusp singularities. The Poincaré surface of section in Fig. 3.7 displays the dependence of momentum component p_{2x} of reflected rays on coordinate x at a given distance y_2 from x axis. We can see familiar loops with constant area and predict the failure of semiclassical approximation when this area becomes smaller than $\hbar$. The figure implicitly assumes that classically only a single scattering event takes place before a ray leaves the wall permanently. If corrugation is deep enough ($\varepsilon > \varepsilon_{\max}$, where $\varepsilon_{\max} < 1$), multiple scattering will occur for any incident angle α_1. The larger ε gets (within the range $0 < \varepsilon < \varepsilon_{\max}$), the smaller the maximum allowed incident angle α_1. Let us therefore consider a wall with very shallow corrugation ($\varepsilon = 0.2$) and a small angle of incidence ($\alpha_1 = 0.2$), a situation which classically allows only a single reflection. We also choose the incident-wave length $\lambda = \frac{2\pi}{k}$ to be 0.3 times the period of corrugation. The surprising result we shall obtain below is that although there exist seven real Bragg peaks in the scattered wave, the semiclassics break down while the single-scattering approximation using replacement manifolds works with excellent accuracy.

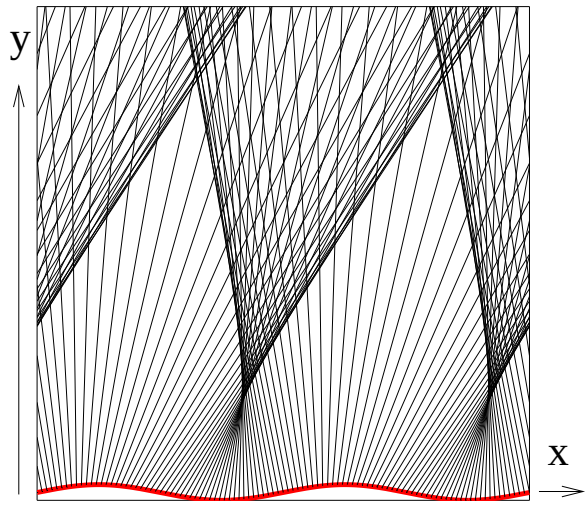

Figure 3.6: Ray picture for a two-dimensional scattering from a corrugated wall. Only reflected rays are shown.

Before applying the replacement-manifold method, let us briefly mention what *exact* and *semiclassical* solutions are used for comparison.

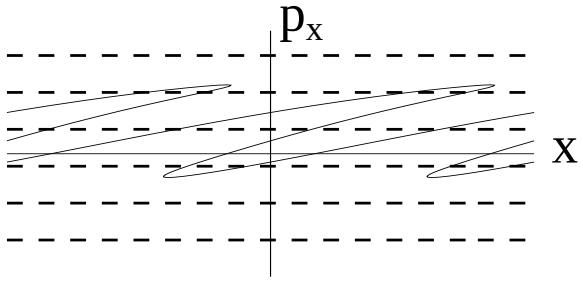

Figure 3.7: Original (solid line) and replacement manifolds (dashed lines) on the Poincaré surface of section at $y_2 = 4\pi/\beta$.

The most direct, Rayleigh approach [105, 6] to find the exact solution relies on expanding the scattered wave in Fourier modes

$$\psi_{scat}(\mathbf{r}) = \frac{1}{2\pi} \sum_{n=-\infty}^{\infty} a_n e^{i\mathbf{k}_{2,n}\cdot\mathbf{r}} \tag{3.37}$$

and finding the coefficients a_n so that the total wave function vanishes along the boundary. The full derivation is presented in Appendix B. Garcia and Cabrera [44] have thoroughly compared merits of this and various other methods. The main issue is the solution's convergence, which improves with decreasing corrugation parameter ε. However, we can safely use

the Rayleigh method since it has been shown to converge for $\varepsilon < 0.448$ [82] and this regime overlaps with the small-loop limit in which we are interested. The resulting probability density is shown in Fig. 3.8.

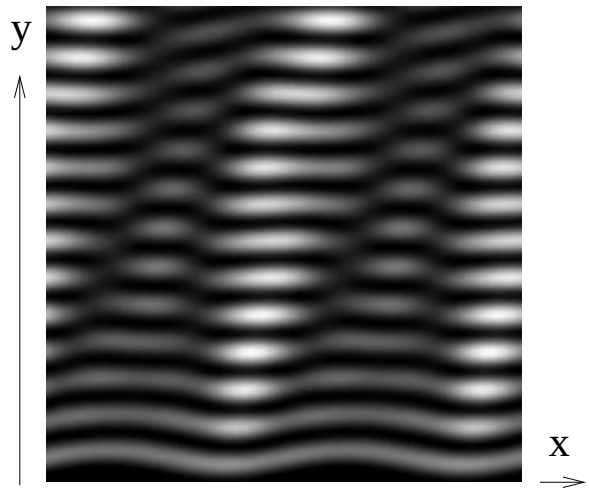

Figure 3.8: Probability density plot for the exact quantum solution. Plot of the replacement-manifold solution is indistinguishable to the eye. For detailed comparison, see Fig. 3.10.

The simple semiclassical wave function may be evaluated by tracing individual rays and employing the Van Vleck propagator (2.4) [129]. The action must be adjusted by correct Maslov indices, corresponding to reflection from a hard wall and to passage through caustics [49]. A probability density plot of the semiclassical wave function is shown in Fig. 3.9. Note the caustics, which clearly separate regions with one, three, and five contributions to the scattered wave. Between caustics, solution looks qualitatively the same as the exact quantum analog in Fig. 3.8. By looking at a surface of section at $y_2 = 4\pi/\beta$ (corresponding to the top edge of Fig. 3.9 where there are at least three contributions for any x) in Fig. 3.7, we expect that semiclassical and quantum wave functions should disagree everywhere. This guess is confirmed in Fig. 3.10.

The application of replacement manifolds is facilitated if the whole scattering problem is formulated using an analog to the smooth-potential Lippmann-Schwinger equation. Invoking the Green's theorem, it can be shown that the total wave function satisfies

$$|\psi_{tot}\rangle = |\psi_{inc}\rangle + \hat{G}_0 \int_{boundary} dx\, |\mathbf{r}\rangle\, \hat{n}(x) \cdot \nabla \psi_{tot}(\mathbf{r}) \tag{3.38}$$

where $|\psi_{inc}\rangle$ is the incident wave, $\hat{G}_0$ is the free-space Green's operator and $\hat{n}(x)$ is a normal

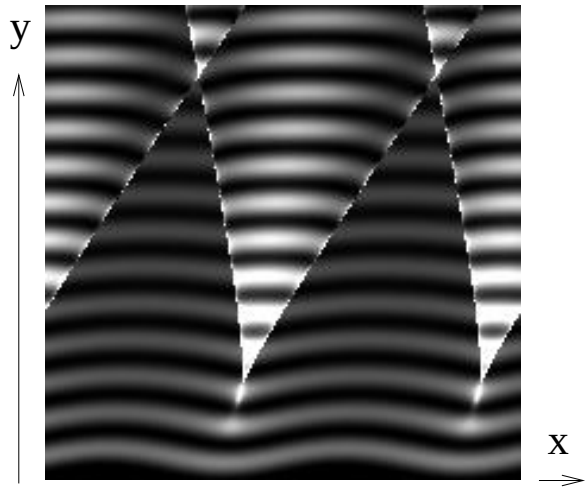

Figure 3.9: Probability density plot for the semiclassical solution.

unit vector at the boundary pointing into free space.

We find $|\psi_{tot}\rangle$ in (3.38) by proceeding in four steps: first we canonically transform the incident wave function to a new coordinate system $\mathbf{r}'$ in which the wall becomes straight. We solve the scattering problem in these coordinates, since there the semiclassical approach is exact. Then we transform back to the original coordinate system in which we propagate the wave using the free-space Green's function to obtain our final answer. Semiclassical approach is used for each separate step but their combination is evaluated exactly.

The wall becomes flat if we apply a canonical transformation

$$x' = x, \quad y' = y - \frac{\varepsilon}{\beta}\sin\beta x$$

generated by

$$F_3(\mathbf{k}, \mathbf{r}') = -k_x x' - k_y(y' + \frac{\varepsilon}{\beta}\sin\beta x'). \tag{3.39}$$

The incident wave function $\psi_{inc}(\mathbf{k}_1)$ can be transformed into new coordinates using

$$\langle \mathbf{r}'|\mathbf{k}\rangle_{sc} = \frac{1}{2\pi}\, e^{-iF_3(\mathbf{k},\mathbf{r}')} \tag{3.40}$$

In primed coordinates, the semiclassical solution of scattering from a straight line is exact and the "angle of incidence" equals the "angle of reflection". Therefore $\hat{n}' \cdot \nabla\psi_{tot}(\mathbf{r}')$ may be replaced by $2\hat{n}' \cdot \nabla\psi_{inc}(\mathbf{r}')$ in equation (3.38). The non-diagonal part of the semiclassical scattering matrix becomes

$$\hat{T} = \hat{S} - \hat{1} = 2\int dx'\, |\mathbf{r}'\rangle\, \hat{n}' \cdot \nabla' \langle \mathbf{r}'| \Big|_{y'=0} \tag{3.41}$$

where $\hat{n}' = \hat{y}'$. Transformation back to original coordinates is achieved by a complex conjugate of (3.40). The free-space propagation is accomplished by the semiclassical Green's function, exact in mixed representation

$$\langle k_{2x}, y_2|\hat{G}_0^{sc}|\mathbf{k}\rangle = \frac{\delta(k_{2x}-k_x)\, e^{ik_y y_2}}{\sqrt{2\pi}(k^2-k_2^2+i\epsilon)} \tag{3.42}$$

Putting all four pieces together, we obtain an expression for the scattered wave on a surface of section,

$$\begin{aligned}\langle k_{2x}, y_2|\hat{G}_0^{sc}\hat{T}\,|\mathbf{k}_1\rangle &= 2\int d^2k \int dx' \langle k_{2x}, y_2|\hat{G}_0^{sc}|\mathbf{k}\rangle\langle\mathbf{k}|\mathbf{r}'\rangle\, \partial_{y'}\langle\mathbf{r}'|\mathbf{k}\rangle_{sc}\Big|_{y'=0} \\ &= \frac{2ik_{1y}}{(2\pi)^{5/2}}\int d^2k\, \frac{\delta(k_{2x}-k_x)\, e^{ik_y y_2}}{\sqrt{2\pi}(k^2-k_2^2+i\epsilon)} \\ &\quad\times \int dx'\, \exp[i(k_{1x}-k_x)x' + i(k_{1y}-k_y)\frac{\varepsilon}{\beta}\sin\beta x'] \end{aligned} \tag{3.43}$$

Before we proceed, it should be noted that the outcome of this four-step process, an integral representation of the scattered wave, can be viewed as a continuous superposition of waves emanating from sources along the boundary, with strength proportional to the normal derivative of the incident wave. It can be shown, in fact, that this process is equivalent to a generalized Kirchhoff diffraction method.[5]

Returning to expression (3.43), we recognize that the exponent in integral over x' corresponds to a classical manifold

$$k_x = k_{1x} + (k_{1y}-k_y)\varepsilon\cos\beta x' \tag{3.44}$$

which is "begging" to be replaced by a series of manifolds $k_{x,n} = k_{1x} + n\beta x'$ with weights $J_n(\epsilon)$ because

$$|\epsilon| = |k_{1y}-k_y|\frac{\varepsilon}{\beta} \lesssim \frac{2k\varepsilon}{\beta} < 1$$

[5]The Kirchhoff diffraction method starts from the Weber integral representation (analog of a more familiar Helmholtz representation in three dimensions)

$$\psi(\mathbf{r}_2) = \int_C ds\left(\psi\frac{\partial}{\partial n}H_1^{(0)}(kR) - H_1^{(0)}(kR)\frac{\partial\psi}{\partial n}\right),$$

where $R = |\mathbf{r}_2 - \mathbf{r}|$, $\mathbf{r}$ is the coordinate vector of points on the closed curve C, $\frac{\partial}{\partial n}$ is the derivative in the direction of an *outward* pointing normal vector $\hat{\mathbf{n}}$. For derivation of Weber and Helmholtz representations see, e.g., Refs. [5, 15].

Kirchhoff method consists in approximating usually unknown values of ψ and $\frac{\partial\psi}{\partial n}$ in the integrand. Originally, it was only used in the case of a plane screen with an aperture: Kirchhoff set ψ and $\frac{\partial\psi}{\partial n}$ equal to zero on the dark side of the screen and equal to the unperturbed values (ψ_{inc} and $\frac{\partial\psi_{inc}}{\partial n}$) in the aperture. The term "Kirchhoff method" is now sometimes used for a more general approximation encompassing our example of corrugated wall, whereby ψ and $\frac{\partial\psi}{\partial n}$ at any point of the surface are approximated by the values that would be present on the tangent plane at that point. See, e.g., p. 20 of [6].

for the classically allowed momenta. The integral over x' is then simple to evaluate and is equal to

$$\int dx' \sum_{n=-\infty}^{\infty} J_n(\epsilon) \exp[i(k_{1x} + n\beta - k_x)\, x'] = 2\pi \sum_{n=-\infty}^{\infty} J_n(\epsilon)\, \delta(k_{1x} + n\beta - k_x)$$

Using this result and evaluating the trivial integral over k_x, expression (3.43) becomes

$$\langle k_{2x}, y_2 | \hat{G}_0^{sc} \hat{T} \, |\mathbf{k}_1\rangle = \frac{2ik_{1y}}{(2\pi)^{3/2}} \sum_{n=-\infty}^{\infty} \int dk_y \, \frac{e^{ik_y y_2}}{\sqrt{2\pi}(k^2 - k_2^2 + i\epsilon)} \, J_n(\epsilon)\, \delta(k_{2x} - k_{2x,n})$$

where $k_{2x,n} = k_{1x} + n\beta$. Integral over k_y picks up a pole at $k_y = k_{2y,n} = \sqrt{k^2 - k_{2x,n}^2}$ and the final answer is

$$\langle k_{2x}, y_2 | \hat{G}_0^{sc} \hat{T} \, |\mathbf{k}_1\rangle = \frac{k_{1y}}{\sqrt{2\pi}} \sum_{n=-\infty}^{\infty} e^{ik_{2y,n} y_2} \, \frac{J_n(\epsilon_n)\, \delta(k_{2x} - k_{2x,n})}{k_{2y,n}} \tag{3.45}$$

where $\epsilon_n = (k_{1y} - k_{2y,n})\frac{\varepsilon}{\beta}$. The uniform scattered wave is in the form (3.37) of a superposition of traveling and evanescent waves with wave vectors $\mathbf{k}_{2,n}$ and coefficients

$$a_{n,\text{unif}} = \frac{k_{1y}}{k_{2y,n}} J_n(\epsilon_n). \tag{3.46}$$

These turn out to be numerically very close to the coefficients of the exact solution, but here we have avoided having to solve a truncated linear system, which was necessary in Rayleigh or other exact methods (see Appendix B or Ref. [6]).

A two-dimensional plot of probability density does not reveal any difference from the exact quantum result in Fig. 3.8 while the corresponding semiclassical plot clearly shows caustics (see Fig. 3.9). Even if we look at the Poincaré surface of section in a region with many classical caustics, the quantum and uniform solutions agree while the semiclassical solution fails miserably (see Fig. 3.10). The uniform solution agrees with one found differently by Garibaldi et al.[45] and is somewhat more accurate than the same result without the $k_{1y}/k_{2y,n}$ prefactor obtained by Hubbard and Miller [61] by the semiclassical perturbation approximation. As Garibaldi et al. (who obtain three different solutions differing only by prefactors) point out, these prefactors "should not be taken too seriously." We agree: for traveling modes, they do not cause large errors, and since all these solutions neglect multiple scattering, we cannot expect high accuracy of the already small coefficients of evanescent modes.

Now we explain how semiclassical and single-scattering regimes differ. As mentioned above, the single-scattering approximation was guaranteed by the choice $\varepsilon \ll 1$,

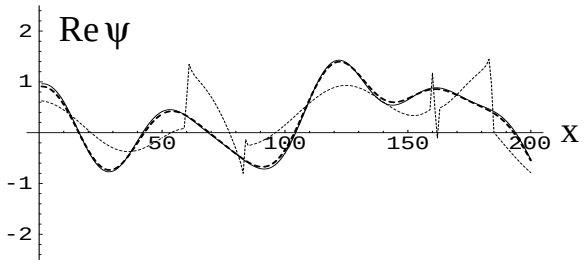

Figure 3.10: Wave function on the surface of section at $y = 4\pi/\beta$. Comparison of the exact quantum (dashed line), replacement-manifold (solid line), and semiclassical (dotted line) wave functions.

$\alpha \ll 1$. At first, it appears that the simple semiclassical approximation should be accurate for this regime of very shallow corrugation, since scattering from a flat wall has an exact semiclassical answer. The correct criterion, however, is based on the area of loops in phase space (see Fig. 3.7). In this case, for small ε and α, the height of loops is equal to the momentum kick received in the region of maximum slope, approximately $p\varepsilon$ and the width is half the period of corrugation, $\frac{\pi}{\beta}$. The loop area is smaller than $p\varepsilon\frac{\pi}{\beta} = \pi kd\hbar$ (d is the depth of corrugation) and has to be compared to $\hbar$. We arrive at a surprising result that the validity of semiclassical approximation is unrelated to the periodicity of corrugation, but only depends on the product of wave vector and corrugation depth. If this product is small, semiclassical approximation breaks down. It works in the opposite case, although we might have to take into account classical trajectories corresponding to multiple scattering if $\varepsilon \geq 1$.

It would be interesting to see in detail how uniform and semiclassical solutions get closer when both $kd \gg 1$ and $\varepsilon \ll 1$. While this could be shown explicitly, as in Section 3.5, by evaluating integrals in (3.43) by the stationary phase method, Berry and Bodenschatz demonstrate the agreement for a similar problem of waves propagating normally from a sinusoidal wavefront [11], using the Talbot interference effect.[6]

[6]This remarkable effect appears also in our case (for ψ_{scat} only) when $k_{1x} = 0$: Note that then paraxial approximation

$$k_{2y,n} = \sqrt{k^2 - (\beta n)^2} \approx k - \frac{\beta^2 n^2}{2k} \tag{3.47}$$

(valid for $\varepsilon \ll 1$) implies that the scattered wave in both exact and replacement-manifold solutions has the property

$$\psi_{scat}(x - \frac{\pi}{\beta}, y + y_T) = \psi_{scat}(x, y)e^{iky_T} \tag{3.48}$$

where $y_T = 2\pi k/\beta^2$ is the Talbot distance.

3.7 Conclusion

In this chapter, we have successfully applied the replacement-manifold idea to uniformize semiclassical wave functions in several situations where repeated small areas or loops in phase space result in the complete failure of the standard WKB approximation. We have shown how the notion of replacement manifolds can rejuvenate physical intuition about the quantum wave function and also be a very convenient way to obtain accurate results. While we have focussed on two physically motivated cases (the homoclinic-like oscillation and the corrugated wall), the present method should work in more complicated time-dependent problems if used in conjunction with Miller's initial value representation of the Van Vleck semiclassical propagator. After replacement manifolds are identified, the perturbative expansion contributions to the wave function could be found by the stationary phase approximation applied to these manifolds.

Chapter 4

Uniform semiclassical wave function for coherent two-dimensional electron flow

In this chapter, we find a uniform semiclassical wave function describing coherent branched flow through a two-dimensional electron gas (2DEG), a phenomenon recently discovered by direct imaging of the current using scanned probed microscopy [121, 122]. The formation of branches has been explained by classical arguments [122], but the semiclassical simulations necessary to account for the coherence are made difficult by the proliferation of catastrophes in phase space. In this chapter, expansion in terms of replacement manifolds is used to obtain a uniform semiclassical wave function for a cusp singularity. The method is then generalized and applied to calculate uniform wave functions for a quantum-map model of coherent flow through a 2DEG. Finally, the quantum-map approximation is dropped and the method is shown to work for a continuous-time model as well.

4.1 Introduction

There is no doubt that detailed understanding of the electron transport through mesoscopic devices is needed to take the full advantage of the possibilities of novel electronics these systems offer. On the experimental side, great progress was made with the use of scanned probe microscopy [41, 30, 121]. The theory has kept up: the present knowledge

has already been summarized in several monographs [114, 34, 62].

Quantum effects have become central as devices have become smaller, cooler, and containing fewer impurities. Remarkably many quantum properties of the electron flow through nanostructures can be explained by semiclassical methods. These methods are based on classical mechanics: the relevant classical manifolds form the "skeleton" to which the wave function is attached. Semiclassical methods need to be substituted for classical ones when coherence is maintained over distances on the order of the size of the device, and when interference effects are playing a role.

In their simplest form, the semiclassical techniques fail when nonlinear classical dynamics create complicated structures in phase space. In particular, the semiclassical approximation breaks down whenever there are multiple contributions to the wave function within the volume of a single Planck's cell. These so-called catastrophes have been classified [118, 3] and various methods have been devised to correct the semiclassical wave functions in cases when there exist only several coalescing contributions [9, 18, 97]. In the setting of mesoscopic devices, improved semiclassical methods have been applied, e.g., to the scattering through ballistic microstructures [138] or to the magnetotransport through a resonant tunneling diode [90].

In Chapter 3 (also see Ref. [125]), we successfully explored a new approach which worked even in situations with an infinite number of coalescing contributions, occurring e.g. in the case of the homoclinic tangle near an unstable periodic orbit.[1] The uniform method of Chapter 3 is based on the idea of replacing a complicated classical manifold by a series of new simpler manifolds. When standard semiclassical methods are applied to these "replacement manifolds," accurate uniform wave functions are obtained in situations where direct semiclassical evaluation of the original manifold fails miserably.

In Chapter 3, this method was used in special, although common cases with an infinite number of oscillations with the same phase-space area. In Section 4.2 we demonstrate that this special property is not necessary, and that similar approach may be used more generally, even in cases with localized perturbations. In Section 4.3, the method is used to uniformize a cusp singularity. In Section 4.4, we apply the generalized method to find a uniform wave function in a quantum-map model of a two-dimensional electron flow through a sample with impurities, where multiple cusp catastrophes are present. The

[1] For the definition of a homoclinic tangle see, e.g., Ref. [2].

quantum-map approximation is relaxed in Section 4.5 and it is shown how the replacement manifolds are formed in a continuous-time model. In Section 4.6, we discuss the merits of the replacement-manifold method and relate it to other semiclassical techniques. While most of this chapter is concerned with what happens to the twisted manifold under the shear of phase space, for completeness Appendix C addresses the other major phase space motion: rotation.

4.2 Replacement-manifold method and its generalization

As described in Chapter 3, the replacement-manifold method works for wave functions of the form

$$\psi(q) = A(q)e^{iS(q)/\hbar} \tag{4.1}$$

with

$$S(q) = S_0(q) + \hbar\epsilon \sin f(q), \tag{4.2}$$

that can be associated with classical manifolds in which the momentum depends on the position as

$$p(q) = \frac{\partial S}{\partial q} = \frac{\partial S_0}{\partial q} + \hbar\epsilon f'(q)\cos f(q). \tag{4.3}$$

Here S_0 and S are the unperturbed and full action, respectively, ϵ is a parameter controlling the strength of the perturbation, $A(q)$ gives the local weight of the manifold, and $f(q)$ is a smooth function defining the shape of the perturbation.

We can expand the wave function as

$$\psi_{RM}(q) = \sum_{n=-\infty}^{\infty} A_n(q)\exp\left[\frac{i}{\hbar}S_n(q)\right], \tag{4.4}$$

and interpret each term of the sum as a contribution from a classical "replacement" manifold $p_n(q) = \partial S_n/\partial q$ with a weight $A_n = A(q)J_n(\epsilon)$ and an action $S_n(q) = S_0(q) + n\hbar f(q)$. The advantage of the replacement-manifold expansion is appreciated after moving to the momentum representation with caustics where semiclassical form $\sum_j A_j^{SC}(p)\exp[iS_j^{SC}(p)/\hbar]$ fails while the sum over replacement manifolds gives an accurate result.

A slightly different and more general approach than in Chapter 3 does not require an oscillatory behavior of the action. If

$$S(q) = S_0(q) + \epsilon\Delta S(q), \tag{4.5}$$

we may Taylor expand the wave function as

$$\psi(q) = A(q)\exp\left[\frac{i}{\hbar}S_0(q)\right]\sum_{n=0}^{\infty}\frac{1}{n!}\left[\frac{i}{\hbar}\epsilon\Delta S(q)\right]^n$$
$$= \sum_{n=0}^{\infty} A_n(q)\exp\left[\frac{i}{\hbar}S_n(q)\right] \tag{4.6}$$

corresponding to replacement manifolds with weights

$$A_n(q) = A(q)(i\epsilon)^n/n!$$

and actions

$$S_n(q) = S_0(q) - i\hbar n\log[\Delta S(q)/\hbar].$$

Defining a new function $f(q)$ by $\Delta S(q) \equiv \hbar\exp[f(q)]$, the nth replacement-manifold action becomes

$$S_n(q) = S_0(q) - i\hbar n f(q) \tag{4.7}$$

It will "help" the convergence of expansion (4.6) if $\lim_{q\to\pm\infty} f(q) = -\infty$. This, however, is a natural property of localized perturbations.

The simplest nontrivial example is obtained by choosing $f(q) = -q^2$. Besides allowing an analytic solution, this choice will yield exactly the manifold needed in our model of a two-dimensional electron flow in Section 4.4. Expanding the function $p(q)$ around $q = 0$,

$$p(q) = -2\epsilon\hbar q e^{-q^2} \approx 2\epsilon\hbar(q^3 - q) + O(q^4), \tag{4.8}$$

we find that this case falls into the second simplest universality class (called cusp) of catastrophe theory [118, 3] (see Fig. 4.1).[2] Assuming that the weighting of this manifold is $A(q) = const. = (2\pi\hbar)^{-1/2}$, the corresponding semiclassical wave function is

$$\psi_{SC}(q) = (2\pi\hbar)^{-1/2}\,\exp\left(i\epsilon e^{-q^2}\right). \tag{4.9}$$

Since for all positions q, there exists only a single contribution to $\psi_{SC}(q)$, the semiclassical position wave function is accurate, $\psi(q) \approx \psi_{SC}(q)$, and the momentum wave function is given by the Fourier transform

$$\psi(p) = (2\pi\hbar)^{-1/2}\int dq\,\psi_{SC}(q)\,e^{-ipq/\hbar}. \tag{4.10}$$

[2] Another choice, $f(q) = -\frac{1}{4}q^4 + \frac{1}{2}q^2$, would give an example of another universality class: the so-called butterfly catastrophe.

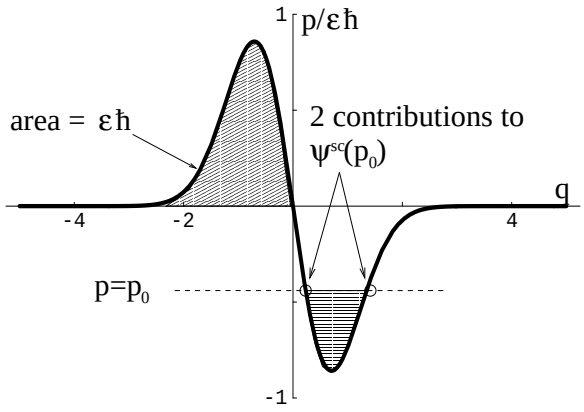

Figure 4.1: Initial manifold of Eq. (4.8) and areas important to the semiclassical approximation of $\psi(p)$.

Evaluating this integral by the stationary phase approximation yields the semiclassical momentum wave function $\psi_{SC}(p)$. The semiclassical momentum wave function has two contributions from two stationary phase points (Fig. 4.1). The horizontally filled-in area gives the phase between two contributions; if it becomes smaller than $\hbar$, the stationary phase approximation breaks down. Therefore $\psi_{SC}(p)$ will be singular for all classically allowed momenta when $\epsilon \leq 1$.

The replacement-manifold momentum can be found from Eq. (4.7) with $f(q) = -q^2$ as

$$p_n(q) = \frac{\partial S_n}{\partial q} = p_0(q) - i\hbar n f'(q) = 2in\hbar q.$$

Note that $p_n(q)$ is purely imaginary for all q and that the corresponding manifold has no caustics. The uniform momentum wave function is found as

$$\psi_{RM}(p) = (2\pi\hbar)^{-1/2} \int dq\, e^{-ipq/\hbar} \sum_{n=0}^{\infty} A_n e^{iS_n(q)/\hbar} \tag{4.11}$$

$$= \delta(p) + \frac{\sqrt{\pi}}{2\pi\hbar} \sum_{n=1}^{\infty} \frac{(i\epsilon)^n}{n!} n^{-1/2} \exp\left(\frac{-p^2}{4n\hbar^2}\right)$$

$$= \delta(p) + \sum_{n=1}^{\infty} \tilde{A}_n e^{i\tilde{S}_n(p)/\hbar} \tag{4.12}$$

where

$$\tilde{A}_n = \frac{\sqrt{\pi}}{2\pi\hbar} \frac{(i\epsilon)^n}{n!} n^{-1/2}, \tag{4.13}$$

$$\tilde{S}_n(p) = -\int dp\, q_n(p) = \frac{ip^2}{4n\hbar}. \tag{4.14}$$

We can in general evaluate all replacement manifolds for $n \geq 1$ by the stationary phase method, although in this case the answer turns out to be equal to the exact Fourier transform because the action S_n is quadratic.

4.3 Uniformization of a cusp singularity

The formation of manifolds with a double-loop structure like the one in Fig. 4.1 is a generic feature of nonlinear Hamiltonian systems. This pattern forms, for instance, whenever an ensemble of trajectories encounters a dip or a bump in the potential surface. Assuming that the particles have energy greater than the maximum of the potential, the dip or bump act as a convex or concave lens, respectively. After it is created, the double loop does not remain stationary: depending on the Hamiltonian, the structure will generally start to shear and rotate in phase space (see Fig. 4.2). In most of this chapter we are concerned with the shear only, but for completeness, in Appendix C we present analytic formulae for the replacement-manifold expansion of an original manifold that is arbitrarily rotated with respect to the q and p axes.

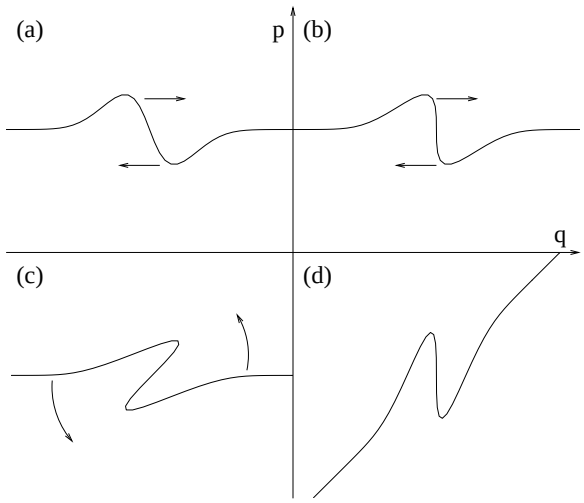

Figure 4.2: An example of a manifold with the double loop structure that has been sheared (a-c) and rotated (c-d) in phase space. While shear and rotation are generic phase space motions, here they were implemented by $H = p^2/2$ and $H = p^2/2 + q^2/2$, respectively.

For now imagine that after the manifold (4.8) with two loops has been formed, the

system evolves freely (with Hamiltonian $H = p^2/2m$). Hamilton's equations of motion are

$$\begin{aligned} \dot{q} &= \frac{p}{m}, \\ \dot{p} &= 0, \end{aligned} \tag{4.15}$$

resulting in a shear of phase-space. The semiclassical position wave function, which was accurate at time $t = 0$, will break down around time

$$t_{\text{cusp}} = \frac{m}{2\epsilon\hbar} \tag{4.16}$$

when a cusp singularity [97] develops (see Fig. 4.3).

This will be remedied if we apply any of the standard semiclassical evolution methods to the first few replacement manifolds instead of directly to the original manifold,[3]

$$\begin{aligned} \psi_{RM}(q,t) &= \int dq'\, K_f(q,q';t)\, \psi_{RM}(q',0) \\ &= \sum_{n=0}^{\infty} \int dq'\, K_f(q,q';t)\, A_n e^{iS_n(q)/\hbar} \end{aligned} \tag{4.17}$$

where the free-space propagator

$$K_f(q'',q';t) = \Big(\frac{m}{2\pi\hbar i t}\Big)^{1/2} \exp\left[\frac{im}{2\hbar t}(q''-q')^2\right] \tag{4.18}$$

and at $t = 0$, using expression (4.6),

$$\psi_{RM}(q,0) = (2\pi\hbar)^{-1/2} \sum_{n=0}^{\infty} \frac{(i\epsilon)^n}{n!} e^{-nq^2}. \tag{4.19}$$

In our case, since the replacement-manifold terms are Gaussian wave packets, their semiclassical evolution (i.e., the stationary phase integration in the second row of Eq. (4.17)) can be performed analytically and is exact,

$$\psi_{RM}(q,t) = (2\pi\hbar)^{-1/2} \sum_{n=0}^{\infty} \frac{(i\epsilon)^n}{n!} (1 + 2in\hbar t/m)^{1/2} \exp\left(\frac{-nq^2}{1+2in\hbar t/m}\right). \tag{4.20}$$

For comparison, the exact quantum evolution was performed by switching to the momentum representation, using the fast Fourier transform and trivially evolving the wave function there. To find the primitive semiclassical evolution, we used a method described by Berry et al. [10]. All three methods are compared in Fig. 4.3, showing the classical manifold

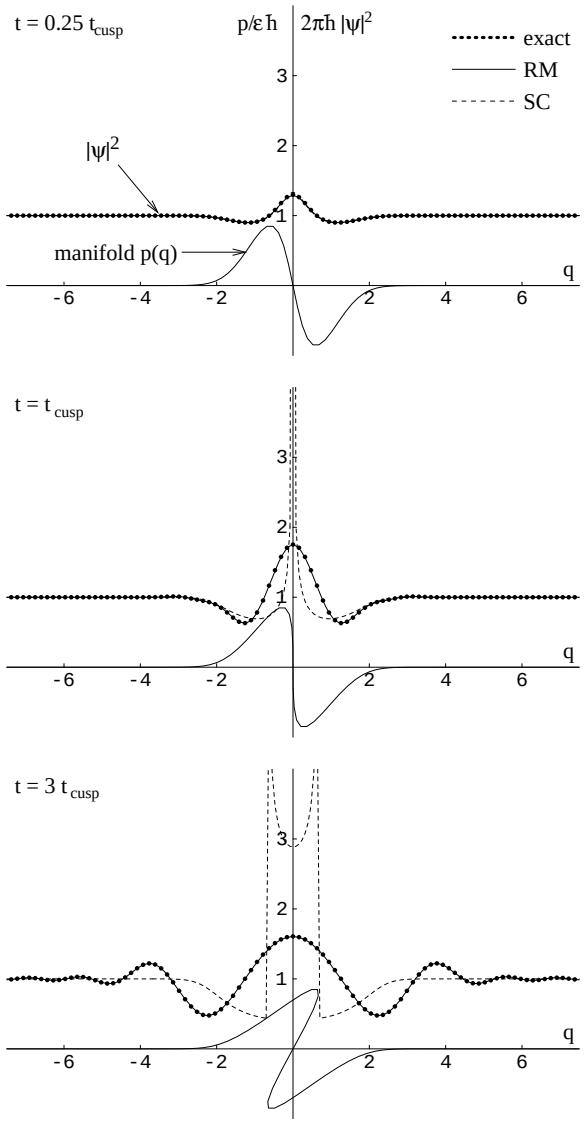

Figure 4.3: Evolution of the manifold and the comparison of the exact (dots), replacement-manifold (RM, solid line) and semiclassical (SC, dashed line) wave functions at a time instant before ($t = 0.25\,t_{\rm cusp}$, top), at ($t = t_{\rm cusp}$, middle), and after ($t = 3\,t_{\rm cusp}$, bottom) the cusp. In these plots, $\epsilon = 1$ and the first five replacement manifolds were used in Eq. (4.20).

and corresponding exact, semiclassical, and replacement-manifold wave function at a time instant before, at, and after the cusp.

In the following section, we show that the replacement-manifold method can treat situations in which more cusps are continuously formed. However, the advantage of the replacement manifolds over the Van Vleck propagation or other standard semiclassical methods can be appreciated already when the rough region of the potential is localized in time and only one or a few cusps are created. As can be seen from Fig. 4.3, even if the potential is simply flat after certain time, the region of q in which the semiclassical approximation breaks down expands. Unlike the simple semiclassical approximation which deteriorates with time, the accuracy of the replacement-manifold method is preserved after leaving the rough area of the potential: once the Gaussian wavepackets corresponding to the replacement manifolds are formed, their number remains constant and their propagation is exact in any potential with up to quadratic terms (see Fig. 4.3).

4.4 Quantum-map model of a two-dimensional electron flow through a sample with impurities

We are now prepared to address the problem of the two-dimensional electron flow in a semiconductor nanostructure with impurities. The electron transport in such a system is neither strictly ballistic nor strictly diffusive. Instead, the experiment has revealed that reality lies somewhere in between and the phenomenon has been termed "branched flow" [122]. Figures 4.4 and 4.5 show respectively the exact electron density (obtained by the exact quantum evolution using the fast Fourier transform) and the representative classical trajectories in the model described below. The name of the phenomenon comes from the shape of the regions with enhanced electron density in Fig. 4.4 or the corresponding clusters of classical electron trajectories in Fig. 4.5. It turns out, however, that these do *not* correspond to the valleys in the potential [122]. Although the branches can already be seen in the classical simulations, Fig. 4.5 also shows that scattering by impurities leads to abundant cusp singularities in phase space, and therefore we expect deviations in both classical and primitive semiclassical approximations from the exact quantum dynamics.

Here we analyze a simple model which can nevertheless exhibit all these proper-

[3] I.e., instead of evaluating the integral in the first row by stationary phase, we apply the stationary phase approximation to the integrals in the second row of Eq. (4.17).

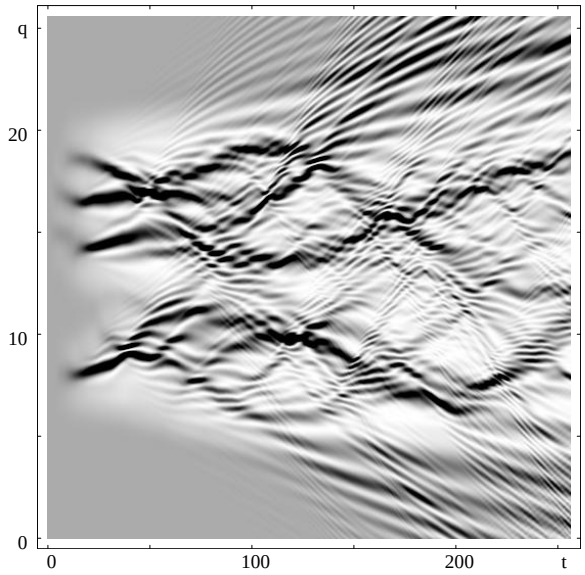

Figure 4.4: Electron density $|\psi(q,t)|^2$ in the model of a two-dimensional electron flow (obtained by the exact quantum evolution using the fast Fourier transform, replacement manifolds were not used). For Hamiltonian, see Eq. (4.26). In this plot, $V_0/v = -0.0125$, $\epsilon = 2.22$, and there were 256 impurities.

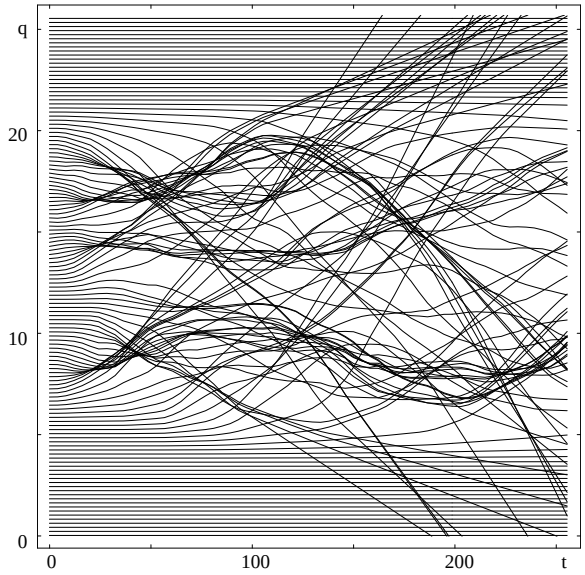

Figure 4.5: Representative classical electron trajectories, corresponding to the electron density in Fig. 4.4.

ties. Namely, we discuss a two-dimensional system with fast electrons, incident along the x-axis and scattered by small isolated Gaussian impurities randomly distributed in the xy plane. Following Topinka et al. [121, 122] who observed branched flow in a similar system, we consider the electron kinetic energy to be much larger than the amplitude of impurities. In fact, we assume the kinetic energy to be high enough to justify an impulse approximation: the electron propagates freely between effectively instantaneous kicks from impurities that affect its momentum but not position. Moreover, while the transverse momentum changes by a small impulse from an impurity, the longitudinal momentum remains effectively constant, allowing the transformation of the original two-dimensional problem into a one-dimensional problem with a time-dependent Hamiltonian. To be precise, we start with a two-dimensional Hamiltonian

$$H(x, y, p_x, p_y) = \frac{p_x^2 + p_y^2}{2m} + \sum_{j=1}^{n} V_0 \exp\left[-\frac{(x - x^{(j)})^2 + (y - y^{(j)})^2}{a^2}\right] \tag{4.21}$$

where n, a, and $x^{(j)}$, $y^{(j)}$ are respectively the number, radius, and coordinates of the centers of the impurities. We assume that

$$\dot{x} = p_x/m \approx \text{const.} = v \tag{4.22}$$

where v is the initial velocity of the electron. This is justified when

$$mv^2/|V_0| \gg \sqrt{n}. \tag{4.23}$$

For simplicity of calculations, we distribute the impurities randomly in the y direction, but regularly along the x axis, at intervals $v\tau$. Each electron will be affected by a single impurity at a time if

$$v\tau \gg a. \tag{4.24}$$

To simplify notation, we take a, τ, and m to be respectively the units of length, time, and mass. Then we define dimensionless quantities $q = y/a$, $p = p_y\tau/ma$, etc. While we do not change the names of all other quantities, it should be understood that they have been made dimensionless as well. After this rescaling, we obtain an effective, one-dimensional time-dependent Hamiltonian

$$H(q, p, t) = \frac{p^2}{2} + \sum_{j=1}^{n} V_0 \exp\left[-(q - q^{(j)})^2 - v^2(t - j)^2\right] \tag{4.25}$$

In this section we consider that the change of the transverse momentum due to the impurity is instantaneous, yielding a further simplification, represented by a periodically "kicked" Hamiltonian,

$$H(q,p,t) \approx \frac{p^2}{2} + \sqrt{\pi}\frac{V_0}{v}\sum_{j=1}^{n} e^{-(q-q^{(j)})^2}\delta(t-j). \tag{4.26}$$

(A generalized analysis without this approximation is presented in Section 4.5.) In the impulse approximation, classical position q of an electron does not change during an interaction with jth impurity.[4] Classical dynamics may therefore be expressed in terms of a map,

$$\begin{aligned} q_{j+1} &= q_j + p_j, \\ p_{j+1} &= p_j + \Delta p(q_{j+1}, q^{(j+1)}) \end{aligned} \tag{4.27}$$

where subscripts denote time in units τ and the change of momentum is

$$\Delta p(q, q^{(j)}) \approx -\int_{-\infty}^{\infty} dt\, \frac{\partial H}{\partial q} = 2\sqrt{\pi}\frac{V_0}{v}(q-q^{(j)})e^{-(q-q^{(j)})^2}, \tag{4.28}$$

implying that a single impurity transforms a momentum state exactly into the two-loop manifold (4.8) from Section 4.2. We can read off the loop area from (4.28) to be $\sqrt{\pi}|V_0|/v$.

In quantum mechanics, another important parameter enters: $\hbar$. Accuracy of the semiclassical approximation will depend on how

$$\epsilon = \sqrt{\pi}\frac{|V_0|}{v\hbar} \tag{4.29}$$

compares to 1. In the impulse approximation, the exact quantum dynamics is described by a quantum map

$$|\psi_{j+1}\rangle = U\,|\psi_j\rangle \tag{4.30}$$

where the subscript again denotes time in units τ and U is the one-step evolution operator

$$\begin{aligned} U &= T\exp\left(-\frac{i}{\hbar}\int_0^1 H\,dt\right) \\ &= \exp\left(-\frac{i}{\hbar}\int_{-\infty}^{\infty} V\,dt\right)\exp\left(-\frac{i}{\hbar}\frac{p^2}{2}\right) = \exp\left(i\epsilon\, e^{-q^2}\right)\exp\left(-\frac{i}{\hbar}\frac{p^2}{2}\right). \end{aligned} \tag{4.31}$$

The easiest way to evolve a quantum state numerically is to use the fast Fourier transform to switch back and forth between position and momentum representations and apply the impulsive part of U in q-representation and the kinetic part of U in p-representation.

[4] With this approximation, the only classical parameter remaining is V_0/v.

We now demonstrate that not only do the replacement manifolds lack singularities (present in the classical and semiclassical analysis), but that they can also correctly reproduce all the details of the exact quantum solution. When the next impurity is encountered, each wave packet develops a loop in its phase-space representation which would soon lead to a new cusp singularity. We therefore replace it with a series of simpler manifolds, as in Section 4.3, avoiding this problem.

In our model we exploit the fact that the replacement-manifold terms are Gaussian wave packets, allowing their analytic evaluation with only a slight generalization of the calculations in Section 4.3. Each term in the replacement-manifold sum at time j has a Gaussian form,

$$\psi_j(q) = c\, e^{aq - bq^2}, \quad \mathrm{Re}\, b > 0. \tag{4.32}$$

After the kinetic propagation, just before next impurity is encountered,

$$\begin{aligned} \tilde{\psi}_{j+1}(q) &= \int K_f(q, q'; 1)\, \psi_j(q')\, dq' \\ &= \frac{c}{(1+2ib)^{1/2}} \exp\left(\frac{ia^2/2 + aq - bq^2}{1+2ib}\right). \end{aligned} \tag{4.33}$$

After receiving an impulse from the $(j+1)$-st impurity,

$$\begin{aligned} \psi_{j+1}(q) &= \tilde{\psi}_{j+1}(q) \exp\left[i\epsilon\, e^{-(q-q^{(j+1)})^2}\right] \\ &= \tilde{\psi}_{j+1}(q) \sum_{n=0}^{\infty} \frac{(i\epsilon)^n}{n!} \exp\left[-n\,(q - q^{(j+1)})^2\right]. \end{aligned} \tag{4.34}$$

Each term in this sum gives rise to a new Gaussian wave packet of the form (4.32), which is propagated further in the same manner.

Figure 4.6 shows a comparison of the exact and RM evolution for $\epsilon = 1.11$ up to a time when eight impurities are encountered. Four replacement manifolds are used to replace each incident wave packet at each impurity. Although the classical manifold (also shown in the figure) has developed many structures smaller than $\hbar$, the agreement remains excellent.

4.5 Continuous version of the model

In certain situations, we may be interested in a detailed evolution of the electron wave function during the collision with the impurity, rather than just in the appearance of

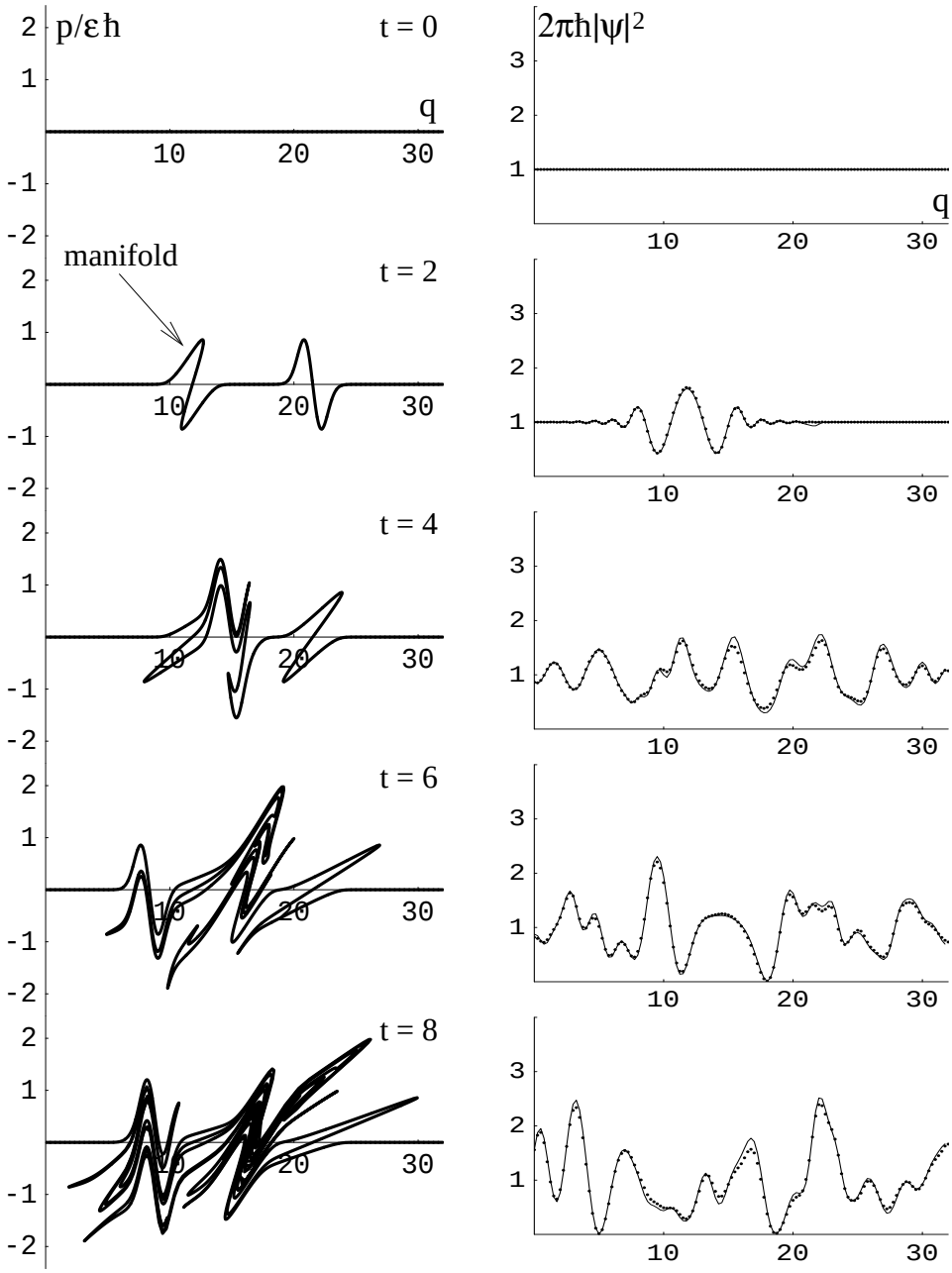

Figure 4.6: Evolution of the manifold (left) and comparison of the corresponding exact (dots) and replacement-manifold (RM, solid line) wave functions (right). The semiclassical wave function is not shown since already at time $t = 6$ it has caustic singularities almost everywhere along the q axis. In this plot, $V_0/v = -0.0625$ and $\epsilon = 1.11$ was chosen to show that the replacement-manifold method is not restricted to $\epsilon < 1$. Only the first four replacement-manifold terms were used in every step (4.34). Two new impurities were encountered at each time interval between the consecutive rows.

the wave function after the collision. Below, we present an analytical solution of this problem in case that the electrons move slowly enough that the collision cannot be considered instantaneous, but fast enough that the transverse displacement of the electrons does not change significantly during the collision.[5]

To simplify the notation, we consider only a single impurity located at position $q = 0$ and time $t = 0$, so that the effective one-dimensional time-dependent Hamiltonian (4.25) becomes

$$H(q,p,t) = \frac{1}{2}p^2 + V_0 \exp\left(-q^2 - v^2t^2\right). \tag{4.35}$$

Assuming that q changes little during the collision we find that the momentum change is

$$\begin{aligned}\Delta p = p(t) - p(-\infty) &= \int_{-\infty}^{t} dt'\, \dot{p}(t') = -\int_{-\infty}^{t} dt'\, \frac{\partial H}{\partial q} \\ &= 2qV_0 e^{-q^2} \int_{-\infty}^{t} dt'\, \exp\left(-v^2 t'^2\right) \\ &= \sqrt{\pi} V_0 v^{-1} q e^{-q^2} \left[1 + \operatorname{erf}(vt)\right]\end{aligned} \tag{4.36}$$

At time $t = -\infty$, we start with a momentum eigenstate with momentum $p = 0$,

$$\begin{aligned}\psi(p, t = -\infty) &= \delta(p), \\ \text{or } \psi(q, t = -\infty) &= (2\pi\hbar)^{-1/2},\end{aligned} \tag{4.37}$$

represented by a horizontal line in phase space. As the electron wave passes through the impurity, a double loop develops in the manifold (curve) representing the wave function. The position representation of the semiclassical wave function at time t is (see, e.g., Ref.[10])

$$\psi(q_f, t) = (2\pi\hbar)^{-1/2} \left|\frac{dq_i}{dq_f}\right|^{1/2} \exp\left[\frac{i}{\hbar}(S_1 + S_2)\right],$$

where q_i is the position at time $t' = -\infty$ that evolves to position q_f at time $t' = t$. In our approximation $q_f \approx q_i$, the Van Vleck determinant $|dq_i/dq_f| = 1$, which is the reason that the semiclassical position wave function remains accurate throughout the collision. S_1 is the action along the trajectory of a reference point $q = x$ on the manifold,

$$S_1 = \int_{-\infty}^{t} dt' L\left[x(t'), \dot{x}(t'), t'\right].$$

[5]For even slower electrons, the coupling between the longitudinal and transverse motion during the collision would prevent us from obtaining closed analytic expressions presented below. However, we could still find the replacement manifolds numerically.

S_2 is the reduced action along the evolved manifold at time t,

$$S_2 = \int_{x_f}^{q_t} dq_t' \, p_t\left(q_t'\right)$$

($p_t(q)$ is the momentum dependence on position at time t). For convenience, we choose $x(-\infty) = -\infty$, giving $\dot{x}(t) = 0$ and $x(t) = const. = -\infty$. Since $V(x = -\infty, t) = 0$, also $L(x, \dot{x}, t) = 0$ and $S_1 = 0$. Finally, since $p_{t=-\infty}(q) = 0$,

$$\begin{aligned} S_2 &= \int_{-\infty}^{q} dq' \, \Delta p_t(q') = \sqrt{\pi} V_0 v^{-1} \left[1 + \mathrm{erf}\,(vt)\right] \int_{-\infty}^{q} dq' \, q' \, e^{-q'^2} \\ &= \sqrt{\pi} V_0 v^{-1} \frac{1}{2} \left[1 + \mathrm{erf}\,(vt)\right] \, e^{-q^2} \end{aligned} \tag{4.38}$$

The semiclassical position wave function at time t is

$$\psi_{SC}(q,t) = (2\pi\hbar)^{-1/2} \exp\left\{ \frac{i}{\hbar} \sqrt{\pi} V_0 v^{-1} \frac{1}{2} \left[1 + \mathrm{erf}\,(vt)\right] \, e^{-q^2} \right\} \tag{4.39}$$

Remembering that $\sqrt{\pi} V_0 v^{-1} \hbar^{-1} = \epsilon$ and that $\mathrm{erf}\,(\pm\infty) = \pm\infty$, we can easily check that this general expression gives the correct limiting forms (4.37) and (4.9) at times $t = -\infty$ and $t = \infty$, respectively. The primitive semiclassical momentum wave function (obtained by the stationary phase approximation of the Fourier transform of (4.39)) fails for the same reasons as in Section 4.2. If we expand $\psi_{SC}(q,t)$ in terms of replacement manifolds, and apply the stationary phase approximation directly to the replacement manifolds, we find an accurate answer. The only difference from expression (4.11) is an extra factor $\left\{ \frac{1}{2} \left[1 + \mathrm{erf}\,(vt)\right] \right\}^n$ for replacement-manifold coefficients A_n or $\tilde{A}_n$ (4.13),

$$\tilde{A}_n = \frac{\sqrt{\pi}}{2\pi\hbar} \frac{(i\epsilon)^n}{n!} n^{-1/2} \left\{ \frac{1}{2} \left[1 + \mathrm{erf}\,(vt)\right] \right\}^n .$$

Since the expression in the large parentheses goes smoothly from 0 at $t = -\infty$ to 1 at $t = \infty$, we see that the replacement manifolds emerge even before the center of the impurity is encountered (at $t = 0$). However, the weight of the manifolds with larger n becomes appreciable only after the impurity is passed.

4.6 Discussion and conclusions

We have shown that the replacement-manifold method is not limited to infinitely repeating phase-space structures if we allow the replacement manifolds to have complex

momenta. Propagation of replacement manifolds gives uniform semiclassical wave functions long after the primitive semiclassical approximation breaks down.

Putting aside the accuracy, the replacement-manifold approach may seem intimidating from a numerical point of view because as described, the algorithm has exponential complexity. But let us remember that the same–exponential proliferation of contributions–is true of the primitive semiclassical solution–which, however, would give a completely wrong result in our case! Moreover, there appear to be at least two possible ways to speed up the replacement-manifold calculations: For $\epsilon < 1$, we could prune the contributions to keep only terms up to a certain "total" power of ϵ (which is different from keeping all terms up to a given power at each impurity). Or we could consolidate the number of wavepackets after certain time by projecting on a suitable basis (because the exponentially growing number of replacement-manifold terms is obviously over-complete) and starting the replacement-manifold propagation afresh.

The question of computational complexity would not even arise if we were interested in a system where the electron wave hits only one or a few impurities and after that propagates in a relatively smooth potential. The small number of Gaussian wavepackets spawned at the last impurity would suffice for all subsequent times and the accuracy of the approximation would be preserved. As discussed in Section 4.3, this should be contrasted with the standard semiclassical approximation which deteriorates even when a manifold with a single cusp propagates in a flat potential (see Fig. 4.3).

Besides providing a uniform wave function the replacement-manifold method gives an intuitive explanation of how quantum mechanics smoothes out the classical detail. Moreover, in the present case of replacement manifolds with a complex momentum, the method appears to provide a link between the semiclassical perturbation approximations [85] and various Gaussian wavepacket techniques [54, 59, 79, 80], because replacement manifolds in the expansion (4.19) are nothing but Gaussian wavepackets. One advantage of the replacement-manifold method over other Gaussian wavepacket methods lies in that it gives an analytic expression for the coefficients of the wavepackets. Other Gaussian wavepacket methods (such as the frozen Gaussians [54], the Herman-Kluk propagator [59] and the full multiple spawning [79, 80]) rely on variational or *ad hoc* methods to obtain optimal wavepacket coefficients numerically.

Chapter 5

Semiclassical evaluation of quantum fidelity in the Fermi-golden-rule and Lyapunov regimes

This chapter presents a numerically feasible semiclassical method to evaluate quantum fidelity decay (Loschmidt echo) in a classically chaotic system. It was thought that such evaluation would be intractable, but instead it is shown here that a uniform semiclassical expression not only is tractable but it gives remarkably accurate numerical results for the standard map in both the Fermi-golden-rule and Lyapunov regimes. Remarkably, it also explicitly contains the "building blocks" of analytical theories of recent literature, and thus permits a direct test of the approximations made by other authors in these regimes, rather than an *a posteriori* comparison with numerical results. Extended validity of the classical perturbation approximation is explained in more detail and it is shown that within this approximation,"diagonal approximation" of Ref. [66] is automatic and does not require ensemble averaging.

5.1 Introduction

The question of stability of quantum motion, originally formulated by Peres in Ref. [98], has recently attracted much interest, due to its relevance to quantum computation and decoherence[1] in complex systems. Peres defined stability in terms of quantum fidelity $M(t)$, the overlap at time t of two states, which were identical at time $t = 0$, but afterwards propagated in slightly different dynamical systems, described by Hamiltonians H^0 and $H^V = H^0 + V$,

$$M(t) = \left|\left\langle \psi^V(t)|\psi^0(t)\right\rangle\right|^2, \tag{5.1}$$

where

$$\psi^0(t) = \exp\left(-iH^0 t/\hbar\right)|\psi\rangle \quad \text{and} \quad \psi^V(t) = \exp\left(-iH^V t/\hbar\right)|\psi\rangle\,.^2$$

This quantity is also equivalently called Loschmidt echo, because it can be interpreted as an overlap of an initial state with this state propagated forward for time t with H^0 and then backward for time t with H^V,

$$M(t) = \left|\left\langle \psi\left|\exp\left(iH^V t/\hbar\right)\exp\left(-iH^0 t/\hbar\right)\right|\psi\right\rangle\right|^2. \tag{5.2}$$

We consider H^0 to be strongly chaotic, although our method is not limited to this case. Even with this restriction, the decay of fidelity has a surprisingly rich behavior: Most surprising recently was the derivation in Ref. [66] that for certain range of perturbations the decay rate is independent of the perturbation strength.

The Loschmidt echo is physically realizable, for example in NMR spin echo experiments, where back-propagation under a slightly different Hamiltonian is feasible [106, 95, 123, 96]. There are other examples, which often go unnoticed, such as neutron scattering, where the scattering kernel can be written as in Eq. (5.1), with H^V a momentum boosted version of H^0. Many numerical investigations of fidelity decay have been undertaken in various chaotic systems [1, 7, 8, 19, 20, 31, 32, 33, 37, 39, 64, 63, 65, 99, 100, 101, 102, 103, 113, 130, 131, 139, 140]. Depending on the strength of perturbation, there exist at least four qualitatively different regimes of the decay in chaotic systems [31]: As the perturbation increases, these regimes are perturbative (PT), Fermi-golden-rule (FGR), Lyapunov (L), and the strong semiclassical regime.

[1] For semiclassical approach to decoherence, see Ref. [115, 42].

[2] In this chapter, superscript V denotes quantities in the perturbed system.

In Section 5.2, we overview these three types of fidelity decay. In Section 5.3 we explain how Gaussian decay is obtained from the first order perturbation theory. The main result of this chapter–the uniform semiclassical expression–is derived in Section 5.4. Section 5.5 discusses how this uniform expression gives rise to the Fermi-golden-rule and Lyapunov decay in various limits. Numerical results for the standard map are presented in Section 5.6. Before concluding this chapter in Section 5.9 we briefly discuss fidelity in quasi-integrable systems in Section 5.7 and the short-time behavior of fidelity in Section 5.8.

5.2 Regimes of fidelity decay in chaotic systems

In the perturbative regime, in which the characteristic matrix element of the perturbation is smaller than the mean level spacing Δ, the decay can be described by a combination of perturbation theory and random matrix theory, and is Gaussian [19, 31],

$$M_{PT}(t) \approx \exp\left(-\overline{V_{nn}^2}\, t^2/\hbar^2\right). \tag{5.3}$$

In the intermediate regime, the decay follows Fermi's golden rule [65] and is exponential,

$$M_{FGR}(t) \approx \exp\left(-\Gamma t/\hbar\right) = \exp\left(-2Kt/\hbar^2\right) \tag{5.4}$$

where $\Gamma = 2\pi\overline{V^2}/\Delta$ and K is the classical action diffusion constant,

$$K = \int_0^\infty dt\ \langle V[\mathbf{r}(t)]\, V[\mathbf{r}(0)]\rangle .$$

The second equality in (5.4) has been confirmed in Refs. [19, 31]. It is shown there that $\Gamma = 2K/\hbar$, in other words that the Fermi-golden-rule decay is equivalent to the exponential decay derived semiclassically in Refs. [66, 19].

In the Lyapunov regime, derived in Ref. [66], fidelity decay actually does not depend on the strength of perturbation, but only on the Lyapunov exponent λ of the chaotic system,

$$M_L(t) \sim \exp(-\lambda t). \tag{5.5}$$

5.3 Perturbative regime ($V_{nm} \ll \Delta$)

Before we discuss the semiclassical approach, let us mention how the Gaussian decay (5.3) is obtained in the perturbative regime. When perturbation is very small, the

decay can be described by the first order perturbation theory. Let E_n^0 be the eigenenergies of H^0 with corresponding eigenstates $|n\rangle$. By "very small" we mean a perturbation V whose matrix elements $V_{nm} = \langle n|V|m\rangle$ are much smaller than the mean level spacing Δ of H^0. To first order, the eigenenergies of H^V are

$$E_n^V = E_n^0 + V_{nn} \quad \text{with} \quad V_{nn} = \langle n|V|n\rangle.$$

Expanding the initial state in terms of eigenstates of H^0,

$$|\psi\rangle = \sum_n a_n|n\rangle,$$

allows us to write the evolved state (to lowest order in the perturbation) as

$$|\psi^V(t)\rangle = \sum_n a_n|n\rangle \exp\left[-i\left(E_n^0 + V_{nn}\right)t/\hbar\right]$$

giving the fidelity

$$M(t) \approx \left|\sum_n |a_n|^2 \exp\left(-iV_{nn}t/\hbar\right)\right|^2 \tag{5.6}$$

This expression is valid for all H^0, V and $|\psi(0)\rangle$. It can be simplified if we make several further assumptions. First, in order to be able to use statistical properties of V_{nn}, we assume that the initial state has an overlap with many eigenstates of H^0. For instance, if the initial state were an eigenstate of H^0, the first order perturbation theory would give no decay. Second, it is assumed that the functions a_n and V_{nn} are uncorrelated. That is reasonable since a_n depends only on the initial state whereas V_{nn} only depends on the perturbation. Third, we assume that matrix elements V_{nn} are uncorrelated for different n. Finally and most importantly, we regard the Bohigas-Giannoni-Schmit conjecture [13] to be valid. This conjecture states that there exists a generic connection between the random matrix theory and the level statistics of quantum analogs of classically chaotic systems. In our case, we only use the consequence that level velocities $v_n = \partial E_n/\partial\epsilon$ are Gaussian distributed (ϵ is a dimensionless parameter controlling the strength of perturbation, $V = \epsilon\widetilde{V}$, where $\widetilde{V}$ is a fixed potential) [19]. The sum can then be replaced by a Gaussian integral over the probability distribution

$$P(v) = \left(2\pi\sigma_v^2\right)^{-1/2} \exp\left(-v^2/2\sigma_v^2\right),$$

where σ_v^2 is the variance of level velocities, giving

$$M(t) \approx \left|\int_{-\infty}^{\infty} dv\, P(v) \exp\left(-i\epsilon vt/\hbar\right)\right|^2 = \exp\left(-\epsilon^2\sigma_v^2\, t^2/\hbar^2\right) = \exp\left(-\overline{V_{nn}^2}t^2/\hbar^2\right).$$

5.4 Semiclassical approach

In this section, we describe a numerically feasible semiclassical method to evaluate fidelity decay in the Fermi-golden-rule and Lyapunov regimes. We will use the method in the following sections to directly test all approximations made in the derivation of results (5.4) and (5.5) from Refs. [66, 19]. Our method starts with a semiclassical approach based on the classical perturbation approximation [66, 19], and ends with a form of the initial value representation (see Section 2.4 or Ref. [83]) which makes the numerical calculation manageable and the semiclassical approximation itself more accurate.

Following notation of Ref. [66], we want to find fidelity decay for an initial Gaussian wave packet

$$\psi\left(\mathbf{r};0\right)=\left(\pi\sigma^{2}\right)^{-d/4}\exp\left[\frac{i}{\hbar}\mathbf{p}_{0}\cdot\left(\mathbf{r}-\mathbf{r}_{0}\right)-\frac{\left(\mathbf{r}-\mathbf{r}_{0}\right)^{2}}{2\sigma^{2}}\right]. \tag{5.7}$$

It is centered at $\mathbf{r}_0$ with dispersion σ and has an average momentum $\mathbf{p}_0$. In general, the evolved state at time t is obtained using the quantum mechanical propagator $K(\mathbf{r}'',\mathbf{r}';t)$,

$$\psi\left(\mathbf{r};t\right)=\int d^{d}r'\,K(\mathbf{r},\mathbf{r}';t)\,\psi\left(\mathbf{r}';0\right).$$

We make the semiclassical approximation by replacing the exact propagator by the semiclassical Van Vleck-Gutzwiller propagator (2.4)

$$K^{sc}(\mathbf{r}'',\mathbf{r}';t)=\sum_{j}\left(2\pi i\hbar\right)^{-d/2}C_{j}^{1/2}\exp\left(\frac{i}{\hbar}S_{j}-i\frac{\pi}{2}\nu_{j}\right). \tag{5.8}$$

Here $C_j=\left|\det\left(\partial^{2}S_{j}/\partial\mathbf{r}''\partial\mathbf{r}'\right)\right|$ is the absolute value of the Van Vleck determinant, which guarantees the conservation of classical probabilities. The phase is determined by the action $S_j\left(\mathbf{r}'',\mathbf{r}';t\right)$ along the jth classical trajectory connecting $\mathbf{r}'$ with $\mathbf{r}''$ in time t,

$$S_{j}\left(\mathbf{r}'',\mathbf{r}';t\right)=\int_{0}^{t}dt'L\left[\mathbf{r}\left(t'\right),\dot{\mathbf{r}}\left(t'\right),t'\right].$$

Finally, Maslov index ν_j gives correction to the phase due to the passage through conjugate points where Van Vleck determinant is singular.

Expanding each contribution in the Van Vleck propagator (5.8) about a central trajectory [120],

$$K_{j}^{sc}\left(\mathbf{r}'',\mathbf{r}';t\right)\approx K_{j}^{sc}\left(\mathbf{r}'',\mathbf{r}_{0};t\right)\exp\left[\frac{i}{\hbar}\left.\frac{\partial S_{j}}{\partial\mathbf{r}'}\right|_{\mathbf{r}'=\mathbf{r}_{0}}\cdot\left(\mathbf{r}'-\mathbf{r}_{0}\right)\right],$$

and applying this new form to the initial state (5.7), yields the evolved state at time t,

$$\begin{aligned}\psi^{sc}(\mathbf{r};t) &\approx \left(\pi\sigma^2\right)^{-d/4}\sum_j K_j^{sc}(\mathbf{r},\mathbf{r}_0;t)\\ &\quad\times\int d^dr'\exp\left[\frac{i}{\hbar}\left(\mathbf{p}_0-\mathbf{p'}_j\right)\cdot\left(\mathbf{r'}-\mathbf{r}_0\right)-\left(\mathbf{r'}-\mathbf{r}_0\right)^2/2\sigma^2\right]\\ &= \left(4\pi\sigma^2\right)^{d/4}\sum_j K_j^{sc}(\mathbf{r},\mathbf{r}_0;t)\exp\left[-\left(\mathbf{p'}_j-\mathbf{p}_0\right)^2\sigma^2/2\hbar^2\right]. \end{aligned} \tag{5.9}$$

It should be noted that this does not amount to linearizing the dynamics. The nonlinearity is still accounted for by retaining the full number of terms in the propagator. Using expression (5.9) for states evolved with H^0 and H^V, respectively, we find the overlap amplitude

$$\begin{aligned}O(t) &= \left\langle\psi^{sc,V}(t)\,|\psi^{sc}(t)\right\rangle\\ &= \left(\sigma^2/\pi\hbar^2\right)^{d/2}\int d^dr\sum_{j,j'}\left(C_j^V C_{j'}\right)^{1/2}\exp\left[\frac{i}{\hbar}\left(S_j^V-S_{j'}\right)-\frac{i\pi}{2}\left(\nu_j^V-\nu_{j'}\right)\right]\\ &\quad\times\exp\left\{-\left[\left(\mathbf{p}'_j-\mathbf{p}_0\right)^2+\left(\mathbf{p}'_{j'}-\mathbf{p}_0\right)^2\right]\sigma^2/2\hbar^2\right\}\end{aligned} \tag{5.10}$$

where $S_j = S_j(\mathbf{r},\mathbf{r}_0;t)$. At this point, two crucial approximations are made in Refs. [66, 19]: First, only the *diagonal terms* $j = j'$ are considered. Ref. [66] claims that these are the only terms surviving the average over impurities in disordered systems [107, 108]. Below we show that this is not a separate approximation, but that it follows from the classical perturbation approximation and does not require any ensemble averaging. The *classical perturbation approximation*, the second approximation used in Refs. [66, 19] is based on an apparently hopeless assumption that the perturbation does not affect trajectories (i.e., $C_j^V \approx C_j$ and $\nu_j^V \approx \nu_j$) but only affects the actions, through

$$\Delta S_j = S_j^V - S_j = -\int_0^t dt'\,V\left[\mathbf{r}_j(t')\right]. \tag{5.11}$$

Of course this assumption is wrong for individual trajectories which deviate exponentially with time. The reason why the approximation works in quantum mechanics is subtle: The first step to understanding why it yields accurate wave functions lies in the structural stability of the manifolds, as pointed out in Ref. [19]. Assuming that perturbation does not cause a bifurcation and does not significantly change the stable manifold, the evolved manifolds almost exactly overlap whereas the same initial points deviate exponentially by sliding along the manifold [19].

The second step goes as follows: consider trajectories $A(t)$, $A^V(t)$, $t \in [0, t_0]$, under the flow of H^0, H^V, respectively. Let $A(0) = A^V(0)$ be a point on the Lagrangian manifold supporting the wave function at $t = 0$. While $A^V(t)$ exponentially diverges from $A(t)$, if the evolved manifolds (almost) exactly overlap, we can find a point $B(0)$ on the manifold at $t = 0$ such that $B^V(t_0)$ (almost) coincides with $A(t_0)$. Because of the exponential sensitivity to the initial conditions, point $B(0)$ will be exponentially close to $A(0)$. Trajectories $A(t)$ and $B(t)$ remain exponentially close for all intermediate times from $t = 0$ to $t = t_0$, so if we use these particular trajectories to find $\psi(t)$ and $\psi^V(t)$, respectively, the classical perturbation approximation will be justified.

The diagonal approximation and classical perturbation approximation enormously simplify expression (5.10) for the overlap amplitude:

$$O(t) = \left(\sigma^2/\pi\hbar^2\right)^{d/2} \int d^d r \sum_j C_j \exp\left[i\Delta S_j/\hbar - \left(\mathbf{p}'_j - \mathbf{p}_0\right)^2 \sigma^2/\hbar^2\right]. \qquad (5.12)$$

Expression (5.12) for the overlap would be still very difficult to implement numerically for three reasons: First, in chaotic systems there is an exponentially growing number of contributing trajectories. Second, the accuracy would be compromised by proliferating caustic singularities in the Van Vleck determinant C_j whenever $\partial\mathbf{r}/\partial\mathbf{p}'_j = 0$. Finally, for each trajectory we would have to perform a computationally expensive root-search to find initial momentum $\mathbf{p}'_j$ that satisfies $\mathbf{r}\left(\mathbf{r}_0, \mathbf{p}'_j, t\right) = \mathbf{r}$. Because of these difficulties, both Refs. [66, 19] at this point resort to statistical arguments to obtain analytical results.

Our goal was to find a way around these difficulties and obtain a numerically implementable semiclassical expression to test these statistical arguments. Indeed, there exists a beautiful and simple way to eliminate the exponentially growing number of terms, caustic singularities and the root search, all at the same time. All three problems can be solved if we evaluate the overlap (5.10) in the initial momentum instead of final position representation. Exactly one point on the evolved manifold corresponds to each initial momentum, so no summation is necessary. The new "Van Vleck determinant" is exactly 1, so there will be no Maslov indices either. With all these simplifications, the semiclassical evaluation becomes tractable; in principle, it yields the same result that an arduous evaluation of (5.12) would:

$$O(t) = \left(\sigma^2/\pi\hbar^2\right)^{d/2} \int d^d p' \exp\left[i\Delta S\left[\mathbf{r}\left(\mathbf{r}_0, \mathbf{p}', t\right), \mathbf{r}_0, t\right]/\hbar - \left(\mathbf{p}' - \mathbf{p}_0\right)^2 \sigma^2/\hbar^2\right]. \qquad (5.13)$$

The only assumption required to derive (5.13) is the validity of the classical perturbation approximation, in the extended sense described above. Ensemble averaging used in Ref. [66]

is unnecessary: result (5.13) is also correct for pure states and for a fixed potential. Expression (5.13) is a special form of the initial value representation (Section 2.4) [83]. We note the unique property of the initial value representation: in this representation, fidelity decay is only due to dephasing. In other representations, the decay can also have a component due to the decay of classical overlaps.

5.5 Limiting cases of the uniform semiclassical result

We proceed by discussing how the uniform method helps to analyze various regimes of decay. The uniform semiclassical expression (5.13), which does not take into account correlations in the discrete quantum mechanical spectrum, cannot describe the perturbative regime except for short times (before the Heisenberg time). In this section we therefore focus on larger perturbations and show how the uniform expression leads to the Fermi-golden-rule and Lyapunov regimes as its special limiting cases.

These two types of decay, discussed first in Ref. [66], exist already within the classical perturbation approximation. First, there is decay related to dephasing of trajectories with uncorrelated actions. Second, there is decay related to dephasing of very near trajectories with correlated actions. As we show more rigorously in a moment, the fraction f of trajectories that have not dephased almost at all decreases as $f \sim e^{-\lambda t}$. Roughly speaking, the fidelity will decay as

$$\begin{aligned} M(t) &\sim (1-f)M_{FGR}(t) + f \\ &\sim \exp(-\Gamma t/\hbar) + e^{-\lambda t}. \end{aligned}$$

For smaller perturbations, the first type of decay is slower and dominates the behavior of fidelity: this happens in the Fermi-golden-rule regime. For larger perturbations, dephasing of uncorrelated trajectories is so fast that the quantum overlap is determined by the fraction of near trajectories that have remained in phase. This is the case in the Lyapunov regime.

Let us derive the two regimes more carefully: Using Eq. (5.13), fidelity can be written as a weighted average of terms $\exp\left[i(\Delta S' - \Delta S'')/\hbar\right]$,

$$\begin{aligned} M_{\text{unif}}(t) = \left(\frac{\sigma^2}{\pi\hbar^2}\right)^d \int d^d p' \int d^d p'' \exp\left[\frac{i}{\hbar}(\Delta S' - \Delta S'')\right] \\ \times \exp\left\{-\left[\left(\mathbf{p}' - \mathbf{p}_0\right)^2 + \left(\mathbf{p}'' - \mathbf{p}_0\right)^2\right]\sigma^2/\hbar^2\right\} \end{aligned} \tag{5.14}$$

where $\Delta S' \equiv \Delta S(\mathbf{r}_0, \mathbf{p}', t)$ corresponds to a trajectory with initial position $\mathbf{r}_0$ and momentum $\mathbf{p}'$, and similarly $\Delta S'' \equiv \Delta S(\mathbf{r}_0, \mathbf{p}'', t)$. Assuming the averaging window (i.e., the momentum width of the wavepacket) is large enough, we can make the replacement

$$\exp\left[i(\Delta S' - \Delta S'')/\hbar\right] \approx \left\langle \exp\left[i(\Delta S' - \Delta S'')/\hbar\right] \right\rangle \tag{5.15}$$

in Eq. (5.14) where averaging is over all initial momenta p', p''. As we show below, the difference $\Delta S' - \Delta S''$ is quite generally Gaussian distributed with a zero average, and consequently the average in Eq. (5.15) becomes

$$\left\langle \exp\left[i(\Delta S' - \Delta S'')/\hbar\right] \right\rangle = \exp\left[-\langle(\Delta S' - \Delta S'')^2\rangle/2\hbar^2\right]. \tag{5.16}$$

The important remaining question is whether the distributions $\Delta S'$ and $\Delta S''$ are correlated. The variance of $\Delta S' - \Delta S''$ depends on the answer to this question. Of course the transition between perfect correlation and no correlation is not abrupt, but depending on which situation is dominant, we also obtain two different regimes of fidelity decay.

5.5.1 Fermi-golden-rule regime

Due to the chaotic nature of H^0, action differences $\Delta S'$ and $\Delta S''$ are not correlated for long enough times t or for large enough difference of the initial momenta $|\mathbf{p}'' - \mathbf{p}'|$. In this case, the variance of $\Delta S'$ and $\Delta S''$ is just twice the variance of ΔS and is independent of the initial momenta,

$$\left\langle \left[\Delta S\left(p'\right) - \Delta S\left(p''\right)\right]^2 \right\rangle = 2\sigma^2_{\Delta S}. \tag{5.17}$$

The same conclusion can be reached from Eq. (5.15) by writing

$$\left\langle \exp\left[i(\Delta S' - \Delta S'')/\hbar\right] \right\rangle \approx \left\langle e^{i\Delta S'/\hbar} \right\rangle \left\langle e^{-i\Delta S''/\hbar} \right\rangle \tag{5.18}$$

for uncorrelated factors and using the result

$$\left\langle \exp\left(i\Delta S/\hbar\right) \right\rangle = \exp\left[i\left\langle \Delta S \right\rangle/\hbar - \sigma^2_{\Delta S}/2\hbar^2\right] \tag{5.19}$$

for Gaussian distributed ΔS. We can intuitively understand why ΔS is Gaussian distributed if we think of integral (5.11) as a continuous limit of a "random-walk" whose step at time t is the perturbation $V\left[\mathbf{r}\left(t'\right)\right]$ at position $\mathbf{r}\left(t'\right)$,

$$\Delta S = S^V - S = -\int_0^t dt'\, V\left[\mathbf{r}\left(t'\right)\right] = -\lim_{n\to\infty} \sum_{j=1}^{n} V\left[\mathbf{r}\left(j\,\Delta t\right)\right] \Delta t, \quad \Delta t = \frac{t}{n}.$$

For strongly chaotic Hamiltonians H^0, the correlations are quickly lost, and the central limit guarantees that the distribution of ΔS indeed approaches a Gaussian with a linearly increasing action variance

$$\sigma_{\Delta S}^2 = 2Kt. \tag{5.20}$$

How this diffusive process comes about can be seen explicitly by writing the variance of action differences as

$$\left\langle (\Delta S)^2 \right\rangle (t) = \int_0^t dt' \int_0^t dt'' \left\langle V\left[\mathbf{r}\left(t'\right)\right] V\left[\mathbf{r}\left(t''\right)\right]\right\rangle .$$

Changing variables to $\overline{t} = \left(t' + t''\right)/2$, $\tau = t'' - t'$ and assuming that the correlation of the potential is translationally invariant, gives

$$\begin{aligned}\left\langle (\Delta S)^2 \right\rangle &\approx \int_0^t dt' \int_{-\infty}^{\infty} d\tau \left\langle V\left[\mathbf{r}\left(t'\right)\right] V\left[\mathbf{r}\left(t'+\tau\right)\right]\right\rangle \\ &\approx 2\int_0^t dt' \int_0^{\infty} d\tau \left\langle V\left[\mathbf{r}\left(0\right)\right] V\left[\mathbf{r}\left(\tau\right)\right]\right\rangle \approx 2Kt,\end{aligned}$$

with the classical action diffusion constant

$$K = \int_0^{\infty} d\tau \left\langle V\left[\mathbf{r}\left(0\right)\right] V\left[\mathbf{r}\left(\tau\right)\right]\right\rangle .$$

Applying approximations (5.15), (5.16), (5.17), and result (5.20) in Eq. (5.14), gives the exponential Fermi-golden-rule decay (5.4) [66, 19].

5.5.2 Lyapunov regime

No matter how strongly chaotic H^0 is, action differences $\Delta S'$ and $\Delta S''$ are uncorrelated for short enough times t or for small enough differences of the initial momenta $|\mathbf{p}'' - \mathbf{p}'|$. In this case simplification (5.18) is not possible. However, we can make another simplification: in order for the action differences $\Delta S'$ and $\Delta S''$ to remain uncorrelated, the trajectories must be near to each other, justifying the approximation

$$\Delta S' - \Delta S'' = \int_0^t dt' \left\{V\left[\mathbf{r}''\left(t'\right)\right] - V\left[\mathbf{r}'\left(t'\right)\right]\right\} \approx \int_0^t dt' \nabla V\left[\mathbf{r}'\left(t'\right)\right] \cdot \left[\mathbf{r}''\left(t'\right) - \mathbf{r}'\left(t'\right)\right].$$

In chaotic systems, there is an exponential divergence of trajectories,

$$\left|\mathbf{r}''\left(t\right) - \mathbf{r}'\left(t\right)\right| \sim \left|\mathbf{p}'' - \mathbf{p}'\right| e^{\lambda t} \tag{5.21}$$

With this approximation, we have a "random walk with an exponentially increasing step,"

$$\Delta S' - \Delta S'' \sim \int_0^t dt' \left|\nabla V\left[\mathbf{r}'\left(t'\right)\right]\right| \left|\mathbf{p}'' - \mathbf{p}'\right| e^{\lambda t'}.$$

If the growth of the random-walk step is slow enough that the central-limit-theorem equilibrium is achieved for all times, we find that the growth of the variance is governed by the equation

$$d\left\langle \left(\Delta S' - \Delta S''\right)^2 \right\rangle \sim 2Ce^{2\lambda t}dt \tag{5.22}$$

where the diffusion constant C is given by

$$\begin{aligned} C &= \left(\mathbf{p}'' - \mathbf{p}'\right)^2 D, \\ D &= \int_0^\infty d\tau \, \left\langle \nabla V\left[\mathbf{r}\left(0\right)\right] \cdot \nabla V\left[\mathbf{r}\left(\tau\right)\right] \right\rangle. \end{aligned} \tag{5.23}$$

Eq. (5.22) can be integrated analytically, giving

$$\left\langle \left(\Delta S' - \Delta S''\right)^2 \right\rangle (t) \sim \frac{C}{\lambda}\left(e^{2\lambda t} - 1\right).$$

Approximation (5.21) is only valid for $\lambda t \gg 1$, so we can finally write

$$\left\langle \left(\Delta S' - \Delta S''\right)^2 \right\rangle (t) \sim \frac{D}{\lambda}\left(\mathbf{p}'' - \mathbf{p}'\right)^2 e^{2\lambda t}. \tag{5.24}$$

Using approximations (5.15), (5.16) together with the result (5.24) in Eq. (5.14) gives

$$\begin{aligned} M\left(t\right) \sim \left(\frac{\sigma^2}{\pi\hbar^2}\right)^d \int d^d p' \int d^d p'' \exp\left[-\frac{D}{2\lambda\hbar^2}\left(\mathbf{p}'' - \mathbf{p}'\right)^2 e^{2\lambda t}\right] \\ \times \exp\left\{-\left[\left(\mathbf{p}' - \mathbf{p}_0\right)^2 + \left(\mathbf{p}'' - \mathbf{p}_0\right)^2\right]\frac{\sigma^2}{\hbar^2}\right\}. \end{aligned}$$

Changing variables to $\mathbf{p}_1 = \left(\mathbf{p}' + \mathbf{p}'' - 2\mathbf{p}_0\right)/\sqrt{2}$, $\mathbf{p}_2 = \left(\mathbf{p}'' - \mathbf{p}'\right)/\sqrt{2}$, factors the integral as

$$M\left(t\right) \sim \left(\frac{\sigma^2}{\pi\hbar^2}\right)^d \int d^d p_1 \exp\left(-\mathbf{p}_1^2\frac{\sigma^2}{\hbar^2}\right) \int d^d p_2 \exp\left[-\left(\frac{D}{\lambda\hbar^2}e^{2\lambda t} + \frac{\sigma^2}{\hbar^2}\right)\mathbf{p}_2^2\right]$$

giving

$$M\left(t\right) \sim \left(1 + e^{2\lambda t}D/\lambda\sigma^2\right)^{-1/2} \approx \left(\lambda\sigma^2/D\right)^{1/2} e^{-\lambda t}, \tag{5.25}$$

in agreement with Eq. (5.5).

5.6 Numerical results

In this section, we test our uniform semiclassical expression (5.13) numerically. In previous numerical experiments analytical predictions of Gaussian or exponential decay have been compared to an exact quantum calculation [7, 19, 31, 39, 65, 100, 139]. While we also have an exact quantum benchmark[3] with which to compare the expressions for various regimes, we reiterate that it would be hard from a mere comparison of analytical with final numerical results for $M(t)$ to determine the source of errors.

We chose to test our method on the standard map, described below in Section 5.6.1, for which there is an analytical expression for the diffusion constant K [19]. We note that results of exact quantum and semiclassical computations which we present in Sections 5.6.2-5.6.4 are for initial position eigenstate with $q_0 = 0.5$ rather than a wavepacket.

5.6.1 Standard map

Standard (also called *Chirikov*) *map* [23] is a symplectic map on a torus, defined by equations,

$$\begin{aligned} q_{j+1} &= q_j + p_j \pmod 1, \\ p_{j+1} &= p_j - \frac{k}{2\pi}\sin\left(2\pi q_{j+1}\right) \pmod 1, \end{aligned}$$

with a single parameter k. This discrete map can be understood as a Poincaré map of dynamics due to a time-dependent "kicked" Hamiltonian

$$\begin{aligned} H(q,p,t) &= \frac{1}{2}p^2 + V(q,t), \\ V(q,t) &= -\frac{k}{(2\pi)^2}\cos\left(2\pi q\right)\sum_{j=-\infty}^{\infty}\delta\left(t-j\right). \end{aligned}$$

For $k = 0$ this is an integrable system, but as k is increased, larger and larger part of phase space becomes chaotic.

Quantum version of this map,

$$|\psi_{j+1}\rangle = \hat{U}\,|\psi_j\rangle,$$

uses a one-step evolution operator

$$\hat{U} = \exp\left(-i\hat{V}/\hbar\right)\,\exp\left(-i\hat{p}^2/2\hbar\right).$$

[3] Our exact quantum calculation uses the fast Fourier transform algorithm.

As usual, the numerical evolution of $|\psi\rangle$ is best accomplished using the fast Fourier transform algorithm. The kinetic evolution is performed in the momentum representation while the potential evolution is performed in the coordinate representation. The Hilbert space is n-dimensional, which fixes the value of the effective Planck's constant to be

$$\hbar = (2\pi n)^{-1}\,.$$

Following Ref. [19], the perturbation for our fidelity calculations is achieved by changing the kicking strength k by a small amount ϵ,

$$k \to k + \epsilon.$$

5.6.2 Perturbative regime

In the perturbative regime (see Fig. 5.1), we do not expect any semiclassical approach to work very well except for short times (much shorter than the Heisenberg time $t_H = h/\Delta$). The random-matrix-theory analytical result M_{PT} from Ref. [19] gives an excellent agreement in this case. The inset shows, however, that before the Gaussian decay M_{PT} sets in at the Heisenberg time, the uniform expression follows M_{exact} much better.

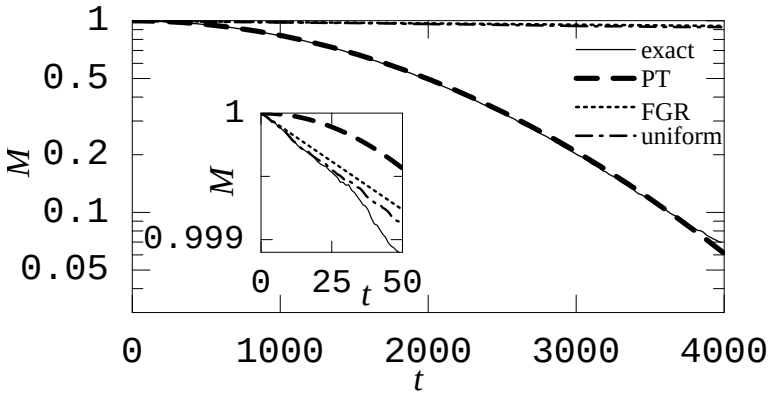

Figure 5.1: Fidelity in the perturbative regime ($k = 18$, $\lambda \approx 2.21$, $\epsilon = 10^{-4}$, $t_H \approx n = 350$). Inset: detail for short times.

5.6.3 Fermi-golden-rule regime

Transition from the perturbative to Fermi-golden-rule regime occurs for $\epsilon^2 \approx 32\pi^2 n^{-3}[1 + 2J_2(k)]^{-1}$ [19] when most of the overlap has decayed before Heisenberg time.

Fig. 5.2 shows fidelity decay in the Fermi-golden-rule regime. It is apparent that M_{unif} matches M_{exact} better than the M_{FGR} since M_{unif} takes into account the precise initial conditions without the averaging assumption (5.15) and since M_{FGR} uses an analytic result for K, which is only approximate [19]. In the inset, histogram of action differences is compared with a Gaussian fit, confirming assumption (5.19). Careful inspection of the short time regime (not shown) reveals that M_{unif} agrees with M_{exact}, since unlike M_{FGR}, M_{unif} does not depend on the central limit theorem which guarantees the Gaussian assumption (5.19) at later times.

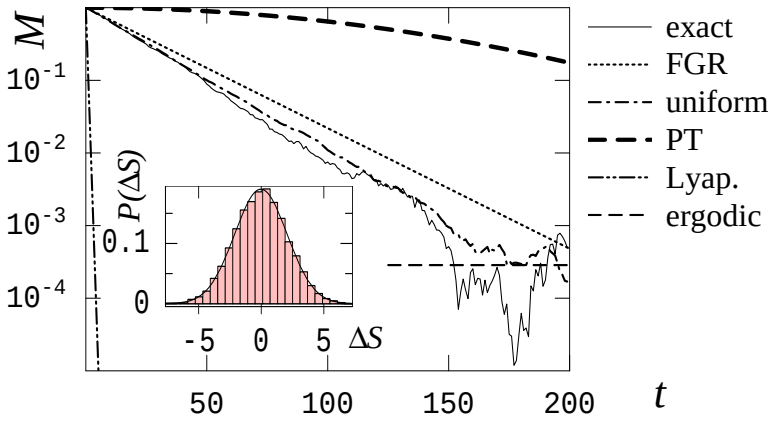

Figure 5.2: Fidelity in the Fermi-golden-rule regime ($k = 18$, $\lambda \approx 2.21$, $\epsilon = 5 \times 10^{-4}$, $n = 3500$). Horizontal dashed line ("ergodic") is the limit of fidelity decay due to the finite size of Hilbert space. Inset: Histogram of action differences compared to a Gaussian fit.

5.6.4 Lyapunov regime

Transition from the Fermi-golden-rule to Lyapunov regime occurs for $\epsilon^2 \approx 8\pi^2 \lambda n^{-2}[1+2J_2(k)]^{-1}$ when the Fermi-golden-rule decay rate is larger than λ.

Fig. 5.3 displays $M(t)$ in the Lyapunov regime. It shows that while M_L gives an accurate average decay only for $\lambda t \gg 1$, M_{unif} correctly follows the behavior of M_{exact} even for short times $t \sim \lambda^{-1}$. The inset shows the variance of $\Delta S(p') - \Delta S(p'')$ as a function of $p' - p''$ at a fixed time and justifies the assumption made in Ref. [66] in derivation of perturbation independent decay: for near trajectories, the variance grows quadratically with $p' - p''$ (fitted line gives an exponent 2.003), in accordance with Eq. (5.24),

$$\left\langle \left(\Delta S' - \Delta S''\right)^2 \right\rangle (t) \sim \frac{D}{\lambda} \left(p'' - p'\right)^2 e^{2\lambda t}, \tag{5.26}$$

while for distant trajectories, in accordance with the derivation of the Fermi-golden-rule regime (Eqs. (5.17) and (5.20)), the variance is independent of $p' - p''$,

$$\left\langle \left[\Delta S\left(p'\right) - \Delta S\left(p''\right)\right]^2 \right\rangle = 2\sigma^2_{\Delta S} = 4Kt. \tag{5.27}$$

The time dependence of $\left\langle \left[\Delta S\left(p'\right) - \Delta S\left(p''\right)\right]^2 \right\rangle$ for fixed $p' - p''$ is shown in Fig. 5.4.

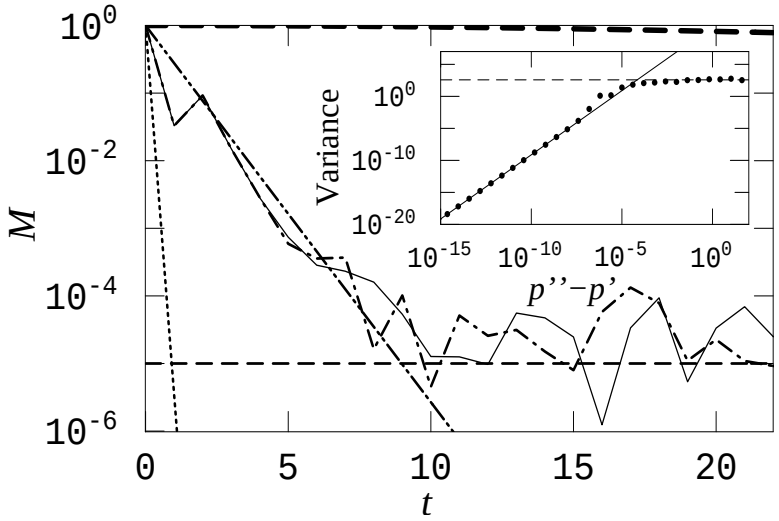

Figure 5.3: Fidelity in the Lyapunov regime ($k = 7$, $\lambda \approx 1.28$, $\epsilon = 5 \times 10^{-4}$, $n = 10^5$). Meaning of lines same as in Fig. 5.2. Inset: Variance of $\Delta S\left(p''\right) - \Delta S\left(p'\right)$ as a function of $p'' - p'$ at time $t = 7$. Dots are numerically calculated, dashed line is the horizontal asymptote $2\sigma^2_{\Delta S}$ from Eq. (5.27), solid line is a linear fit for small $p'' - p''$, in agreement with Eq. (5.26).

Part a) shows that for short times when trajectories are still correlated, this dependence is exponential, in agreement with Eq. (5.26). Part b) shows that for longer times, when correlation is lost, the dependence is linear, as expected from Eq. (5.27).

5.7 Fidelity in quasi-integrable systems

Most of this chapter was concerned with quantum fidelity in classically chaotic systems. Is the situation different if H^0 is integrable or quasi-integrable? Various authors have studied this question and observed several regimes, again depending on the strength of perturbation. Although the research of fidelity for integrable systems has not been so extensive as for chaotic systems, it appears that with increasing perturbation strength, the fidelity decay can be Gaussian [100, 20], exponential [64], or algebraic [64]. The Gaussian

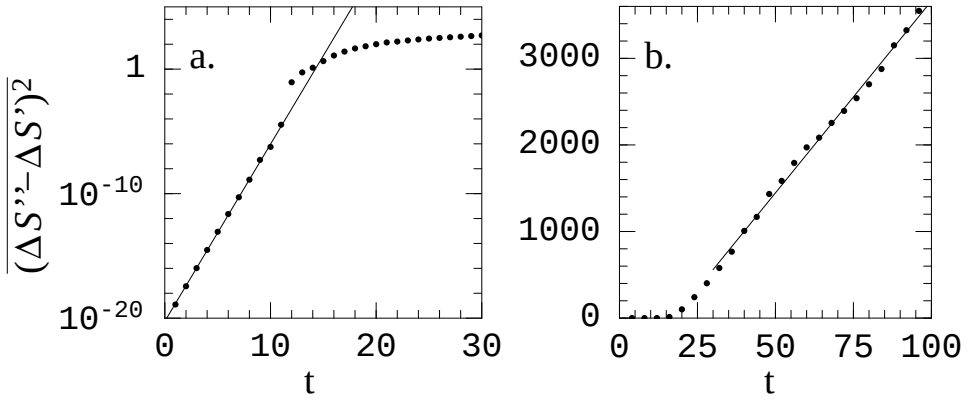

Figure 5.4: Variance of $\Delta S\left(p''\right)-\Delta S\left(p'\right)$ as a function of t for $p''-p'=10^{-11}$: a) exponential dependence for short times (see Eq. (5.26)) , b) linear dependence for long times (see Eq. (5.27)) .

and exponential regimes are analogous to the perturbative and Fermi-golden-rule regimes for chaotic systems from Sections 5.3 and 5.5.1. For strong perturbations, fidelity decays very differently in chaotic and quasi-integrable systems: while in chaotic systems, the decay is exponential (Lyapunov regime of Section 5.5.2), in quasi-integrable systems, it is algebraic [64],

$$M_{\mathrm{alg}}(t)\sim t^{-3d/2}. \tag{5.28}$$

where d is the number of degrees of freedom.

Here we present a simple derivation of this regime from the uniform expression (5.13). That our uniform expression is valid for regular systems should not be surprising, since no part of the derivation in Section 5.4 relied on chaoticity of H^0. In fact, as was mentioned there, it is easier to understand the classical perturbation approximation in quasi-integrable systems. We can use very similar reasoning as in the derivation of the Lyapunov regime in Section 5.5. The difference comes in Eq. (5.21): in quasi-integrable systems, the divergence of trajectories is only a linear function of time,

$$\mathbf{r}''\left(t\right)-\mathbf{r}'\left(t\right)\approx\left(\mathbf{p}''-\mathbf{p}'\right)\,t. \tag{5.29}$$

We have a "random walk with a linearly growing step,"

$$\Delta S'-\Delta S''\approx\int_0^t dt'\,\nabla V\left[\mathbf{r}'\left(t'\right)\right]\cdot\left(\mathbf{p}''-\mathbf{p}'\right)\,t'.$$

If the growth of the random-walk step is slow enough that the central-limit-theorem equilibrium is achieved for all times, we find that the growth of the variance is governed by the

equation

$$d\left\langle \left(\Delta S' - \Delta S''\right)^2 \right\rangle \approx 2Ct^2 dt \tag{5.30}$$

where the diffusion constant C is the same as in Section 5.5.2. Eq. (5.30) can be integrated analytically, giving

$$\left\langle \left(\Delta S' - \Delta S''\right)^2 \right\rangle (t) \approx \frac{2}{3} C\, t^3 \sim \frac{2}{3} D\, \left(\mathbf{p}'' - \mathbf{p}'\right)^2 t^3. \tag{5.31}$$

Using approximations (5.15), (5.16) together with the result (5.31) in Eq. (5.14) we find

$$\begin{aligned} M(t) \approx \left(\frac{\sigma^2}{\pi\hbar^2}\right)^d \int d^d p' \int d^d p'' \exp\left[-\frac{1}{3\hbar^2} D\, \left(\mathbf{p}'' - \mathbf{p}'\right)^2 t^3\right] \\ \times \exp\left\{-\left[\left(\mathbf{p}' - \mathbf{p}_0\right)^2 + \left(\mathbf{p}'' - \mathbf{p}_0\right)^2\right] \frac{\sigma^2}{\hbar^2}\right\}. \end{aligned} \tag{5.32}$$

Changing variables to $\mathbf{p}_1 = \left(\mathbf{p}' + \mathbf{p}'' - 2\mathbf{p}_0\right)/\sqrt{2}$, $\mathbf{p}_2 = \left(\mathbf{p}'' - \mathbf{p}'\right)/\sqrt{2}$, factors the integral as

$$M(t) \sim \left(\frac{\sigma^2}{\pi\hbar^2}\right)^d \int d^d p_1 \exp\left(-\mathbf{p}_1^2 \frac{\sigma^2}{\hbar^2}\right) \int d^d p_2 \exp\left\{-\left(\frac{2}{3\hbar^2} D\, t^3 + \frac{\sigma^2}{\hbar^2}\right) \mathbf{p}_2^2\right\},$$

giving

$$M(t) \sim \left(1 + 2D\, t^3/3\sigma^2\right)^{-d/2} \approx \left(2D/3\sigma^2\right)^{d/2} t^{-3d/2},$$

in agreement with Eq. (5.28).

5.8 Short-time behavior of fidelity

While the main focus of this chapter has been the fidelity decay after the transient behavior at very short times, for completeness we briefly address this short-time behavior in this section.

5.8.1 Quadratic decay

Independently of the nature of the Hamiltonian H^0, for very short times the perturbation-theory result (5.6) gives a quadratic decay [98],

$$M_{\text{quadr}}(t) \approx 1 - (\Delta V)^2 \frac{t^2}{\hbar^2} + O\left((\Delta V)^4 \frac{t^4}{\hbar^4}\right) \tag{5.33}$$

where

$$\begin{aligned} (\Delta V)^2 &= \sum_n |a_n|^2 V_{nn}^2 - \left(\sum_n |a_n|^2 V_{nn}\right)^2 \\ &= \left\langle \psi \left| V^2 \right| \psi \right\rangle - \left\langle \psi \left| V \right| \psi \right\rangle^2. \end{aligned}$$

This initial decay depends only on the perturbation V and the initial state ψ, and not on the unperturbed Hamiltonian H^0. Fidelity decays quadratically for times

$$t \ll \frac{\hbar}{\Delta V}.$$

5.8.2 Double exponential decay

The Lyapunov decay (5.5) of fidelity derived for large perturbations in chaotic systems in Section 5.5.2 sets in only after the Ehrenfest time

$$t_E = \frac{1}{2}\lambda^{-1} \log \frac{\Omega}{\hbar^d}$$

when the system forgets completely the precise initial conditions. In the expression above, Ω is the volume of accessible phase space. As pointed out in Ref. [113], before Ehrenfest time, the fidelity decay of a pure state follows a double exponential

$$M_{\text{d.exp.}}(t) \sim \exp\left(-\text{const.} \times \frac{\epsilon^2}{\hbar} e^{2\lambda t}\right), \quad t \ll t_E. \tag{5.34}$$

This result would be obtained from Eq. (5.32) if $(\mathbf{p}' - \mathbf{p}'')^2$ were replaced by the expected value $\hbar^2/\sigma^2$ since diffusion constant (5.23) $D \propto \epsilon^2$ and the dispersion of a wavepacket symmetric in phase space is $\sigma \propto \hbar^{1/2}$. In any case, result (5.34) is consisted with expression (5.25) for times

$$t \ll \frac{1}{2\lambda} \log \frac{\lambda \sigma^2}{D},$$

since then both expressions (5.34) and (5.25) reduce to

$$M(t) \approx 1 - \frac{D}{2\lambda\sigma^2} e^{2\lambda t}.$$

5.9 Conclusion

To conclude, we have explicitly evaluated semiclassical expression for quantum fidelity. While it was thought that such semiclassical expression would be intractable numerically, we have obtained remarkably accurate results for fidelity decay in both the Fermi-golden-rule and Lyapunov regimes. We provided a more detailed explanation why classical perturbation approximation can be used in chaotic systems and employed our method to test other approximations used in Refs. [66, 19]. The success of the semiclassical approach depends on the use of the initial momentum representation which avoids the singularities in

the Van Vleck determinant. In fact, Van Vleck determinant in this representation is simply equal to one, and the decay is entirely due to dephasing. In this sense, the initial momentum representation is special, because in other representations, fidelity decay is generally due to both dephasing and to the decay of classical overlaps [64]. The derivation of various regimes of fidelity decay is particularly simple from this "dephasing picture" expressed in our uniform expression (5.13): whether the decay is Fermi-golden-rule, Lyapunov or algebraic, only depends on how the variance of action differences $\left\langle [\Delta S(p') - \Delta S(p'')]^2 \right\rangle$ grows with time.

Chapter 6

Survival probability and the local density of states for one-dimensional Hamiltonian systems

For chaotic systems there is a theory for the decay of survival probability, and for the parametric dependence of the local density of states. This theory leads to the distinction between "perturbative" and "non-perturbative" regimes, and to the observation that standard semiclassical tools are useful in the latter case. This chapter discusses what is left from this theory in the case of one-dimensional systems. It is shown here that a remarkably accurate *uniform* semiclassical approximation captures the physics of *all* the different regimes, though it cannot take into account the effect of strong localization.

6.1 Introduction

The quantum mechanical state of a particle, or of a system, is represented by the probability matrix ρ. This object corresponds to a classical distribution $\rho^{cl}(Q,P)$ in phase space, where Q and P are the canonical coordinates of the system. One way to represent the probability matrix is by using the Wigner function $\rho(Q,P)$. Many calculations in quantum mechanics reduce eventually to calculation of a trace over a pair of probability

matrices. This includes in particular calculations of the local density of states (LDOS) [28], and calculations of the survival probability $\mathcal{P}(t)$ [56]. Strongly related are calculations of Franck-Condon factors for non-adiabatic transitions between Born-Oppenheimer surfaces [68, 112]. In Chapter 5 we obtained a uniform expression for "quantum fidelity" (also known as "Loschmidt echo") which has drawn a great amount of interest lately, especially in the context of decoherence and quantum computation [66, 31, 32, 33, 7, 19, 100, 99, 102, 37, 113, 65, 140, 127]. This "fidelity" is in fact a synonym for the survival probability $\mathcal{P}(t)$ which is calculated for a particular dynamical scenario (namely, the forward evolution is followed by a reversed evolution with a perturbed Hamiltonian).

The calculation of a trace over a pair of probability matrices has a clear classical limit. To be specific let us consider the survival probability, which is defined as

$$\mathcal{P}(t) = |\langle\psi_0|\psi_t\rangle|^2 = \mathrm{trace}(\rho_t\rho_0). \tag{6.1}$$

where ρ_t and ψ_t are the probability matrix and the associated wave function of an evolving quantum mechanical pure state. In the Wigner representation the trace operation means $dQdP/(2\pi\hbar)^d$ integral over phase space, where d is the number of freedoms. It should be emphasized that the Wigner representation is quantum-mechanically exact. The classical limit/approximation is obtained by treating $\rho(P,Q)$ as a classical distribution, whose evolution is governed by classical equations of motion.

To take the classical limit as a leading order approximation for $\mathcal{P}(t)$ is one possibility. Another possibility is to use perturbation theory, in particular "Fermi golden rule" (FGR). It should be obvious that the results that are obtained by using these methods are typically very different from each other.

A major objective of recent studies[1] is to understand the limitations of perturbation theory on the one hand, and to explore the capabilities of the semiclassical tools, on the other. A specific question is whether the decay of $\mathcal{P}(t)$ is of perturbative nature (e.g., FGR type[2]), or else whether it is of classical nature ("semiclassical" type). The main approach towards this question is to allow the specification of a control parameter that represents some "strength" of a perturbation. Depending on the value of of this control parameter one may have either perturbative or semiclassical behavior. The first publications

[1] For a pedagogical presentation, including references, see Refs. [27] and [25].

[2] In Section 6.5 we explain that perturbation theory can lead to either no decay, or Gaussian decay, or Wigner type decay. The latter can be regarded as the outcome of FGR transitions.

[24, 28] that have taken this approach, led to the distinction between perturbative and non-perturbative regimes, and to the realization that the semiclassical behavior is contained in the non-perturbative regime. Later [65] the idea was adopted into the context of quantum fidelity studies.

The above mentioned studies have mainly concentrated on quantized chaotic systems. The chaos assumption allows simplification of certain calculations. In particular one can invoke the random matrix theory (RMT) conjecture [13], in order to obtain some generic results. The natural question that arises is whether some of the general theory regarding the LDOS and $\mathcal{P}(t)$, applies also to the world of one dimensional ($d = 1$) systems.

A central observation in the theory of quantized chaotic systems is the existence of two distinct energy scales. One is the mean level spacing ($\Delta \propto \hbar^d$), while the other is the bandwidth ($\Delta_b \propto \hbar$). The latter is semiclassically related to the correlation time of the classical motion. The dimensionless bandwidth is defined as $b = \Delta_b/\Delta$. The classical limit ($\hbar \to 0$) of quantized chaotic system ($d > 1$) is characterized by $\Delta \ll \Delta_b$ and hence $b \gg 1$. But in one dimensional systems ($d = 1$) we do not necessarily have this separation of energy scales. For some typical perturbations $b = \mathcal{O}(1)$. We shall explain that in such case there is no FGR regime in the theory. A necessary, but not sufficient condition for having FGR regime in one-dimensional systems is to have $b \gg 1$. This means that "small features" should characterize the phase space manifolds that support the perturbed (or evolving) quantum mechanical states.

The analysis of one dimensional ($d = 1$) systems is highly non-universal, but typically allows analytical calculations that go well beyond the leading semiclassical approximation. In particular we demonstrate the capabilities and the limitations of the uniform approximation [125, 126].

The outline of this chapter is as follows: Section 6.2 defines several simple prototype models. In Section 6.3 we define the main objects of the studies which are the LDOS and the survival probability $\mathcal{P}(t)$. In Section 6.4 we discuss the issue of quantum-classical correspondence and make the distinction between semiclassical and perturbative approximations. Section 6.5 describes the various possible regimes in the context of the LDOS studies. In Section 6.6 and Section 6.7 we discuss the existence of the LDOS regimes in one-dimension within the framework of a uniform approximation. Section 6.8 considers the implication of the strong localization effect. Results of previous sections are extended in Section 6.9, into the context of survival probability studies. Conclusion and final remarks

are summarized in Section 6.10. Appendix D contains details of derivations, which have not been integrated into the main text in order to simplify the presentation of the physical picture.

6.2 Definition of models

In this chapter we are going to consider one-dimensional model systems. The simplest is the deformable harmonic oscillator:

$$\mathcal{H}(Q,P;x) = \tfrac{1}{2}(xP)^2 + \tfrac{1}{2}(Q/x)^2. \tag{6.2}$$

where (Q,P) are the canonical coordinates, and x is a constant parameter. The energy surfaces $\mathcal{H}(Q,P;x) = E$ are ellipses in phase space. We shall assume that $E \gg 1$. Without loss of generality we shall regard $x = x_0 = 1$ as the "unperturbed" value of the parameter x. Later we shall assume that $\delta x \equiv (x - x_0)$ is small in a *classical* sense. Namely $\delta x \ll 1$. Then it is possible to write the Hamiltonian as $\mathcal{H} = \mathcal{H}_0 + \delta\mathcal{H}$, where

$$\mathcal{H}_0 = \mathcal{H}(Q,P;x_0{=}1) \;=\; \frac{1}{2}(P^2+Q^2), \tag{6.3}$$

$$\delta\mathcal{H} = \delta x \left.\frac{\partial\mathcal{H}}{\partial x}\right|_{x=1} \;=\; \delta x\ (P^2 - Q^2) \tag{6.4}$$

Note that the perturbation δx is allowed to be large in a quantum mechanical sense: many levels can be mixed by the perturbation $\delta\mathcal{H}$.

A more complicated case is to consider a particle in a ring (= one dimensional box with periodic boundary conditions). The Hamiltonian is of the general form

$$\mathcal{H}(Q,P;x) = \frac{1}{2\mathsf{m}}P^2 + x\ V(Q) \tag{6.5}$$

Without loss of generality we can take $\mathsf{m} = 1$ as the mass of the particle, and $L = 2\pi$ as the perimeter (length) of the ring. The parameter x controls the "height" of the potential landscape. Naturally we shall regard $x_0 = 0$ as the unperturbed value of x. We shall consider the case of a single "bump" where

$$V(Q) = V_0 \exp\left[-\left(Q - Q_0\right)^2/2\ell^2\right] \tag{6.6}$$

It is implicitly assumed that $\ell \ll L$. The Fourier components of this potential are $|\tilde{V}(k)| = V_0\ell \exp\left[-(k\ell)^2/2\right]$. Hence the non-vanishing ($|k\ell| < 1$) Fourier components satisfy $|\tilde{V}(k)| \approx$

$V_0\ell$. If we have many bumps, then we have a "disordered" potential

$$V(Q) = \sum_{\alpha}(\pm\text{random})V_0 \exp\left[-\left(Q-Q_\alpha\right)^2/2\ell^2\right] \tag{6.7}$$

Here we implicitly assume that the bumps are non-overlapping and randomly distributed along the ring, such that the correlation function $\langle V(Q+r)V(Q)\rangle$ is characterized by the correlation length ℓ. Consequently the non-vanishing ($|k\ell| < 1$) Fourier components of the potential satisfy $|\tilde{V}(k)| \approx V_0\ell \times \sqrt{L/\ell}$. Note that the phases of the Fourier components look "random", unlike the case of a single bump.

All models that we have introduced are of the generic form $\mathcal{H} = \mathcal{H}_0 + \delta\mathcal{H}$. The representation in the basis that is determined by the unperturbed Hamiltonian is

$$\mathcal{H} \mapsto \mathbf{E} + \delta x \mathbf{B} \tag{6.8}$$

where $\mathbf{E} = \{E_n\}$ is a diagonal matrix consisting of the eigenenergies of the unperturbed Hamiltonian. With scaled parameters, such that $\hbar = 1$, the mean level spacing of the eigenenergies is $\Delta = 1$ for Hamiltonian (6.2) and $\Delta = \sqrt{2E}$ for Hamiltonian (6.5). The matrix $\mathbf{B}$ corresponds to the perturbation. It is a banded matrix. The bandwidth is b. It is defined such that $2b$ is the number of the levels which are coupled by the perturbation. For the Hamiltonian (6.2) we have $b = 1$, because only neighboring levels of the de-symmetrized Hamiltonian ($|n-m| = 2$) are coupled by the perturbation $\delta\mathcal{H}$. For the Hamiltonian (6.5) the bandwidth is $b = L/\ell$. See Section 6.6 for details. Thus for the latter model we may have $b \gg 1$.

6.3 Definitions of $P(n|m)$ and $\mathcal{P}(t)$

Let $|n(x)\rangle$ and $E_n(x)$ be the eigenstates and the corresponding eigenvalues of the Hamiltonian $\mathcal{H}(Q,P;x)$. We define the parametric kernel

$$P(n|m) = |\langle n(x)|m(x_0)\rangle|^2 = \text{trace}(\rho_n\rho_m). \tag{6.9}$$

Note that for $\delta x = 0$ we have $P(n|m) = \delta_{nm}$. Given a reference state $|m(x_0)\rangle$ this kernel can be regarded as a probability distribution with respect to n. The LDOS is just a scaled version of this kernel, namely

$$P(\omega) = \sum_n P(n|m)\ 2\pi\delta\Big(\omega - [E_n(x) - E_m(x_0)]\Big) \tag{6.10}$$

One important measure that characterizes the LDOS is its variance:

$$\delta E^2 = \sum_n P(n|m)\ (E_n - E_m)^2 \tag{6.11}$$

In the next section we shall explain that the variance has a special role in the theory of the LDOS.

The survival probability of the state $|m(x_0)\rangle$ for evolution which is generated by the perturbed Hamiltonian $\mathcal{H}(Q,P;x)$ can be written as $\mathcal{P}(t) = |F(t)|^2$, where

$$F(t) = \langle m(x_0)|\mathrm{e}^{-it(\mathcal{H}-E_m)}|m(x_0)\rangle \tag{6.12}$$

In the above definition we have taken $E = E_m$ as the natural reference for the energy. With this definition we see that $F(t)$ is just the Fourier transform of the LDOS. We note that in more complicated scenarios a simple Fourier transform relation between $F(t)$ and $P(\omega)$ does not exist [140].

6.4 Quantum-classical correspondence

The classical limit/approximation for the LDOS kernel $P(n|m)$ is obtained by taking for the Wigner function $\rho_n(Q,P) \approx \rho_n^{cl}(Q,P)$, where

$$\rho_n^{cl}(Q,P) \propto \delta\left[\mathcal{H}(Q,P;x) - E_n(x)\right]$$

is the corresponding classical microcanonical distribution. For the deformable harmonic oscillator one obtains (D.1):

$$P^{cl}(n|m) \approx \frac{1}{\pi}\frac{1}{\sqrt{4(\delta x/x)^2E^2 - (E_n - E_m)^2}} \tag{6.13}$$

The dispersion (square root of the variance) is

$$\delta E^{cl} = \sqrt{2}\left(\frac{\delta x}{x}\right)E \tag{6.14}$$

What about the quantum mechanical LDOS? The simplest limit that can be considered is the first order perturbation theory (FOPT). One obtains (D.2):

$$P^{PT}(n|m) \approx \delta_{nm}\ +\ \frac{1}{4}\left(\frac{\delta x}{x}E\right)^2\ \delta_{|n-m|,2} \qquad \text{[FOPT]} \tag{6.15}$$

This result is very different from the classical result. Therefore we say that there is no "detailed quantum-classical correspondence". On the other hand one easily calculates the

variance. One obtains $\delta E = \delta E^{cl}$. We call the latter equality "restricted quantum-classical correspondence".

It is possible to write an exact analytical expression for the quantum mechanical LDOS (see D.1). But this expression is not very useful since its complexity makes it virtually impossible to extract the simple limits in various regimes. It is more illuminating to obtain a uniform approximation (D.3)

$$P^{\rm unif}(n|m) \approx \left[J_{(m-n)/2}\left(\frac{\delta x}{x}E\right)\right]^2 \tag{6.16}$$

In Figure 6.1 we demonstrate that the uniform approximation is almost indistinguishable from the exact result for any value of δx. One can verify that this approximation reduces to the FOPT result (6.15) in the parametric regime $\delta x \ll (x/E)$. Disregarding an oscillatory component it reduces to the semiclassical result (6.13) in the parametric regime $\delta x \gg (x/E)$. The two regimes are separated by the quantum mechanical parametric scale $\delta x_{PT} = (\hbar\omega_{osc}/E)x$. For the the convenience of the reader we have reverted here to non-scaled units (with our scaling $\omega_{osc} = 1$ and $\hbar = 1$.)

The example above demonstrates some general observations regarding the LDOS. On the one hand we have restricted quantum-classical correspondence, which means $\delta E = \delta E^{cl}$. It can be proved that this type of quantum-classical correspondence holds in general [26]. The proportionality $\delta E \propto \delta x$ is guaranteed by the classical linearization condition ($\delta x \ll x$), which is a fixed assumption in this chapter. On the other hand we do not have in general detailed quantum-classical correspondence, which means that the approximation $P(n|m) \approx P^{cl}(n|m)$ holds only in a specific parametric regime. In the above example we have only two parametric regimes:

- The "perturbative regime" ($\delta x \ll \delta x_{PT}$)
  in which (in this example) FOPT can be used.
- The "non-perturbative regime" ($\delta x > \delta x_{PT}$)
  in which (in this example) the semiclassical approximation can be used.

Hence upon quantization there is only one parametric scale in the theory ($\delta x_{PT} \propto \hbar$). This parametric scale marks a border between the perturbative and the non-perturbative regimes.

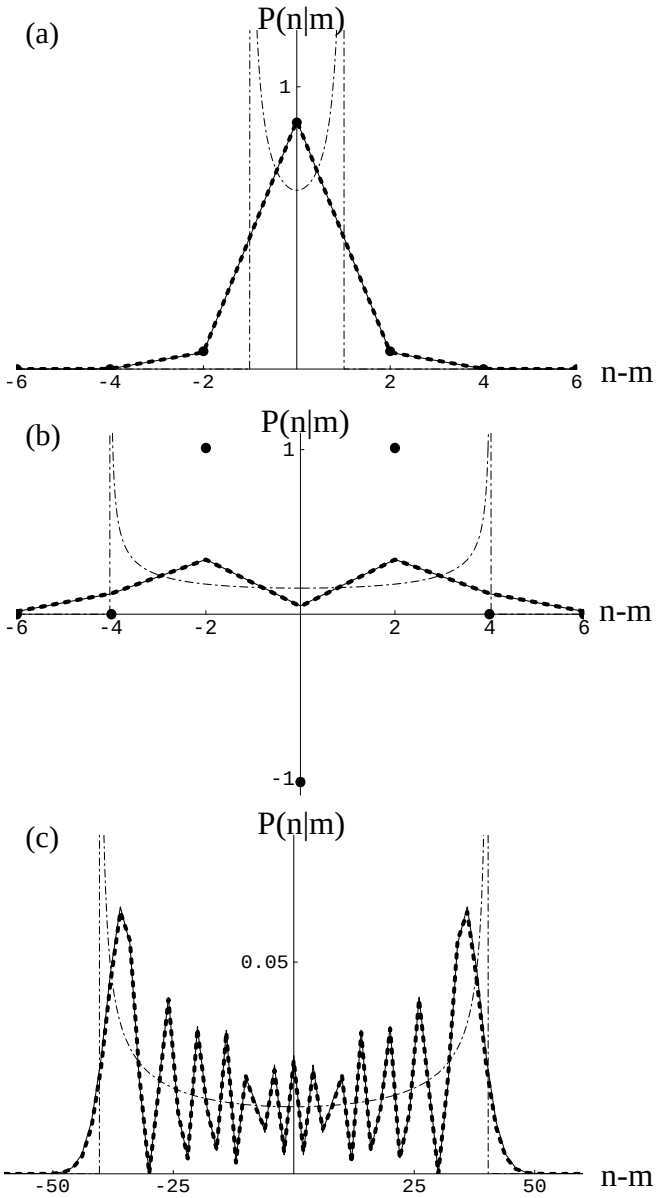

Figure 6.1: The local density of states for E=100. (a) For $(\delta x/x)E = 0.5$ (perturbative regime). (b) For $(\delta x/x)E = 2$ (intermediate regime). (c) For $(\delta x/x)E = 20$ (semiclassical regime). In each panel the thick dashed line is the exact result, the solid line is the uniform result, the dashed-dotted line is the classical result, and the solid circles are the perturbative result. The classical result is divided by 2 for a reason which is explained at the end of D.1.

6.5 Regimes: chaotic versus one-dimensional systems

In case of chaotic systems the generic case is having three regimes. The perturbative regime is subdivided into the FOPT regime and the Wigner/Lorentzian/ core-tail/FGR regime. In the latter case the various names mean the same, and we shall use from now on the term "Wigner regime". The FOPT regime is defined as the parametric regime where we can use the first order perturbation theory (FOPT):

$$P^{PT}(n|m) \approx \delta_{nm} + \delta x^2 \frac{|\mathbf{B}_{nm}|^2}{(E_n - E_m)^2} \qquad \text{[FOPT]} \tag{6.17}$$

The condition for the validity of this approximation is $\delta x \ll \delta x_c$, where $\delta x_c = \Delta/\sigma$. Here Δ is the mean level spacing, and σ is defined as the root-mean-square value of the "in-band" off-diagonal elements of the $\mathbf{B}$ matrix.

Outside of the FOPT regime we can still use first order perturbation theory for the *tails* of the LDOS [25]. This leads to a generalized Wigner's Lorentzian (a more meaningful name is "core-tail structure"):

$$P^{PT}(n|m) \approx \delta x^2 \frac{|\mathbf{B}_{nm}|^2}{[\Gamma(\delta x)/2]^2 + (E_n - E_m)^2} \qquad \text{[Wigner]} \tag{6.18}$$

The width parameter $\Gamma(\delta x)$ is determined so as to have proper normalization,

$$\sum_n P(n|m) = 1.$$

For strongly chaotic systems, for which the band profile is quite flat, it follows that the "core" width is $\Gamma \approx (\delta x/\delta x_c)^2 \Delta$. The "core-tail" approximation makes sense as long as we have separation of energy scales $\Gamma(\delta x) \ll \Delta_b$, where $\Delta_b = b\Delta$ is the bandwidth in units of energy. This translates into the condition $\delta x \ll \delta x_{PT}$ where

$$\delta x_{PT} = \sqrt{b}\ \delta x_c. \tag{6.19}$$

The "core-tail" approximation (6.18) can be regarded as the outcome of perturbative summation of diagrams to infinite order: The FOPT diagrams are re-iterated, while the interference terms are neglected. In time domain analysis this corresponds to a *Markovian approximation* for the survival probability $\mathcal{P}(t)$, leading to an exponential decay. Hence we say that there is a *perturbative regime* that includes the FOPT sub-regime, and the Wigner sub-regime. In the Wigner sub-regime we need *all orders* of perturbation theory leading to

FGR transitions and Wigner decay. On the other hand in the FOPT sub-regime there is *no decay*. This can be easily deduced by Fourier transforming the LDOS which is associated with Eq. (6.17): Up to negligible first order correction, the survival amplitude $F(t)$ comes out as a pure phase factor, whose absolute value squared is $\mathcal{P}(t) \approx 1$. It is appropriate at this point to make a connection with the analysis of quantum fidelity in Chapter 5. There, we considered the dynamics of a wavepacket that was a superposition of many eigenstates. Consequently there was an effective averaging over the survival amplitude $F(t)$, leading (in the FOPT regime) to a slow Gaussian decay (5.3) which can be related (as in Section 5.3) to the statistics of the first order correction to the eigenenergies.

By Weyl law we know that the mean level spacing for a d-dimensional system is $\Delta \propto \hbar^d$. On the other hand the bandwidth $\Delta_b \propto \hbar$ is inversely proportional to the period, or to the correlation time of the dynamics. For chaotic systems (with $d > 1$) we generally have $b = \Delta_b/\Delta \gg 1$. But for $d = 1$ systems we can have $b = \mathcal{O}(1)$, as in the example of equation (6.2). Therefore in the latter case $\delta x_{PT} \sim \delta x_c$, and we do not have a "Wigner regime" where the LDOS has a Lorentzian-like structure. Note again that in order to have exponential decay of $\mathcal{P}(t) = |F(t)|^2$ the LDOS should have a Lorentzian structure. While this latter statement strictly holds for the specific scenario which has been defined by equation (6.12), it typically holds also in more complicated circumstances [65]. Thus we conclude that the FGR picture cannot be applicable to the analysis of the dynamics unless $b \gg 1$.

At this stage of the discussion we can say that in order to have three regimes (FOPT, Wigner, semiclassical) in the theory of one-dimensional systems, we have to consider models where the perturbation is characterized by a large bandwidth ($b \gg 1$). In the next sections we would like to further discuss the following:

- A uniform approximation can be applied in order to address both the perturbative and the non-perturbative regimes.
- We can have $b \gg 1$ by considering potentials that have small (or sharp) features. (For example "bump" or "disorder").
- It is possible to get a Lorentzian-like LDOS from the uniform approximation, but $b \gg 1$ is not a sufficient condition.
- The uniform approximation does not take into account the effect of strong localization.
- Three LDOS regimes can be observed in case of disordered potential in spite of the strong localization effect.

6.6 Perturbations with large bandwidth

For any one-dimensional system we can find the action-angle variables, in which the problem becomes essentially equivalent to the problem (6.5) of a particle in a ring. Consider for example the deformable harmonic oscillator (6.2): We already saw that all the essential physics of the perturbed eigenstates can be obtained via a uniform approximation which is based on action-angle variables description of the system. The Hamiltonian (D.11) of a deformable harmonic oscillator in action-angle variables, and the Hamiltonian (6.5) of a particle in a ring, are similar as far as the semiclassical treatment is concerned. Having a quadratic rather than a linear dispersion relation is not an essential difference.

More generally, we may encounter circumstances where the perturbation creates small phase space structures, as we did in Chapters 3 and 4. This is the new ingredient (compared with the deformable harmonic oscillator) that we are going to consider in the following sections. The problem (6.5) of a particle in a ring constitutes a prototype example of having such small phase space structures. The perturbation $V(Q)$ is characterized by a different, much smaller scale (ℓ), compared with the size of the system (L). This means that we have large bandwidth ($b \gg 1$) rather than $b = \mathcal{O}(1)$.

In the absence of a perturbation ($x = x_0 = 0$), the eigenenergies of a particle in a ring are $E_n = p_n^2/2\mathsf{m}$, where n is an integer index, and $p_n = (2\pi\hbar/L)n$. The perturbation

matrix is related to the Fourier components of the potential:

$$\mathbf{B}_{nm} \;=\; \frac{1}{L}\tilde{V}(p_n - p_m) \tag{6.20}$$

The expressions for $\tilde{V}(k)$ in case of either the "bump" (6.6) or the "disorder" (6.7), were given in Section 6.2. Upon substitution in (6.20) it follows that

$$\Delta = 2\pi\hbar v_E/L \tag{6.21}$$

$$\Delta_b = 2\pi\hbar v_E/\ell \tag{6.22}$$

$$b = L/\ell \tag{6.23}$$

where $v_E = \sqrt{2E/\mathsf{m}}$. One difference between the two models is related to the coupling parameter σ, which has been defined in the beginning of Section 6.5 as the RMS value of the in-band off-diagonal elements. Hence

$$\sigma = (\ell/L)V_0 \qquad \text{for the bump} \tag{6.24}$$

$$\sigma = (\ell/L)^{1/2}V_0 \qquad \text{for the disorder} \tag{6.25}$$

This leads to

$$\delta x_c^{\text{bump}} = \Delta/\sigma = (\Delta_b/V_0) \tag{6.26}$$

$$\delta x_c^{\text{disorder}} = \Delta/\sigma = (\Delta_b/V_0)/\sqrt{b} \tag{6.27}$$

The difference in σ, and hence in δx_c is not the significant difference between the "bump" potential and the "disorder" potential. The significant difference is related to the statistical properties of the $\mathbf{B}$ matrix. In the case of "disorder" the matrix elements look "random", which is not the case for a single bump.

In both cases, of having either single bump or disorder, the FOPT regime is $\delta x \ll \delta x_c$. What do we have beyond the FOPT? More specifically, the question is whether we have, as in the theory of chaotic systems, a distinct parametric scale $\delta x_{PT} = \sqrt{b}\delta x_c$ that distinguishes between the Wigner regime and the semiclassical regime. In the next section we shall try to address this question within the framework of a uniform approximation.

6.7 Regimes within the framework of uniform approximation

There is a general semiclassical procedure that associates wave functions of integrable systems with phase space manifolds. The traditional implementation of this procedure is known as the WKB method. The WKB method is problematic near turning points.

This problem can be solved by uniformization of the solution, the simplest example of which was described in Section 2.3. The simplest point of view regarding uniformization is obtained by using action-angle variables. This leads to a Hamiltonian that looks like that of a particle in a ring. In general the dispersion relation can be different (not quadratic as in (6.5)), but we shall see that this is not an important difference for the issues under study.

The eigenstates of Hamiltonian (6.5) are supported by the manifolds

$$H(Q,P;x) = E_n.$$

An alternate (explicit) way to describe a given manifold is $P = p_n(Q;x)$, where

$$p_n(Q;x) = \sqrt{2\mathsf{m}\left[E_n - \delta x V(Q)\right]} \approx p_n - \delta x\ \hbar\ k(Q) \tag{6.28}$$

and $k(Q) = V(Q)/\hbar v_E$. In the following we use units such that $\hbar = 1$. The semiclassical formula for the corresponding eigenfunction is

$$\langle Q|n(x)\rangle = \frac{1}{\sqrt{L}} \exp\left(i\int_0^Q p_n(Q';x)dQ'\right) \tag{6.29}$$

This can be regarded as a special case of (D.13). Above we approximate the classical pre-exponential prefactor by $1/\sqrt{L}$. This is legitimate because a fixed assumption of this chapter is that we are considering high-lying eigenstates, and assume *classically small* perturbations.[3] We already saw, in the context of the deformable harmonic oscillator (see the end of Appendix D.3), that the numerical error which is associated with this approximation is insignificant. The essential physics of having various "regimes" is not related to this approximation.

The overlap of the semiclassical wave functions is given by the integral

$$\langle n(x)|m(x_0)\rangle = \frac{1}{L}\int_0^L dQ\ \exp\left[-i\left((p_n - p_m)Q - \delta x\int_0^Q k(Q')dQ'\right)\right] \tag{6.30}$$

In case of the bump, $k(Q)$ has an amplitude $k_0 = V_0/\hbar v_E$ over a spatial scale ℓ. The total phase variation in (6.30) is

$$\delta\phi_{\rm bump} = \delta x \times k_0\ell \tag{6.31}$$

This phase variation is in fact the phase space area of the bump. So we have two possibilities: Either $\delta\phi_{\rm bump} \ll 2\pi$ or $\delta\phi_{\rm bump} \gg 2\pi$. This can be shown to be equivalent to either

[3] It can also be regarded as an example of a more general semiclassical perturbation approximation used in Chapter 5 [85, 127].

$\delta x \ll \delta x_c^{\rm bump}$ or $\delta x \gg \delta x_c^{\rm bump}$ respectively. In the former case it is easy to recover the FOPT result (6.17). One should simply put the perturbation off the exponent, and then calculate the integral by parts. For $n \neq m$ it leads to

$$P(n|m) = \left| \frac{1}{L} \int_0^L dQ \frac{{\rm e}^{-i(p_n - p_m)Q}}{p_n - p_m} \, \delta x k(Q) \right|^2 = \delta x^2 \left| \frac{\mathbf{B}_{nm}}{E_n - E_m} \right|^2 \tag{6.32}$$

The other possibility ($\delta\phi_{\rm bump} \gg 2\pi$) guarantees the validity of the standard semiclassical approximation. In such case we cannot put the perturbation off the exponent, but instead we can make the stationary phase approximation.

We see that for a simple bump we can use either the FOPT or the semiclassical approximation. So we have just two regimes, in spite of the fact that $b \gg 1$. This means that large bandwidth is not a sufficient condition for having three parametric regimes. So let us try to make things more complicated by considering a disordered potential with many bumps. Equation (6.31) still describes the phase variation over a single bump. This means that $\delta\phi_{\rm bump} \gg 2\pi$ is still the relevant condition for a semiclassical approximation! What about the first order perturbation theory? The total phase variation in (6.30) for many bumps is

$$\delta\phi_{\rm disorder} = \delta x \times \sqrt{b} \times k_0 \ell \tag{6.33}$$

(note that b is essentially the number of bumps involved). Consequently the validity condition for the first order perturbation theory is $\delta\phi_{\rm disorder} \ll 2\pi$, which can be easily converted into $\delta x \ll \delta x_c^{\rm disorder}$.

The considerations of the previous paragraph imply that for *disordered* potential we have three regimes. In the intermediate regime $\delta x_c \ll \delta x \ll \delta x_{PT}$, we have $\delta\phi_c^{\rm disorder} \gg 2\pi$ while $\delta\phi_c^{\rm bump} \ll 2\pi$. Consequently we can use neither FOPT, nor the semiclassical approximation. This is the Wigner regime where we expect to find a Lorentzian-like LDOS. Let us demonstrate that indeed a Lorentzian-like LDOS can be obtained from the uniform

approximation (6.30). For this purpose we average $P(n|m)$ over realizations of the disorder:

$$\begin{aligned} P(n|m) &= \frac{1}{L^2}\int_0^L\int_0^L dQ_1 dQ_2 \ \mathrm{e}^{-i(p_n-p_m)(Q_2-Q_1)} \left\langle \exp\left[i\delta x \int_{Q_1}^{Q_2} k(Q')dQ'\right]\right\rangle_{\text{disorder}} \\ &= \frac{1}{L^2}\int_0^L\int_0^L dQ_1 dQ_2 \ \mathrm{e}^{-i(p_n-p_m)(Q_2-Q_1)} \\ &\quad \times \exp\left[-\frac{1}{2}\left(\frac{\delta x}{\hbar v_E}\right)^2 \int_{Q_1}^{Q_2}\int_{Q_1}^{Q_2} \langle V(Q')V(Q'')\rangle dQ' dQ''\right] \\ &\approx \frac{1}{L}\int_{-\infty}^{\infty} dr \ \mathrm{e}^{-i(p_n-p_m)r} \exp\left[-\delta x^2\left(\frac{V_0}{\hbar v_E}\right)^2 \ell|r|\right] \end{aligned} \tag{6.34}$$

where $r = Q_2 - Q_1$. The last integral is the Fourier transform of an exponential, leading to the Lorentzian LDOS as defined in (6.18).

6.8 Strong localization effect

Still we have to address the question whether we can trust the uniform approximation, which is based on the WKB wave function (6.29). The answer is known to be negative in case of *disordered* potential. The WKB approximation does not take into account backscattering, which is responsible for the strong localization effect in 1D disordered potential. It is well known [107] that the localization length is equal (in 1D) to twice the mean free path. Up to a numerical prefactor the Born approximation estimate is

$$\frac{1}{L_{\text{loc}}} \approx \frac{1}{\hbar v_E}\frac{\sigma^2}{\Delta} \times \delta x^2 = \left(\frac{\delta x}{\delta x_c}\right)^2 \frac{1}{L} = \left(\frac{\delta x}{\delta x_{PT}}\right)^2 \frac{1}{\ell} \tag{6.35}$$

The condition for *not* being affected by the strong localization effect is $L_{\text{loc}} \gg L$, which leads to $\delta x \ll \delta x_c$. Thus it follows that only in the FOPT regime we can ignore the strong localization effect. The strong localization effect can be ignored neither in the Wigner regime nor in the semiclassical regime.

The above Born approximation assumes $L_{\text{loc}} \gg \ell$. This condition breaks down if $\delta x > \delta x_{PT}$. Recall that we also assume that δx is small in the classical sense ($\delta x V_0 \ll E$). The two inequalities are consistent if and only if the de Broglie wavelength of the particle is much smaller compared with ℓ. In this regime we can analyze the localization using the well known transfer matrix approach: Each bump has some transfer matrix, and the random distance between the bumps provides the phase randomization which is assumed

in "combining" adjacent transfer matrices. Denoting the average transmission of a "bump" by g, one gets

$$\frac{1}{L_{\rm loc}} \approx \ln(1/g) \times \frac{1}{\ell} \tag{6.36}$$

Thus even in the $\delta x > \delta x_{PT}$ regime we can have a very long localization length ($L_{\rm loc} \gg \ell$), which is in fact consistent with the naive expectation.

The implications of the above discussion are, that in spite of the strong localization effect, it is still meaningful to distinguish between three parametric regimes (FOPT, Wigner, semiclassical). We just have to remember that the wave function is not ergodic in real space, so the role of L is taken by $L_{\rm loc}$.

6.9 Survival probability $\mathcal{P}(t)$

We turn to discuss the calculation of the survival probability (6.1) for the specific wavepacket dynamics scenario that has been defined in Section 6.3. We have the following five strategies of calculation:

- Uniform approximation (which is essentially exact)
- Time domain classical approximation
- Energy domain classical approximation ($\rightsquigarrow$ LDOS $\rightsquigarrow$ Fourier transform)
- Time domain perturbation theory
- Energy domain perturbation theory ($\rightsquigarrow$ LDOS $\rightsquigarrow$ Fourier transform)

It can be shown that in typical circumstances the two versions of perturbation theory give in leading order consistent results. This means that we can write a perturbative (essentially first order) result that can be trusted for sufficiently short times (for any perturbation δx) or for sufficiently weak perturbation (for any time t). As an example we consider the deformable harmonic oscillator. Taking equation (6.15) with appropriate second order compensation of normalization, we get after Fourier transform,

$$\mathcal{P}^{PT}(t) \approx 1 - 2\left(\frac{\delta x}{x}\right)^2 E^2 \sin^2 t \tag{6.37}$$

In a strict time domain FOPT we get only t^2 time dependence, while in a strict energy domain FOPT we do not get the correct normalization ($\mathcal{P}^{PT}(0) = 1$). Still we are able to get one consistent result.

The situation is different with the classical approximation. Here time domain and energy domain calculations do not give the same result. As an example we consider again the deformable harmonic oscillator. The calculation of overlap between ρ_t^{cl} and ρ_0^{cl} is simpler in action-angle variables, but otherwise it is similar to the calculation in Appendix D.1, leading to

$$\mathcal{P}^{cl}(t) = \left| 2\pi \frac{\delta x}{x} E \sin t \right|^{-1} \tag{6.38}$$

The energy domain classical approximation is obtained by squaring the Fourier transform of equation (6.10) using the classical approximation (6.13) of $P^{cl}(n|m)$, leading to

$$\mathcal{P}^{cl,E}(t) = \left| J_0 \left(2\frac{\delta x}{x} E t \right) \right|^2 \tag{6.39}$$

Although there is no simple exact expression for $\mathcal{P}(t)$, there again exists a very simple uniform approximation which is remarkably accurate in all regimes and therefore we can regard it as "exact," namely

$$\mathcal{P}^{\text{unif}}(t) = \left| J_0 \left(2\frac{\delta x}{x} E \sin t \right) \right|^2 \tag{6.40}$$

It is derived in D.4 by using semiclassical expressions for the initial and evolved states, while calculating the overlap exactly rather than by the stationary phase approximation.

Results (6.37)-(6.40) are graphically displayed in Figure 6.2. Approximations (6.37)-(6.39) can be regarded as various limits of the uniform approximation (6.40). It is easily seen that (6.40) reduces to the perturbative result (6.37) whenever $2(\delta x/x)E\sin(t) \ll 1$. So as expected the perturbative result can be trusted for either small time t or for small perturbation $\delta x/x$. It is also easy to see that the uniform result (6.40) reduces to the energy domain classical result (6.39) for $t \ll 1$. The relation of (6.40) to the time domain classical result (6.38) is more subtle: For large perturbation the two expressions agree in an asymptotic sense, and either time smoothing or energy averaging is required in order to demonstrate this agreement (see Figure 6.2c).

An important message of this section is that the discussion of regimes in the context of survival probability $\mathcal{P}(t)$ is in one to one correspondence with the discussion of the LDOS regimes.

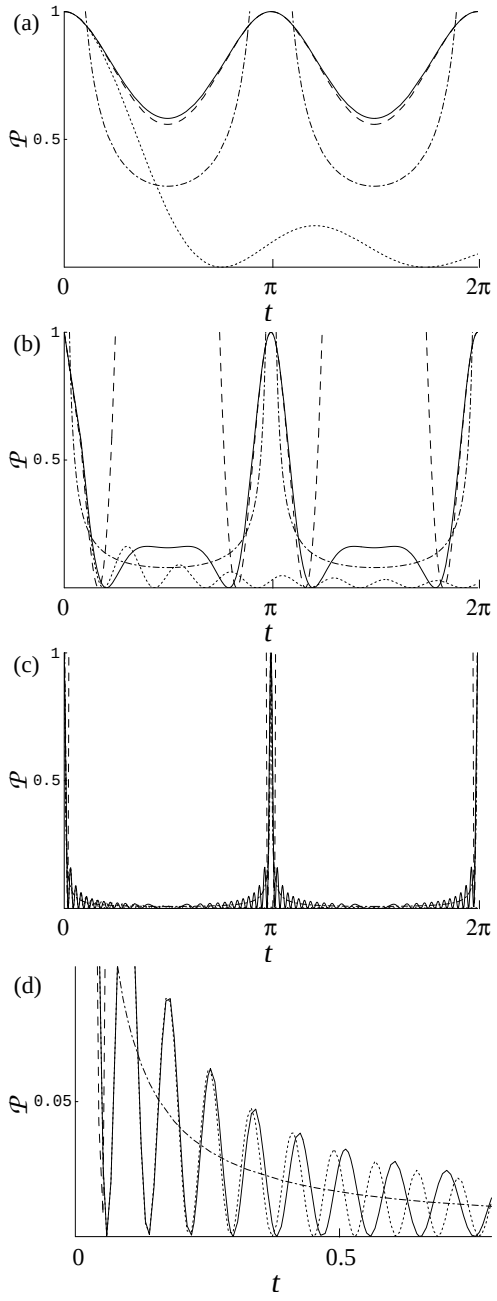

Figure 6.2: The survival probability, using the same parameters as in figure 6.1. (a) Perturbative regime. (b) Intermediate regime. (c) Semiclassical regime. In each panel the solid line is the uniform result (6.40), the dashed line is the perturbative result (6.37), the dashed-dotted line is the time domain classical result (6.38), and the dotted line is the energy domain classical result (6.39). Panel (d) gives a short-time detail of panel (c).

6.10 Conclusions and final remarks

In general, for more complicated wavepacket dynamics scenarios, an explicit reduction to the LDOS theory is not possible [140]. This opens the possibility for chaos in the classical dynamics of one-dimensional systems. A prototype system for chaos studies is the kicked rotator: This is a particle in a ring, which is periodically kicked by a cosine potential. As in the standard formulation of wavepacket dynamics it is common to assume an initial preparation which is supported by a manifold $P = p_m$. As a result of the kicks the initial manifold becomes extremely convoluted. If we want to calculate $\mathcal{P}(t)$ we have to trace the evolving manifold with the initial one. The calculation of this overlap can be carried out using the uniform approximation based on replacement manifolds that were discussed in Chapters 3 and 4.

There is one major difference that makes the chaotic scenario that we have described above different from the LDOS calculation: The issue of strong localization, which has been discussed in Section 6.8 is no longer relevant. The evolving state is distributed over the whole manifold. The only reservation for this statement is the possibility of witnessing a *dynamical localization effect* after an extremely long time (known as the "breaktime"). For small $\hbar$ the existence of a "breaktime" will have a negligible effect on the behavior of $\mathcal{P}(t)$. In fact we should remember that also in non-kicked systems we have a "breaktime", which is just the Heisenberg time.

In view of the above, the calculations presented in this chapter, using the uniform approximation, are in fact generic. In particular we have explained how the Fermi-golden-rule behavior arises within this framework.

The reader can be tempted to reach the conclusion that the discussion of regimes within the framework of the uniform approximation can be trivially generalized to $d > 1$ chaotic systems. This is in fact not quite correct. In order to explain the difficulty let us consider again LDOS calculation. In one-dimensional systems what we have to do is to calculate the overlap of two one-dimensional manifolds. We can do this calculation semiclassically if we can trust the stationary phase approximation. This leads to the "area $\hbar$" condition: the stationary phase approximation is accurate if the phase space area delimited by the two manifolds between two stationary phase points is larger than $\hbar$. What is the generalization of this condition in the $d > 1$ case? Now the manifolds are "surfaces" and they intersect along "curves." So the concept of stationary-phase points becomes inapplicable,

and also the "area $\hbar$" condition becomes meaningless. The way out of this difficulty [25] is to use the Wigner function point of view. Then one realizes that the proper way to formulate the semiclassical condition is to say that the separation between the surfaces should be much larger compared with the "thickness" of Wigner function. This "thickness" is just the bandwidth that we have discussed in this chapter.

Conventionally, semiclassical methods are applied in the semiclassical regime (large enough perturbation). In the perturbative regime people use perturbation theory. A major motivation for the present line of study is to extend the applicability of semiclassical methods into the perturbative regime. Most of the calculations that we have presented under the heading "uniform approximation" can be reformulated using the Wigner function language. This opens the way towards a unified semiclassical understanding of "regimes" in case of $d > 1$ systems.

Chapter 7

Conclusion

The main goal of this thesis was to present several methods improving the WKB approximation in systems with nonlinear classical dynamics. There are two main problems which result in the failure of the standard WKB approximation: Firstly, it is the inaccuracy due to the abundance of caustics in chaotic systems. Secondly, there is a practical problem: many uniform semiclassical methods that correct this inaccuracy are numerically intractable.

Both of these problems were successfully addressed by the three uniform semiclassical methods discussed in this thesis: replacement manifolds of Chapters 3 and 4, the method based on the initial value representation combined with the classical perturbation approximation in Chapter 5, and the uniform method of Chapter 6. Because the standard WKB approximation is based on the stationary phase approximation, it will always lead to singularities whenever the stationary-phase points (or surfaces) coalesce. On the other hand, the uniform approximations are in general based on replacing some [1] of the stationary-phase integrals by their exact analogs. These exact integrals, in turn, can be evaluated numerically (e.g., by the Monte Carlo method) as in Chapter 5, or often analytically, as in Chapters 3, 4, and 6. Another unifying feature of the uniform approximations presented in this thesis is that they all have a simple physically motivated geometric interpretation.

The replacement manifolds of Chapters 3 and 4, e.g., were a natural consequence of the Heisenberg uncertainty principle. Since quantum mechanics cannot distinguish details of classical mechanics on the scale of Planck's constant, we could replace intricate details in Lagrangian manifolds by smoother manifolds that corresponded to the same quantum

[1] I.e., those explicit or implicit stationary-phase integrals that are or potentially could be divergent.

wave function, but did not lead to singularities in the WKB approximation. However, the replacement manifolds did not neglect the small-scale features in phase space altogether: they could take them into account by a rapidly convergent series of corrections. These corrections are exponentially small because they physically represent tunneling contributions. Finally, replacement manifolds are still Lagrangian manifolds and consequently, all results of the semiclassical analysis applicable to usual Lagrangian manifolds are equally applicable to the replacement manifolds.

The semiclassical calculation of quantum fidelity in Chapter 5 was based on the initial value representation of the fidelity amplitude. This representation eliminates caustic singularities in the overlap because there is a unique semiclassical contribution corresponding to each initial momentum, rather than an exponentially growing number of contributions that would be present if final position representation were used. The semiclassical expressions were particularly simple thanks to the use of the classical perturbation approximation. This approximation can be used even in strongly chaotic systems: when such a system is perturbed, individual trajectories diverge exponentially, but the manifold supporting the semiclassical wave function is structurally stable. The main strength of our approach is the ease of numerical implementation. Furthermore, a single uniform expression contains the Fermi-golden-rule, Lyapunov and algebraic regimes of fidelity decay. Each type of decay corresponds to a specific law of dephasing caused by the perturbation.

In Chapter 6 we used another uniform method to discuss various types of the local density of states and regimes of the decay of survival probability in one-dimensional chaotic and disordered systems. This uniform method was based on an exact evaluation of the overlap of the WKB eigenstates of the original and perturbed Hamiltonians in the action-angle variables. The angle representation was advantageous because it did not contain any caustics and also because the overlap could be found analytically in terms of Bessel functions. Most importantly, the uniform approximation was capable of describing the perturbative, Fermi-golden-rule, and semiclassical regimes.

While we gave theoretical arguments justifying each of the methods, we also applied them successfully to various physical problems. We used replacement manifolds to find the wave function for a homoclinic tangle and for the scattering from a corrugated wall in Chapter 3, and for the coherent two-dimensional electron flow in Chapter 4. In Chapter 5, we applied our uniform method to calculate quantum fidelity for the standard map and in Chapter 6, we tested our theory on the perturbed harmonic oscillator and on a particle in

a ring with a disordered potential. The main contributions of this thesis are the following: Firstly, the replacement manifolds of Chapters 3 and 4 provide a new class of semiclassical uniformizations. Because of its intuitive geometric motivation, the replacement-manifold idea should be applicable to a broad range of problems. In particular, it facilitates the understanding of quantum wave functions near a homoclinic tangle. Secondly, the uniform semiclassical method of Chapter 5 has justified several crucial approximations used in the rapidly evolving field exploring quantum fidelity. Because we have shown that the uniform semiclassical expression for fidelity is indeed accurate, others may use our approach for further progress and insight.

Appendix A

Exact evaluation of replacement-manifold terms in the model of homoclinic oscillations

The oscillatory integral (3.14) with $\xi(Q) = \alpha \log(Q/a)$ is made convergent by displacing momentum P with an imaginary infinitesimal term $-i\epsilon$, $\epsilon > 0$,

$$\langle P|p\rangle_{n,\mathrm{unif}} = \frac{1}{2\pi\hbar}\int_0^\infty dQ\, \exp\left\{\frac{i}{\hbar}\left[-(P-i\epsilon-p)Q + n\hbar\alpha\log\frac{Q}{a}\right]\right\}. \tag{A.1}$$

In this form, the answer is found by rotating the contour about the origin of complex plane by $-\frac{\pi}{2}\,\mathrm{sgn}(P-p)$. Let us explicitly solve the case $P > p$. Fig. A.1 shows a contour in complex plane enclosing a region with no singularities, and as a result the sum of integrals along appropriate parts of the contour is zero, $I_1 + I_R + I_2 + I_r = 0$. In the limit $R \to \infty$, $r \to 0$, I_1 becomes our desired integral (A.1) and both I_R and I_r vanish, implying $I_1 = -I_2$. Contour for integral I_2 is the set of complex points $z = -ix = e^{-i\pi/2}x$, $x > 0$. Consequently,

$$-I_2 = \frac{1}{2\pi\hbar}e^{-i\pi/2}\int_0^\infty dx\, \exp\left\{\frac{i}{\hbar}[-(P-p-i\epsilon)(-ix) + n\hbar\alpha\log\frac{xe^{-i\pi/2}}{a}]\right\}. \tag{A.2}$$

Transforming to a dimensionless variable $y = \frac{(P-p-i\epsilon)x}{\hbar}$, the integral becomes

$$\begin{aligned} -I_2 &= \frac{1}{2\pi\hbar}\exp\left\{(n\alpha - i)\frac{\pi}{2} - in\alpha\log\left[(P-p-i\epsilon)a/\hbar\right]\right\} \\ &\quad \times\frac{\hbar}{P-p-i\epsilon}\int_0^\infty dy\, e^{-y}y^{in\alpha}. \end{aligned} \tag{A.3}$$

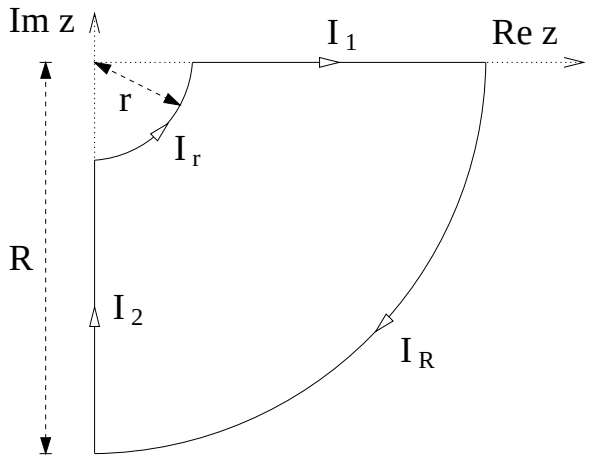

Figure A.1: Contour for evaluation of $\langle P|p\rangle_{n,unif}$ in the case $\xi(Q) = \alpha \log Q/a$.

Recognizing the remaining integral as a Γ function of complex argument $1 + in\alpha$, we may write

$$-I_2 = \frac{\Gamma(1+in\alpha)}{2\pi(P-p-i\epsilon)} \exp\left\{(n\alpha - i)\frac{\pi}{2} - in\alpha \log\left[(P-p-i\epsilon)a/\hbar\right]\right\}. \tag{A.4}$$

For $P < p$, we need to close the contour in the upper half-plane, but otherwise the procedure is analogous. Combining the two cases, we obtain a single analytic expression for the uniform transformation element,

$$\langle P|p\rangle_{n,\mathrm{unif}} = \frac{\Gamma(1+in\alpha)}{2\pi(|P-p| - is\epsilon)} \exp\left[(n\alpha - i)\frac{\pi}{2}s - in\alpha \log \frac{(|P-p| - is\epsilon)a}{\hbar}\right] \tag{A.5}$$

where $s = \mathrm{sgn}(P-p)$. As promised, the uniform (A.5) and semiclassical (3.26) forms have identical dependence on $\hbar$ and $P-p$. The only difference lies in the dependence on $n\alpha$, in particular the semiclassical form is obtained if we keep only the first term in the asymptotic expansion of $\Gamma(1+in\alpha)$ in $\langle P|p\rangle_{n,\mathrm{unif}}$. However, for our conservative choice of $\alpha \approx 33$ the agreement between $\langle P|p\rangle_{n,sc}$ and $\langle P|p\rangle_{n,\mathrm{unif}}$ is such that they may be used interchangeably for any practical purposes.

Appendix B

Exact solution of scattering from a hard sinusoidal wall

From conservation of energy, the scattered and incident waves must have the same magnitude of momentum. Due to the periodicity of the wall in the x direction, the x-component of momentum is constrained by the Bragg condition

$$k_{2x,n} = k_{1x} + n\beta, \quad n \in \mathbb{Z}. \tag{B.1}$$

Corresponding y-component of momentum $k_{2y,n} = \sqrt{k^2 - k_{2x,n}^2}$ will be real only if $|k_{1x} + n\beta| < k$. Otherwise the reflected wave becomes evanescent: it decays exponentially with distance from x-axis because k_{2y} is imaginary. To complete the solution, coefficients a_n in the momentum Green's function

$$\langle \mathbf{k}_{2x} | \mathbf{k}_{1x} \rangle = \sum_{n=-\infty}^{\infty} a_n \, \delta(k_{2x} - k_{2x,n}) \, \delta(k_{2y} - k_{2y,n})$$

must be found. This is accomplished by imposing the Dirichlet boundary condition in coordinate space. Namely, the total wave function $\psi_{tot}(\mathbf{r}) = \psi_{inc}(\mathbf{r}) + \psi_{scat}(\mathbf{r})$ has to vanish along the corrugated wall. Using

$$\begin{aligned} \psi_{inc}(\mathbf{r}) &= \langle \mathbf{r} | \mathbf{k}_1 \rangle = \frac{1}{2\pi} e^{i\mathbf{k}_1 \cdot \mathbf{r}}, \\ \psi_{scat}(\mathbf{r}) &= \int d^2 k_2 \, \langle \mathbf{r} | \mathbf{k}_2 \rangle \langle \mathbf{k}_2 | \mathbf{k}_1 \rangle = \frac{1}{2\pi} \sum_{n=-\infty}^{\infty} a_n e^{i\mathbf{k}_{2,n} \cdot \mathbf{r}}, \end{aligned} \tag{B.2}$$

definition of boundary (3.36) and (B.1) for $k_{2x,n}$, the boundary condition becomes

$$\exp\left[i(k_{1x} x + k_{1y} \frac{\varepsilon}{\beta} \sin \beta x) \right] + \sum_{n=-\infty}^{\infty} a_n \exp\left[i(k_{1x} + n\beta)x + i k_{2y,n} \frac{\varepsilon}{\beta} \sin \beta x \right] = 0.$$

Recalling the identity

$$e^{i\lambda \sin x} = \sum_{m=-\infty}^{\infty} J_m(\lambda)\, e^{imx}$$

and denoting

$$\lambda_1 = \frac{\varepsilon}{\beta} k_{1y}, \quad \lambda_{2,n} = \frac{\varepsilon}{\beta} k_{2y,n}, \quad \theta = \beta x,$$

the boundary condition may be written as

$$\sum_{m=-\infty}^{\infty} \left[J_m(\lambda_1)\, e^{im\theta} + \sum_{n=-\infty}^{\infty} a_n\, J_m(\lambda_{2,n})\, e^{i(n+m)\theta} \right] = 0. \tag{B.3}$$

Replacing m by $p \equiv n+m$ in the second term and by $p \equiv m$ in the first term in the brackets in (B.3), we get

$$\sum_{p=-\infty}^{\infty} e^{ip\theta} \left[J_p(\lambda_1) \, + \sum_{n=-\infty}^{\infty} a_n\, J_{p-n}(\lambda_{2,n}) \right] = 0. \tag{B.4}$$

This equation will be satisfied for all $x = \frac{\theta}{\beta}$ only if coefficients of $e^{ip\theta}$ on the left-hand side vanish,

$$J_p(\lambda_1) \, + \sum_{n=-\infty}^{\infty} a_n\, J_{p-n}(\lambda_{2,n}) = 0, \quad \forall p \in \mathbb{Z}. \tag{B.5}$$

We recognize (B.5) as an infinite system of linear equations for coefficients a_n. In matrix form, $\mathbf{A} \cdot \mathbf{a} = \mathbf{b}$, with $A_{ij} \equiv J_{i-j}\left(\frac{\varepsilon}{\beta}\sqrt{k^2 - (k_{1x} + j\beta)^2}\right)$and $b_i \equiv -J_i(\frac{\varepsilon}{\beta} k_{1y})$. Although this system cannot be solved analytically, expressing the solution in this form is a great improvement compared to what can be done for a general Dirichlet problem satisfying time-independent Schrödinger equation. The system (B.5) can be approximately evaluated numerically by restricting n and p to lie between limiting values $\pm n_{\max}$.

Appendix C

Replacement-manifold expansion in an arbitrarily rotated coordinate system

We show here that the replacement-manifold expansion for the manifold studied in Chapter 4 can be found analytically in an arbitrarily rotated coordinate system. In other words, the method can be readily applied not just in the q or p representations, but in any mixed representation given by a canonical transformation (see Fig. C.1)

$$\begin{aligned} Q &= q\cos\phi + p\sin\phi \\ P &= -q\sin\phi + p\cos\phi \end{aligned} \tag{C.1}$$

In the original coordinate system (q, p), replacement manifolds are straight lines

$$p_n(q) = 2in\hbar q = q\tan\alpha_n \tag{C.2}$$

(where α_n is complex). In the rotated coordinates (Q, P), the replacement manifolds are given by the relationship

$$P_n(Q) = Q\tan(\alpha_n - \phi) = Q\frac{2in\hbar - \tan\phi}{1 + 2in\hbar\tan\phi}. \tag{C.3}$$

The reduced action is

$$S_n(Q) = \int dQ\, P_n(Q) = \frac{1}{2}Q^2\tan(\alpha_n - \phi). \tag{C.4}$$

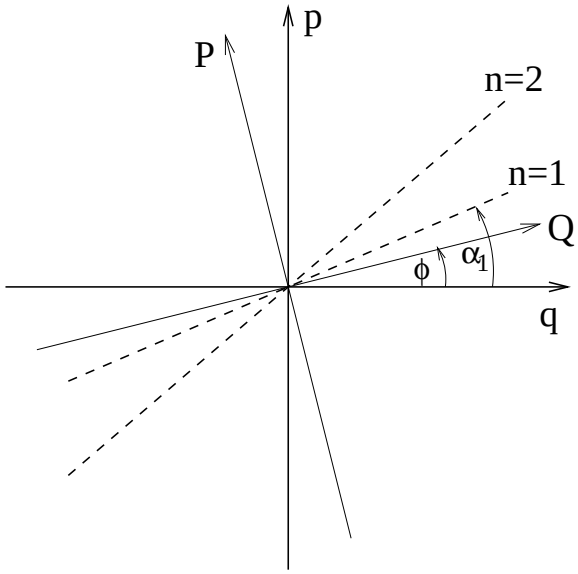

Figure C.1: Original and rotated coordinate systems.

The weight of the nth replacement manifold in the Q representation is the weight in the q representation multiplied by the ratios of the projections on the q and Q axes, respectively. Including the Maslov index μ (0 or 1), we find the correct nth replacement-manifold contribution

$$\psi_{RM,n}(Q) \;=\; \frac{1}{\sqrt{2\pi\hbar}}\frac{(i\epsilon)^n}{n!}\left|\frac{\cos\alpha_n}{\cos(\alpha_n-\phi)}\right|^{1/2}\exp\left[\frac{i}{2\hbar}Q^2\tan(\alpha_n-\phi)-i\mu_n\frac{\pi}{2}\right].$$

After simplification, the full replacement-manifold expansion becomes

$$\begin{aligned}\psi_{RM}(Q) &= \sum_{n=0}^{\infty}\psi_{RM,n}(Q)\\ &= \frac{1}{\sqrt{2\pi\hbar}}\sum_{n=0}^{\infty}\frac{(i\epsilon)^n}{n!}|\cos\phi+2in\hbar\sin\phi|^{-1/2}\\ &\quad\times\exp\left(-Q^2\frac{n+i\tan\phi/(2\hbar)}{1+2in\hbar\tan\phi}-i\mu_n\pi/2\right).\end{aligned}\tag{C.5}$$

It is easy to check that this general result correctly reduces to expressions (4.11) or (4.19) when $\phi=\pi/2$ or $\phi=0$, respectively.

Appendix D

Explicit calculation of $P(n|m)$ and $\mathcal{P}(t)$

D.1 Calculation of $P^{cl}(n|m)$ and $P^{\text{exact}}(n|m)$

We shall demonstrate in this appendix the calculation of $P^{cl}(n|m)$ for the deformable harmonic oscillator of Chapter 6:

$$\begin{aligned} P^{cl}(n|m) &= \int \frac{dQdP}{2\pi}\delta\left[H(Q,P;x_2)-E_n\right]\delta\left[H(Q,P;x_1)-E_m\right] \\ &= \int \frac{dQ}{2\pi}\sum_{P=\pm\sqrt{2E_m-(Q/x_1)^2}/x_1}\frac{\delta[\mathcal{H}(Q,P;x)-E_n]}{x_1^2|P|} \\ &= \frac{1}{\pi}\int dQ\frac{\delta[f(Q)]}{\sqrt{2x_1^2E_m-Q^2}} \\ &= \frac{1}{\pi}\sum_{\pm}\left(2x_1^2E_m-Q_\pm^2\right)^{-1/2}\left|f'(Q_\pm)\right|^{-1} \\ &= \frac{1}{\pi}\frac{x_1x_2}{\sqrt{\left(x_2^2E_n-x_1^2E_m\right)\left(x_2^2E_m-x_1^2E_n\right)}} \end{aligned} \tag{D.1}$$

where

$$f(Q)\equiv\frac{x_2^4-x_1^4}{2x_1^4x_2^2}Q^2+\left(\frac{x_2}{x_1}\right)^2E_m-E_n. \tag{D.2}$$

and $Q_\pm$ are the roots of the equation $f(Q)=0$,

$$Q_\pm=\pm x_1x_2\sqrt{\frac{2(x_2^2E_m-x_1^2E_n)}{x_2^4-x_1^4}} \tag{D.3}$$

for which

$$f'(Q_\pm) = \pm x_1^{-3} x_2^{-1} \sqrt{2(x_2^2 E_m - x_1^2 E_n)(x_2^4 - x_1^4)} \tag{D.4}$$

Equation (6.13) is a simplified version of this result, assuming that $\delta x \ll x$.

It is also possible to obtain an exact result in the quantum mechanical case. The explicit expression for the eigenfunction using Hermite polynomials is

$$\langle Q|n(x)\rangle = (\pi x^2)^{-1/4} (2^n n!)^{-1/2} H_n(Q/x) \mathrm{e}^{-(Q/x)^2/2} \tag{D.5}$$

This leads to

$$\begin{aligned} \langle n(x_2)|m(x_1)\rangle &= (\pi x_1 x_2)^{-1/2} (2^{n+m} n! m!)^{-1/2} \\ &\times \int_{-\infty}^{\infty} dQ H_n(Q/x_2) H_m(Q/x_1) \mathrm{e}^{-\frac{1}{2}(x_1^{-2}+x_2^{-2})Q^2} \end{aligned} \tag{D.6}$$

Upon squaring one obtains $P(n|m)$. The integral in (D.6) becomes highly oscillatory for high-lying eigenstates in which we are interested, and numerical calculation is tricky. To our surprise, this intimidating integral can be evaluated analytically even for $x_1 \neq x_2$, resulting in a finite sum of terms, which is not very elegant, but very simple to evaluate on a computer. For the exact benchmark in the numerical results presented in Chapter 6, we therefore used this analytical expression instead of numerically evaluating the integral (D.6).

Note that both classically and quantum mechanically the overlap $P(n|m)$ depends only on the ratio x_2/x_1. In the classical case n is a real index (E_n can have any real positive value). In the quantum mechanical case n is an integer index ($E_n = n + \frac{1}{2}$). Due to the reflection symmetry of the Hamiltonian there is an overlap only between states with the same parity. The overlap for $|n - m| =$ odd vanishes. Whenever we say that $P(n|m) \approx P^{cl}(n|m)$, it should be interpreted in a coarse grain sense. Therefore, for sake of graphical presentation we have plotted $P(n|m)$ versus $P^{cl}(n|m)/2$. One may say that the plotted $P(n|m)$ and $P^{cl}(n|m)/2$ correspond to a de-symmetrized oscillator.

D.2 Calculation of $P^{PT}(n|m)$

We shall demonstrate in this appendix the calculation of $P^{PT}(n|m)$ for the deformable harmonic oscillator. From first order perturbation theory we know that for $m \neq n$

$$\langle m(x_0)|n(x_0 + \delta x)\rangle \approx \frac{\langle m|\delta\mathcal{H}|n\rangle}{E_n - E_m} \tag{D.7}$$

Using

$$\left\langle m|Q^2|n\right\rangle,\ \left\langle m|P^2|n\right\rangle\ =\ (\tfrac{1}{2}+n)\delta_{mn} \pm \frac{1}{2}\left[\sqrt{(n+1)(n+2)}\delta_{m,n+2} + \sqrt{n(n-1)}\delta_{m,n-2}\right]$$

one obtains

$$P^{PT}(n|m) \approx \delta_{n,m} + \frac{1}{4}\left(\frac{\delta x}{x}\right)^2 \left(E^2 - \frac{1}{4}\right)\delta_{|n-m|,2} \tag{D.8}$$

where $E = (E_n + E_m)/2$. In the text we have presented a simplified version that assumes $E \gg 1$.

D.3 Calculation of $P^{\rm unif}(n|m)$

The following canonical transformation is used in order to transform the Hamiltonian of the harmonic oscillator to action-angle variables:

$$Q = \sqrt{2I}\cos(\phi) \tag{D.9}$$

$$P = \sqrt{2I}\sin(\phi) \tag{D.10}$$

In the vicinity of $x_0 = 1$ it leads to

$$\begin{aligned}\mathcal{H}(\phi, I; x) &= I\left[(1/x)\cos^2\phi + x\sin^2\phi\right] \\ &\approx I - \delta x I\cos(2\phi)) + \mathcal{O}(\delta x^2)\end{aligned} \tag{D.11}$$

The canonical transformation from (ϕ, I) to the action angle variables (ϕ', I') of the perturbed Hamiltonian is derived from a generating function $S(\phi, I')$. The manifold $I' =$ const is determined from the equation $\mathcal{H}(\phi, I; x) =$ const, leading to the relation $I = [1 + \delta x\cos(2\phi)]\, I'$. The generating function should satisfy $I = \partial S/\partial\phi$. Therefore one deduces that

$$S(\phi, I') = [\phi + \delta x\sin(2\phi)]\, I' \tag{D.12}$$

The semiclassical expression for the wave function is

$$\left\langle\phi|I'\right\rangle_{\rm sc} = (2\pi)^{-1/2}\sqrt{\frac{\partial^2 S}{\partial I'\partial\phi}}\ \mathrm{e}^{iS(\phi,I')}. \tag{D.13}$$

The nth semiclassical eigenstate corresponds to the substitution $I' = E_n = n + \frac{1}{2}$. For technical simplicity it is convenient to calculate the overlap between two perturbed wave

functions ($x = x_0 \pm \delta x/2$),

$$\begin{aligned}\langle n(x_0+\delta x/2)|m(x_0-\delta x/2)\rangle &= \int_0^{2\pi} d\phi \langle \phi|I''{=}E_n\rangle^* \langle \phi|I'{=}E_m\rangle \\ &= \frac{1}{2\pi}\int_0^{2\pi} d\phi \sqrt{1-\delta x^2\cos^2 2\phi} \\ &\quad \times \exp\left[i(E_m-E_n)\phi - i\delta x E \sin 2\phi\right] \\ &\approx J_{(m-n)/2}(\delta x E). \end{aligned} \tag{D.14}$$

Above I' and I'' correspond to the perturbations $\pm\delta x/2$, and $E = (E_n + E_m)/2$. In the main text we have reverted to a more general version of this expression that does not assume $x_0 = 1$. It is important to realize that because of the assumption $\delta x \ll x$ the pre-exponential factor (which is in fact a classical factor) can be neglected in leading order. Figure 6.1 confirms the remarkable agreement of the uniform approximation with the exact result.

D.4 Calculation of $\mathcal{P}^{\rm unif}(t)$

For the purpose of calculation it is more convenient to regard the prepared state as a "perturbed state" and the evolution Hamiltonian as the "unperturbed Hamiltonian". This is of course equivalent to the presentation in the text upon the replacement $\delta x \mapsto -\delta x$.

The initial state $|m(x_0+\delta x)\rangle$ is characterized by the action $I' = E_m \equiv E$. It is represented as in Appendix D.3 by

$$\langle \phi|I'{=}E\rangle \approx \frac{1}{2\pi}\exp[i(\phi + \delta x \sin 2\phi)E] \tag{D.15}$$

The evolving state is represented by

$$\langle \phi|\mathrm{e}^{-it\mathcal{H}_0}|I'{=}E\rangle = \langle \phi - t|I'{=}E\rangle \tag{D.16}$$

The overlap between the evolving and the initial state is

$$\frac{1}{2\pi}\int_0^{2\pi} d\phi \exp\Big[i\Big(-t + \delta x\left[\sin 2(\phi-t) - \sin 2\phi\right]\Big)E\Big]$$

For $F(t)$ as defined in (6.12) we obtain (after the required replacement $\delta x \mapsto -\delta x$):

$$F(t) = \frac{1}{2\pi}\int_0^{2\pi} d\phi \exp\left[i\delta x E \sin t \cos(2\phi - t)\right] \;=\; J_0\left(2\delta x E \sin t\right) \tag{D.17}$$

The survival probability is obtained by squaring this result.

Bibliography

[1] Y. Adamov, I. V. Gornyi, and A. D. Mirlin. Preprint `cond-mat/0212065`, 2002.

[2] A. M. Ozorio De Almeida. *Hamiltonian Systems: Chaos and Quantization*. Cambridge University Press, Cambridge, UK, 1990.

[3] V. I. Arnold. *Usp. Mat. Nauk.*, **30**:3, 1975.

[4] V. I. Arnold. *Mathematical Methods of Classical Mechanics*. Springer-Verlag, New York, 1978.

[5] B. B. Baker and E. T. Copson. *The Mathematical Theory of Huygens' Principle, 2nd ed.* Oxford University Press, London, 1950. p. 48.

[6] P. Beckmann and A. Spizzichino. *The Scattering of Electromagnetic Waves from Rough Surfaces*. Artech House, Norwood, 1987.

[7] G. Benenti and G. Casati. *Phys. Rev. E*, **65**:066205, 2002.

[8] G. Benenti, G. Casati, and G. Veble. Preprint `nlin.CD/0208003`, 2002.

[9] M. V. Berry. *Proc. Phys. Soc. London*, **89**:479, 1966.

[10] M. V. Berry, N. L. Balazs, M. Tabor, and A. Voros. *Ann. Phys. (NY)*, **122**:26, 1979.

[11] M. V. Berry and E. Bodenschatz. *J. Mod. Optics*, **46**:349, 1999.

[12] M. V. Berry and M. Tabor. *J. Phys. A: Math. Gen.*, **10**:371, 1977.

[13] O. Bohigas, M. J. Giannoni, and C. Schmit. *Phys. Rev. Lett.*, **52**:1, 1984.

[14] N. Bohr. *Phil. Mag.*, **26**:1, 1913.

[15] M. Born and E. Wolf. *Principles of Optics, 6th ed.* Pergamon Press, Elmsford, 1980. p. 375.

[16] M. Brack and R. K. Bhaduri. *Semiclassical Physics.* Addison-Wesley, Reading, MA, 1997.

[17] L. Brillouin. *Compt. Rend.*, **183**:24, 1926.

[18] G. F. Carrier. *J. Fluid Mech.*, **24**:641, 1966.

[19] N. R. Cerruti and S. Tomsovic. *Phys. Rev. Lett.*, **88**:054103, 2002.

[20] N. R. Cerruti and S. Tomsovic. *J. Phys. A: Math. Gen.*, **36**:3451, 2003.

[21] M. S. Child. *Semiclassical Mechanics With Molecular Applications.* Clarendon Press, Oxford, UK, 1991.

[22] M. S. Child and P. M. Hunt. *Mol. Phys.*, **34**:261, 1977.

[23] B. V. Chirikov. *Phys. Rep.*, **52**:264, 1979.

[24] D. Cohen. *Phys. Rev. Lett.*, **82**:4951, 1999.

[25] D. Cohen. In *New Directions in Quantum Chaos: Proceedings of the International School of Physics Enrico Fermi Course CXLIII,* ed. G. Casati, I. Guarneri, and U. Smilansky. IOS Press, Amsterdam, 2000.

[26] D. Cohen. *Phys. Rev. E*, **63**:36203, 2001.

[27] D. Cohen. In *Dynamics of Dissipation: Proceedings of the 38th Karpacz Winter School of Theoretical Physics,* ed. P. Garbaczewski and R. Olkiewicz. Springer, Berlin, 2002. (pp. 317-350).

[28] D. Cohen and E. J. Heller. *Phys. Rev. Lett.*, **84**:2841, 2000.

[29] J. N. L. Connor and D. Farrely. *J. Chem. Phys.*, **75**:2831, 1981.

[30] R. Crook, C. G. Smith, C. H. W. Barnes, M. Y. Simmons, and D. A. Ritchie. *J. Phys.: Cond. Matt.*, **12**:167, 2000.

[31] F. M. Cucchietti, C. H. Lewenkopf, E. R. Mucciolo, H. M. Pastawski, and R. O. Vallejos. *Phys. Rev. E*, **65**:046209, 2002.

[32] F. M. Cucchietti, H. M. Pastawski, and R. Jalabert. *Physica A*, **283**:285, 2000.

[33] F. M. Cucchietti, H. M. Pastawski, and D. A. Wisniacki. *Phys. Rev. E*, **65**:045206, 2002.

[34] S. Datta. *Electronic Transport in Mesoscopic Systems*. Cambridge University Press, Cambridge, UK, 1997.

[35] M. J. Davis and E. J. Heller. *J. Chem. Phys.*, **75**:246, 1981.

[36] M. Dimassi and J. Sjöstrand. *Spectral Asymptotics in the Semi-Classical Limit*. Cambridge University Press, Cambridge, UK, 1999.

[37] B. Eckhardt. *J. Phys. A: Math. Gen.*, **36**:371, 2003.

[38] A. Einstein. *Verh. Dtsch. Phys. Ges.*, **19**:82, 1917.

[39] J. Emerson, Y. S. Weinstein, S. Lloyd, and D. G. Cory. *Phys. Rev. Lett.*, **89**:284102, 2002.

[40] P. S. Epstein. *Ann. Phys. (Leipzig)*, **50**:489, 1916.

[41] M. A. Eriksson, R. G. Beck, M. Topinka, J. A. Katine, R. M. Westervelt, K. L. Kampman, and A. C. Gossard. *Appl. Phys. Lett.*, **69**:671, 1996.

[42] G. A. Fiete and E. J. Heller. Preprint `quant-ph/0211184`, 2002.

[43] H. Friedrich and D. Wintgen. *Phys. Rep.*, **183**:39, 1989.

[44] N. Garcia and N. Cabrera. *Phys. Rev. B*, **18**:576, 1978.

[45] U. Garibaldi, A. C. Levi, R. Spaldacini, and G. E. Tommei. *Surface Science*, **48**:649, 1975.

[46] W. R. S. Garton and F. S. Tomkins. *Astrophys. Jour.*, **158**:839, 1969.

[47] M. C. Gutzwiller. *J. Math. Phys.*, **8**:1979, 1967.

[48] M. C. Gutzwiller. *J. Math. Phys.*, **12**:343, 1971.

[49] M. C. Gutzwiller. *Chaos in Classical and Quantum Mechanics*. Springer-Verlag, New York, 1990.

[50] B. I. Halperin, A. Stern, Y. Oreg, J. N. H. J. Cremers, J. A. Folk, and C. M. Marcus. *Phys. Rev. Lett.*, **86**:2106, 2001.

[51] H. Hasegawa, M. Robnik, and G. Wunner. *Prog. Theor. Phys. Supplement*, **98**:198, 1989.

[52] E. J. Heller. *J. Chem. Phys.*, **62**:1544, 1975.

[53] E. J. Heller. *J. Chem. Phys.*, **65**:4979, 1976.

[54] E. J. Heller. *J. Chem. Phys.*, **75**:2923, 1981.

[55] E. J. Heller. *Phys. Rev. Lett.*, **53**:1515, 1984.

[56] E. J. Heller. In *Chaos and Quantum Physics,* ed. M.-J. Giannoni, A. Voros, and J. Zinn-Justin. Elsevier, Amsterdam, 1991. (pp. 547-663).

[57] E. J. Heller. *Prog. Theor. Phys. Supplement*, **N116**:45, 1994.

[58] E. J. Heller, S. Tomsovic, and M. A. Sepúlveda. *Chaos*, **2**:105, 1992.

[59] M. F. Herman and E. Kluk. *Chem. Phys.*, **91**:27, 1984.

[60] H. Hoinkes. *Rev. Mod. Phys.*, **52**:933, 1980.

[61] L. M. Hubbard and W. H. Miller. *J. Chem. Phys.*, **78**:1801, 1983.

[62] Y. Imry. *Introduction to Mesoscopic Physics*. Oxford University Press, Oxford, UK, 1997.

[63] P. Jacquod, I. Adagidelli, and C. W. J. Beenakker. *Phys. Rev. Lett.*, **89**:154103, 2002.

[64] P. Jacquod, I. Adagidelli, and C. W. J. Beenakker. *Europhys. Lett.*, **61**:729, 2003.

[65] P. Jacquod, P. G. Silvestrov, and C.W.J. Beenakker. *Phys. Rev. E*, **64**:055203, 2001.

[66] R. A. Jalabert and H. M. Pastawski. *Phys. Rev. Lett.*, **86**:2490, 2001.

[67] H. Jeffreys. *Proc. London Math. Soc.*, **23**:428, 1925.

[68] S. Kallush, B. Segev, A. V. Sergeev, and E. J. Heller. *J. Phys. Chem. A*, **106**:6006, 2002.

[69] L. Kaplan and E. J. Heller. *Ann. Phys. (NY)*, **264**:171, 1998.

[70] J. B. Keller. *Ann. Phys. (NY)*, **4**:180, 1958.

[71] S. Keppeler. *Ann. Phys. (NY)*, **304**:40, 2003.

[72] H. A. Kramers. *Z. Phys.*, **39**:828, 1926.

[73] M. Kuś, F. Haake, and D. Delande. *Phys. Rev. Lett.*, **71**:2167, 1993.

[74] J. Liouville. *J. Math. Pures Appl.*, **20**:137, 1855.

[75] J. Main and G. Wunner. *Phys. Rev. A*, **55**:1743, 1997.

[76] C. M. Marcus, A. J. Rimberg, R. M. Westervelt, P. F. Hopkins, and A. C. Gossard. *Phys. Rev. Lett.*, **69**:506, 1992.

[77] C. M. Marcus, R. M. Westervelt, P. F. Hopkins, and A. C. Gossard. *Chaos*, **3**:643, 1993.

[78] A. Martinez. *An Introduction to Semiclassical and Microlocal Analysis*. Springer-Verlag, New York, 2002.

[79] T. J. Martinez, M. Ben-Nun, and G. Ashkenazi. *J. Chem. Phys.*, **104**:2847, 1996.

[80] T. J. Martinez and R. D. Levine. *Chem. Phys. Lett.*, **259**:252, 1996.

[81] M. L. Mehta. *Random Matrices*. Academic Press, New York, 1991.

[82] R. F. Millar. *Proc. Camb. Phil. Soc.*, **69**:217, 1971.

[83] W. H. Miller. *J. Chem. Phys.*, **53**:3578, 1970.

[84] W. H. Miller. *J. Phys. Chem.*, **105**:2942, 2001.

[85] W. H. Miller and F. T. Smith. *Phys. Rev. A*, **17**:939, 1978.

[86] F. L. Moore, J. C. Robinson, C. F. Barucha, B. Sundaram, and M. G. Raizen. *Phys. Rev. Lett.*, **75**:4598, 1995.

[87] C. Morette. *Phys. Rev.*, **81**:848, 1951.

[88] E. E. Narimanov and A. D. Stone. *Phys. Rev. B*, **57**:9807, 1998.

[89] E. E. Narimanov, A. D. Stone, and G. S. Babinger. *Phys. Rev. Lett.*, **80**:4024, 1998.

[90] E. E. Narimanov, A. D. Stone, and G. S. Boebinger. *Phys. Rev. Lett.*, **80**:4024, 1998.

[91] P. W. O'Connor, S. Tomsovic, and E. J. Heller. *J. Stat. Phys.*, **68**:131, 1991.

[92] P. W. O'Connor, S. Tomsovic, and E. J. Heller. *Physica D*, **55**:340, 1992.

[93] M. Ol'shanii, J. Vaníček, and M. Prentiss. *Quant. Semiclass. Opt.*, **8**:655, 1996.

[94] G. Papadopoulos. *Phys. Rev. D*, **11**:2870, 1975.

[95] H. M. Pastawski, P. R. Levstein, and G. Usaj. *Phys. Rev. Lett.*, **75**:4310, 1995.

[96] H. M. Pastawski, P. R. Levstein, G. Usaj, J. Raya, and J. Hirschinger. *Physica A*, **283**:166, 2000.

[97] T. Pearcy. *Phil. Mag.*, **37**:311, 1946.

[98] A. Peres. *Phys. Rev. A*, **30** :1610, 1984.

[99] T. Prosen. Preprint `quant-ph/0106149`, 2001.

[100] T. Prosen. *Phys. Rev. E*, **65**:036208, 2002.

[101] T. Prosen and T. Seligman. *J. Phys. A: Math. Gen.*, **35**:4707, 2002.

[102] T. Prosen and M. Ždinarič. *J. Phys. A: Math. Gen.*, **34**:681, 2001.

[103] T. Prosen and M. Ždinarič. *J. Phys. A: Math. Gen.*, **35**:1455, 2002.

[104] M. G. Raizen, F. L. Moore, J. C. Robinson, C. F. Barucha, and B. Sundaram. *Quant. Semiclass. Opt.*, **8**:687, 1996.

[105] J. W. Strutt (Baron Rayleigh). *Proc. Roy. Soc. A*, **79**:399, 1907.

[106] W. K. Rhim, A. Pines, and J. S. Waugh. *Phys. Rev. Lett.*, **25**:218, 1970.

[107] K. Richter, D. Ullmo, and R. A. Jalabert. *Phys. Rev. B*, **54**:5219, 1996.

[108] K. Richter, D. Ullmo, and R. A. Jalabert. *J. Phys. A: Math. Gen.*, **37**:5087, 1996.

[109] R. Schinke. *Photodissociation dynamics.* Cambridge University Press, Cambridge, UK, 1993.

[110] M. A. Sepúlveda and E. J. Heller. *J. Chem. Phys.*, **101**:8004, 1994.

[111] M. A. Sepúlveda, S. Tomsovic, and E. J. Heller. *Phys. Rev. Lett.*, **69**:402, 1992.

[112] A. V. Sergeev and B. Segev. *J. Phys. A: Math. Gen.*, **35**:1769, 2002.

[113] P. G. Silvestrov, J. Tworzydlo, and C. W. J. Beenakker. Preprint `nlin.CD/0207002`, 2002.

[114] L. L. Sohn, L. P. Kouwenhoven, and Eds. G. Schön. *Mesoscopic Electron Transport*. Kluwer Academic, Boston, 1997.

[115] A. Stern, Y. Aharonov, and Y. Imry. *Phys. Rev. A*, **41**:3436, 1990.

[116] J. R. Stine and R. A. Marcus. *J. Chem. Phys.*, **59**:5145, 1973.

[117] V. M. Strutinsky. *Nukleonika (Poland)*, **20**:679, 1975.

[118] R. Thom. *Structural Stability and Morphogenesis*. Benjamin, Reading, USA, 1975.

[119] S. Tomsovic and E. J. Heller. *Phys. Rev. Lett.*, **67**:604, 1991.

[120] S. Tomsovic and E. J. Heller. *Phys. Rev. E*, **47**:282, 1993.

[121] M. A. Topinka, B. J. LeRoy, S. E. J. Shaw, E. J. Heller, R. M. Westervelt, K. D. Maranowski, and A. C. Gossard. *Science*, **289**:2323, 2000.

[122] M. A. Topinka, B. J. LeRoy, R. M. Westervelt, S. E. J. Shaw, R. Fleischmann, E. J. Heller, K. D. Maranowski, and A. C. Gossard. *Nature*, **410**:183, 2001.

[123] G. Usaj, H. M. Pastawski, and P. R. Levstein. *Mol. Phys.*, **95**:1229, 1998.

[124] J. Vaníček and D. Cohen. Survival probability and the local density of states for one-dimensional Hamiltonian systems. *Submitted to J. Phys. A*, March 2003. Preprint `quant-ph/0303103`.

[125] J. Vaníček and E. J. Heller. *Phys. Rev. E*, **64**:026215, 2001.

[126] J. Vaníček and E. J. Heller. *Phys. Rev. E*, **67**:016211, 2003.

[127] J. Vaníček and E. J. Heller. Semiclassical evaluation of fidelity in the Fermi-golden-rule and Lyapunov regimes. *Submitted to Phys. Rev. Lett.*, February 2003. Preprint `quant-ph/0302192`.

[128] J. Vaníček, M. Ol'shanii, N. Dekker, and M. Prentiss. Semiclassical and quantum analysis of atomic lens based on laser standing wave. Not published, 1996.

[129] J. H. Van Vleck. *Proc. Nat. Acad. Sci. USA*, **14**:178, 1928.

[130] W. Wang and B. Li. Preprint `nlin.CD/0208013`, 2001.

[131] Y. S. Weinstein, J. Emerson, S. Lloyd, and D. G. Cory. Preprint `quant-ph/0210063`, 2002.

[132] D. Weiss and K. Richter. *Physica D*, **83**:290, 1995.

[133] D. Weiss, K. Richter, A. Menschig, R. Bergmann, H. Schweizer, K. von Klitzing, and G. Weimann. *Phys. Rev. Lett.*, **70**:4118, 1993.

[134] D. Weiss, M. L. Roukes, A. Menschig, P. Grambow, K. von Klitzing, and G. Weimann. *Phys. Rev. Lett.*, **66**:2790, 1991.

[135] G. Wentzel. *Z. Phys.*, **38**:519, 1926.

[136] P. B. Wilkinson, T. M. Fromhold, L. Eaves, F. W. Sheard, N. Miura, and T. Takamasu. *Nature*, **380**:608, 1996.

[137] D. Wintgen, K. Richter, and G. Tanner. *Chaos*, **2**:19, 1992.

[138] L. Wirtz, J.-Z. Tang, and J. Burgdörfer. *Phys. Rev. B*, **56**:7589, 1997.

[139] D. A. Wisniacki. *Phys. Rev. E*, **67**:016205, 2003.

[140] D. A. Wisniacki and D. Cohen. *Phys. Rev. E*, **66**:046209, 2002.